SCIENCE CHINA
Chemistry

•REVIEWS•

December 2021 Vol.64 No.12: 2060–2104
https://doi.org/10.1007/s11426-021-1146-6

Frontiers in circularly polarized luminescence: molecular design, self-assembly, nanomaterials, and applications

Zhong-Liang Gong[1†], Xuefeng Zhu[1†], Zhonghao Zhou[1†], Si-Wei Zhang[2†], Dong Yang[2†], Biao Zhao[3†], Yi-Pin Zhang[4†], Jianping Deng[3*], Yixiang Cheng[4*], You-Xuan Zheng[4*], Shuang-Quan Zang[5*], Hua Kuang[6*], Pengfei Duan[7*], Mingjian Yuan[8*], Chuan-Feng Chen[1,9*], Yong Sheng Zhao[1,9*], Yu-Wu Zhong[1,9*], Ben Zhong Tang[2,10*] & Minghua Liu[1,9*]

[1]*Beijing National Laboratory for Molecular Sciences (BNLMS), CAS Research/Education Center for Excellence in Molecular Sciences, Key Laboratory of Photochemistry, Key Laboratory of Colloid, Interface and Chemical Thermodynamics, Key Laboratory of Molecular Recognition and Function, Institute of Chemistry, Chinese Academy of Sciences, Beijing 100190, China;*
[2]*Department of Chemistry, Hong Kong Branch of Chinese National Engineering Research Center for Tissue Restoration and Reconstruction, The Hong Kong University of Science and Technology, Clear Water Bay, Kowloon, Hong Kong 999077, China;*
[3]*State Key Laboratory of Chemical Resource Engineering, College of Materials Science and Engineering, Beijing University of Chemical Technology, Beijing 100029, China;*
[4]*State Key Laboratory of Coordination Chemistry, Key Lab of Mesoscopic Chemistry of Ministry of Education, Collaborative Innovation Center of Advanced Microstructures, and Jiangsu Key Laboratory of Advanced Organic Materials, School of Chemistry and Chemical Engineering, Nanjing University, Nanjing 210023, China;*
[5]*Henan Key Laboratory of Crystalline Molecular Functional Materials, Henan International Joint Laboratory of Tumor Theranostical Cluster Materials, Green Catalysis Center, College of Chemistry, Zhengzhou University, Zhengzhou 450001, China;*
[6]*Key Lab of Synthetic and Biological Colloids, Ministry of Education, School of Chemical and Material Engineering, State Key Laboratory of Food Science and Technology, Jiangnan University, Wuxi 214122, China;*
[7]*CAS Center for Excellence in Nanoscience, CAS Key Laboratory of Nanosystem and Hierarchical Fabrication, National Center for Nanoscience and Technology (NCNST), Beijing 100190, China;*
[8]*Key Laboratory of Advanced Energy Materials Chemistry (Ministry of Education), College of Chemistry, Renewable Energy Conversion and Storage Center (RECAST), Nankai University, Tianjin 300071, China;*
[9]*School of Chemical Sciences, University of Chinese Academy of Sciences, Beijing 100049, China;*
[10]*Shenzhen Institute of Molecular Aggregate Science and Engineering, School of Science and Engineering, The Chinese University of Hong Kong, Shenzhen, Shenzhen 518172, China*

Received October 5, 2021; accepted October 28, 2021; published online November 10, 2021

The research in circularly polarized luminescence has attracted wide interest in recent years. Efforts on one side are directed toward the development of chiral materials with both high luminescence efficiency and dissymmetry factors, and on the other side, are focused on the exploitations of these materials in optoelectronic applications. This review summarizes the recent frontiers (mostly within five years) in the research in circularly polarized luminescence, including the development of chiral emissive materials based on organic small molecules, compounds with aggregation-induced emissions, supramolecular assemblies, liquid crystals and liquids, polymers, metal-ligand coordination complexes and assemblies, metal clusters, inorganic nanomaterials, and photon upconversion systems. In addition, recent applications of related materials in organic light-emitting devices, circularly polarized light detectors, and organic lasers and displays are also discussed.

†These authors contributed equally to this work.
*Corresponding authors (email: zhongyuwu@iccas.ac.cn; dengjp@mail.buct.edu.cn; yxcheng@nju.edu.cn; yxzheng@nju.edu.cn; zangsqzg@zzu.edu.cn; kuangh@jiangnan.edu.cn; duanpf@nanoctr.cn; yuanmj@nankai.edu.cn; cchen@iccas.ac.cn; yszhao@iccas.ac.cn; tangbenz@cuhk.edu.cn; liumh@iccas.ac.cn)

circularly polarized luminescence, photochemistry, photophysics, aggregation-induced emission, self-assembly, nanomaterials, nanostructures, chiral materials, chirality, organic light-emitting devices, photodetectors, organic lasers

Citation: Gong ZL, Zhu X, Zhou Z, Zhang SW, Yang D, Zhao B, Zhang YP, Deng J, Cheng Y, Zheng YX, Zang SQ, Kuang H, Duan P, Yuan M, Chen CF, Zhao YS, Zhong YW, Tang BZ, Liu M. Frontiers in circularly polarized luminescence: molecular design, self-assembly, nanomaterials, and applications. *Sci China Chem*, 2021, 64: 2060–2104, https://doi.org/10.1007/s11426-021-1146-6

1 Introduction

Polarization is one of the inherent and important properties of light, which is very important in display, remote sensing, target identification, information storage fields and so on [1–4]. Unlike the intensity and wavelength of light, polarization has the ability to distinguish the information of light from three dimensions [5]. In particular, circularly polarized (CP) light can be regarded as the superposition of two linearly polarized lights (LPLs) with the same frequency and vertical polarization direction. Due to the rich optical information and angle independence character, CP light is widely applied for various technologies and devices, including quantum computing and information encryption [6], asymmetric synthesis [7], three-dimensional (3D) displays [8], and light-emitting devices [9].

CP light is traditionally produced from LPL by passing a quarter wave plate. Alternatively, CP light can be directly generated from chiral luminescent materials in the form of circularly polarized luminescence (CPL), which circumvents the energy loss caused during the plate transition process in the traditional method. In order to obtain CPL-active materials, an efficient coupling between the chiral components and luminescent components is generally necessary (Figure 1a). Such coupling can be realized through either covalent or non-covalent bonding. Taking organic luminescent materials with CPL as an example, three common strategies can be applied (Figure 1b) [10]. Firstly, a single-component chiral chromophore could display intrinsic CPL in solution or amplified CPL signal after aggregation. Secondly, the co-assembly of a chiral molecule with an achiral molecule into aggregates could produce CPL by chirality transfer. In this method, either component could be the emissive chromophore or the chirality inducer. Thirdly, symmetry breaking of a single-component achiral chromophore could lead to the separation of aggregates enriched in one type of chirality and thus the emergence of CPL. These strategies can be extended to inorganic and nanomaterials.

For the experimental characterizations of chiral emissive materials, electronic circular dichroism (CD) and CPL spectral measurements are often performed. CD spectroscopy measures the absorption difference of the material toward the left-handed CPL (L-CPL) and right-handed CPL (R-CPL). The magnitude of CD can be quantified by the absorption dissymmetry factor g_{abs} (or g_{CD}), which is determined by Eq. (1):

$$g_{abs} = \frac{\varepsilon_L - \varepsilon_R}{1/2(\varepsilon_L + \varepsilon_R)} = \frac{2(\varepsilon_L - \varepsilon_R)}{\varepsilon_L + \varepsilon_R} \quad (1)$$

where ε_L and ε_R are the molar absorption coefficients of L-CPL and R-CPL, respectively. Experimentally, the g_{abs} value can be determined by Eq. (2):

$$g_{abs} = \frac{\text{ellipticity}}{32980 \times \text{absorbance}} \quad (2)$$

where the "ellipticity (in mdeg)" and "absorbance" values can be directly obtained from CD spectral measurement.

Compared with CD spectra, CPL spectra are associated with the excited state properties of chiral systems. The CPL property can be evaluated by the luminescence dissymmetry factor g_{lum} (g_{PL} and g_{EL} are also used to differentiate the g_{lum} value of photoluminescence and electroluminescence), which is defined by Eq. (3):

$$g_{lum} = \frac{I_L - I_R}{1/2(I_L + I_R)} = \frac{2(I_L - I_R)}{I_L + I_R} \quad (3)$$

where I_L and I_R represent the luminescence intensity of L-CPL and R-CPL, respectively. Theoretically, g_{lum} is predicted to be related to Eq. (4):

$$g_{lum} = 4\cos\theta \frac{|m||\mu|}{|m|^2 + |\mu|^2} \quad (4)$$

where m and μ denote the magnetic and electric transition dipole moments, respectively, and θ is the angle between them. In the case of that m is much less than μ (which is true for most molecular systems), Eq. (4) can be simplified as Eq. (5):

$$g_{lum} \approx 4\cos\theta \frac{|m|}{|\mu|} \quad (5)$$

In this sense, the g_{lum} value is proportional to $|m|$ but inversely proportional to $|\mu|$. A smaller $|\mu|$ value is thus expected to be beneficial for higher g_{lum}. On the other hand, in order to obtain highly-emissive materials with a high emission quantum yield Φ, it is generally required to have a high $|\mu|$. This dilemma leads to the difficulty in achieving materials with both high g_{lum} and Φ (Φ_F and Φ_P are specified in some cases to differentiate the fluorescence and phosphorescence quantum yield, respectively).

According to Eqs. (1) and (3), the values of g_{abs} and g_{lum} are both in the range from −2 to +2. The absolute values $|g_{abs}|$ and $|g_{lum}|$ reflect the magnitude of the Cotton effect and luminescence polarization, respectively. CPL-active materials ($|g_{lum}| \neq 0$) usually display distinct Cotton effects ($|g_{abs}| \neq 0$). However, the observation of Cotton effects does not ne-

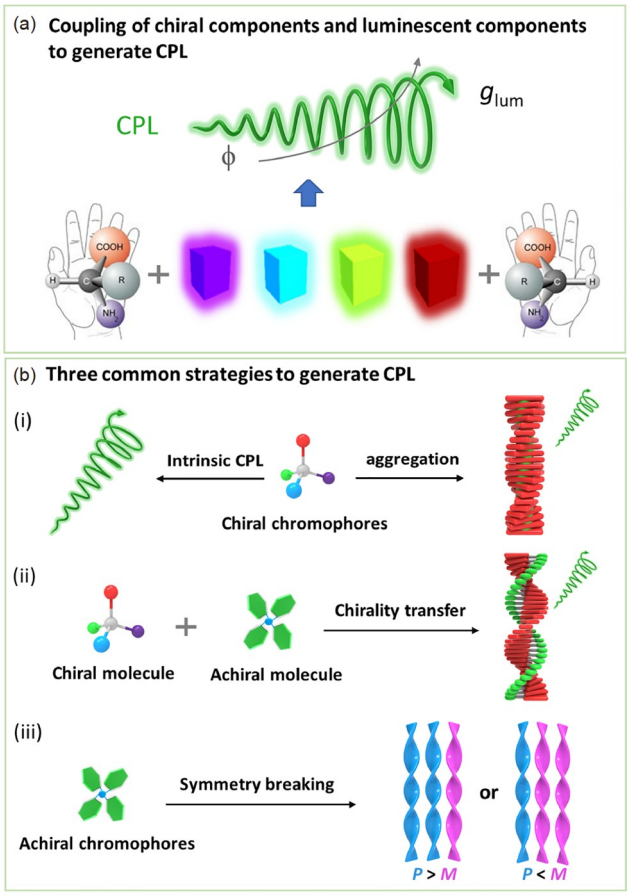

Figure 1 (a) Schematic presentation of the coupling of chiral components and luminescent components to generate CPL. (b) Three common strategies to produce luminescent materials with CPLs (color online).

cessarily point to CPL activity, because they are related to the ground- and excited-state property of the material, respectively.

Since the first report of CPL-active molecular material, chiral hydrindanon, in 1967 [11], much advance has been made in this field to date. In particular, the research in CPL has received intense attention in the past ten years and has now become the frontier of a wide range of scientific fields, including molecular materials, nanoscience and technology, photochemistry, and optoelectronic devices. The research in CPL has been summarized by a number of recent reviews focusing on nanoassemblies and aggregated systems [10,12–15], organic small molecules [16–18], photon upconversion systems [19], or optoelectronic devices [9,20]. We discuss herein the recent frontiers (mostly within five years) of CPL research from a broad range of perspective, including the development of chiral emissive materials based on organic small molecules, compounds with aggregation-induced emissions (AIEs), supramolecular assemblies, liquid crystals (LCs) and liquids, polymers, metal-ligand coordination complexes and assemblies, metal clusters, inorganic nanomaterials, and photon upconversion systems. In addition, the recent applications of related materials in light-emitting devices, CP light detections, and organic lasers and displays are discussed.

2 CPL-active materials

2.1 CPL-active chiral organic small molecules

In the past several years, there have been more and more reports on CPL-active materials by using versatile chiral organic small molecules. In particular, those derivatives with the axially chiral binaphthyls, helicenes, and planar chiral cyclophanes were extensively investigated [21–24]. Compared with chiral polymers, chiral organic small molecules have many advantages, such as easy structural modification, high fluorescence efficiency, fine-tuning of emission wavelength, precise structure-performance relationship, and easy manufacturing process [25].

1,1′-Bi(2-naphthol) (BINOL) is a representative axially chiral compound, whose chirality originates from the restricted rotation between two naphthalene rings. Optically active 1,1′-binaphthyl derivatives have been regarded as one of the most important chiral units for the design of ideal CPL emitters because the binaphthyl skeletal structure at 2,2′-, 3,3′-, 5,5′- or 6,6′-positions can be selectively functionalized at the well-defined molecular level to afford stable chiral configuration and high chiral induction [26]. In this context, Ema's group [27–30] designed a series of CPL-active intramolecular excimers of the chiral quarter naphthyl fluorophores (*R*,*R*,*R*)-**1a**–**1f** (**1a**: g_{lum} = +0.037, **1c**: Φ_F = 0.67) *via* ester linkers (Figure 2a and Table 1) [27]. Interestingly, although these compounds have the same axial chirality, (*R*,*R*,*R*)-**1a**, **1c**, **1d**, and **1f** displayed (+)-CPL whereas (*R*,*R*,*R*)-**1b** and **1e** exhibited (−)-CPL, as a result of the clockwise and counterclockwise orientations of intramolecular proximal aromatic pairs. In 2019, their group [28] also observed that *peri*-xanthenoxanthenes (PXX)-based dyes (*R*)-**3** and (*R*,*R*)-**5** containing bridged chiral binaphthyl moiety emitted strong CPL signals (Figure 2b), demonstrating axially chiral PXX could further promote the chiral amplification effect of the rigid binaphthyl structure. In contrast, the related compounds (*R*)-**2** and (*R*,*R*)-**4** without the methylenedioxy bridges, were essentially CPL-inactive. The bridged structures **3** and **5** were considered to adjust the angle between the vectors of *m* and *μ* to produce intense CPL activity. In 2019, Zhao's group [31] investigated the temperature-dependent dual fluorescences of **6** and **7** based on the chosen amino groups by using 2,2′-diamino-6,6′-diboryl-1,1′-binaphthyls enantiomers (Figure 2c). At higher temperatures (20–80 °C), compound **6** possesses the emission maximum at 478–485 nm. When the temperature is decreased to −20 °C, the emission maximum shifts to 565 nm. While the CPL activity of **6** has not been examined, the enantiomers of **7**

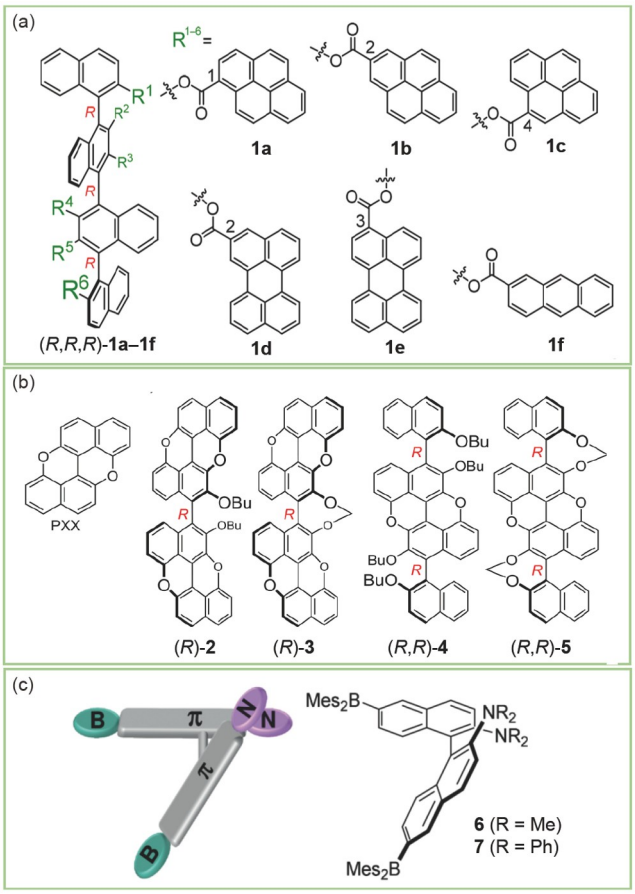

Figure 2 (a) Chemical structures of chiral quarter naphthyl fluorophores (*R*,*R*,*R*)-**1a**–**1f** [27]. (b) Chemical structures of chiral dyes **2**–**5** based on *peri*-xanthenoxanthenes (PXX) structural unit [28]. (c) Chemical structures of chiral dyes **6** and **7** [31] (color online).

Table 1 CPL parameters of organic compounds [a)]

Compound	λ_{em} (nm)	Φ	g_{lum}	Ref.
(*R*,*R*,*R*)-**1a**	540	0.24	+0.037	[27]
(*R*,*R*,*R*)-**1b**	430	0.35	-2.8×10^{-3}	[27]
(*R*,*R*,*R*)-**1c**	490	0.67	+0.014	[27]
(*R*,*R*,*R*)-**1d**	525	0.24	$+3.3 \times 10^{-3}$	[27]
(*R*,*R*,*R*)-**1e**	570	0.38	−0.013	[27]
(*R*,*R*,*R*)-**1f**	450	0.03	$+1.0 \times 10^{-3}$	[27]
(*R*)-**2**	481	0.89	ND	[28]
(*R*)-**3**	497	0.56	$+1.3 \times 10^{-3}$	[28]
(*R*,*R*)-**4**	458	0.57	ND	[28]
(*R*,*R*)-**5**	490	0.67	$+1.0 \times 10^{-3}$	[28]
(+)-**7**(*c*-Hex)	455	0.75	-1.17×10^{-3}	[31]
(+)-**7**(CH_3CN)	524	0.26	$+1.19 \times 10^{-3}$	[31]
(*P*)-**8a**	424	0.33	-2.5×10^{-4}	[37]
(*P*)-**8b**	455	0.19	-4.5×10^{-3}	[37]
(*P*)-**9a**–**9f**	390–440	NR	$+(0.7–1.0) \times 10^{-3}$	[38]
(*P*)-**10a**–**10f**	430–470	NR	$-(3.7–6.8) \times 10^{-3}$	[38]
(*P*)-**10g**	450/530	NR	−0.004/+0.005	[38]
(*P*)-**11**	486	0.25	$+0.77 \times 10^{-3}$	[39]
(*P*)-**12**	532	0.41	$+7.44 \times 10^{-3}$	[39]
(R_p)-**13**	401	0.81	$+1.3 \times 10^{-3}$	[40]
(R_p)-**14**	425	0.75	-1.7×10^{-3}	[40]
(S_p)-**15**	400	NR	$+1.7 \times 10^{-3}$	[41]

a) ND = not determined due to low CPL activity; NR = not reported.

were demonstrated to display solvent-switchable CPL. A change of solvent from nonpolar cyclohexane (*c*-Hex) to highly polar CH_3CN not only shifts the CPL position of (+)-**7** to much longer wavelength with intramolecular charge transfer (ICT) characteristic, but also inverts the (−)-CPL to (+)-CPL (Table 1).

It is worth noting that much attention has been paid to the novel CPL materials from helicene-based derivatives due to their twisted extended π-conjugated molecular structures and strong helical chirality properties [32–39]. Since 2016, Chen's group [32–38] developed versatile CPL-active emitters based on optically stable enantiomeric hydro[5]helicene and [5]helicene derivatives. Compared with the relatively flexible compound **8a**, the rigid helicene **8b** could exhibit stronger CPL (Figure 3a) [37]. Furthermore, inversions of CPL signs were observed by oxidation of the hydro[5]helicene **9a**–**9f** to [5]helicene derivatives **10a**–**10f** or modulation of the ICT from triphenylamine groups of **10g** (Figure 3b) [38]. Interestingly, compound (*P*)-**10g** displayed bisignate CPL spectra with (−)-CPL in the shorter wavelength region (430–470 nm) and (+)-CPL in the longer wavelength region (510–560 nm), respectively, in CH_2Cl_2. In addition, the CPL signals of (*P*)-**10g** were strongly dependent on the solvent polarity, resembling those of the previously discussed ICT compound **7** (Figure 2c). Recently, Narita's group [39] also observed the chiroptical property difference between the π-extended [9]helicene **12** and the parent pristine [7]helicene **11** (Figure 3c). The enantiomers (*P*/*M*)-**12** had 10-fold enhancement in $|g_{lum}|$ (7.44×10^{-3}) and higher Φ_F (0.41) than (*P*/*M*)-**11** ($|g_{lum}| = 0.77 \times 10^{-3}$, Φ_F = 0.25), indicating that the π-extended helicenes could possess high potential for spin transport and superior inductance.

In recent years, planar chirality-based small molecules have been designed and used to construct CPL materials through various fluorophore incorporation [21,40,41]. Morisaki's group [40] found that the V-shaped chiral [2.2]paracyclophanes (PCP) molecule (R_p)-**13** emitted intense opposite CPL signals (λ_{em} = 401 nm, $g_{lum} = +1.3 \times 10^{-3}$, Φ = 81%) compared with the X-shaped PCP (R_p)-**14** (λ_{em} = 425 nm, $g_{lum} = -1.7 \times 10^{-3}$, Φ_F = 75%) (Figure 4a). The sign inversion of CPLs was believed to be caused by their different stacking modes and the orientation of the dipole moments between *m* and *μ*. Meanwhile, they also reported good CPL property of the X-shaped PCP molecule (S_p)-**15** (λ_{em} = 400 nm, $g_{lum} = +1.7 \times 10^{-3}$) at 25 °C in $CHCl_3$ solution

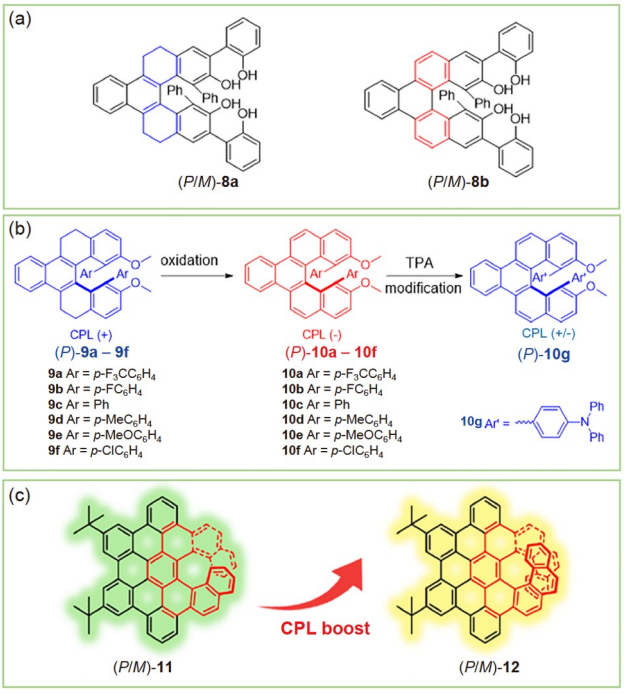

Figure 3 (a) The enantiomers with different flexible (**8a**) or rigid (**8b**) helical skeleton [37]. (b) Sign inversions of CPL by chemically fine-tuning operations on the structures of helical compounds **9a**–**9f** and **10a**–**10g** [38]. (c) Molecular structures of helicene derivatives **11** and **12** [39] (color online).

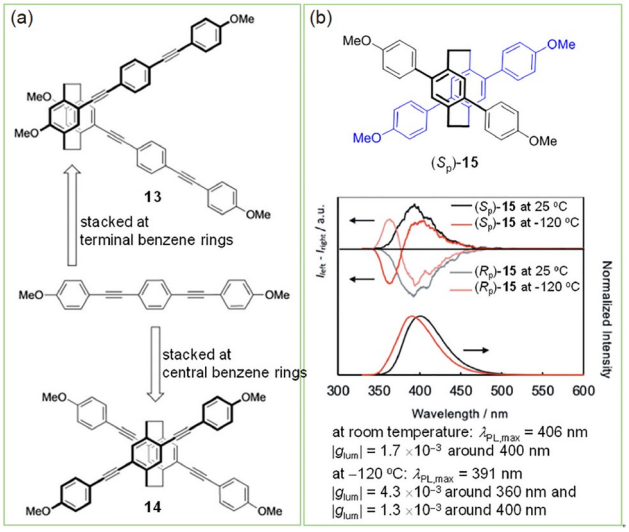

Figure 4 (a) Structures of V-shaped (**13**) and X-shaped (**14**) planar chiral molecules [40]. (b) X-shaped planar chiral molecule **15** and the CPL and emission spectra (S_p)- and (R_p)-**15** in methylcyclohexane (10^{-5} M) at 25 and −120 °C [41] (color online).

(Figure 4b) [41]. Interestingly, an additional CPL peak with an opposite sign was observed in the short-wavelength region (λ_{em} =360 nm, $g_{lum} = -4.3 \times 10^{-3}$) at −120 °C, as a result of the suppression of the rotary motion of the anisolyl units in the excited states and thus the emergence of emissions from two isomers [41].

2.2 CPL from AIE-active aggregates

Chiral organic molecules exhibiting CPL property, with both a large g_{lum} value and a high luminescence efficiency, are highly desired due to their potential applications in the wide range of 3D optical displays, encryptions, biological probes, chiral photoelectric devices, and CPL switches. From the viewpoint of practical application, it is imperative to develop solid-state CPL materials while maintaining a high luminescence efficiency [42–44]. Unfortunately, π-conjugated luminophores always face a general situation of aggregation-caused quenching (ACQ) of luminescence effect in their aggregate or assembly state (Figure 5a), which dramatically deteriorates the CPL performance [45,46]. Recently, the AIE concept (Figure 5b), in which organic fluorophores emit brighter in aggregates caused by the restriction of intramolecular motion, including intramolecular rotation and vibration, has emerged as a potently valuable methodology to fabricate solid-state luminescent materials [47–49]. Thus, integrating chiral luminescent aggregate with a high g_{lum} value into the AIE system can be a promising protocol for designing AIE-CPL systems with both large g_{lum} and Φ values (Figure 5c). Generally speaking, three strategies could be adopted for the generation of AIE-CPL, (1) the chiral and AIE moiety is covalently attached to realize AIE-CPL by helical aggregation; (2) chirality transfer from chiral mole-

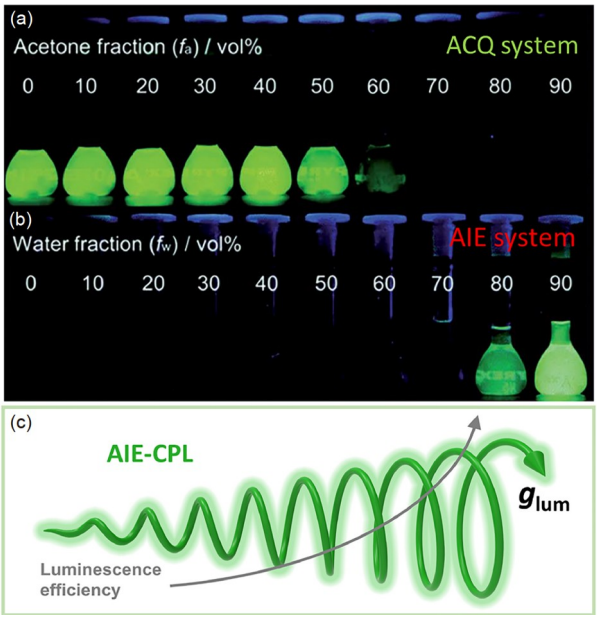

Figure 5 Typical examples of ACQ and AIE systems: fluorescence photographs of (a) fluorescein and (b) hexaphenylsilole (HPS) in the mixtures of (a) water and acetone with different fractions of acetone (f_a) and (b) THF and water with different fractions of water (f_w). (c) Generation of CPL with high g_{lum} from AIE-active aggregate with high luminescence efficiency (AIE-CPL). Panels (a) and (b) are adapted from Ref. [42] (color online).

cules to achiral AIEgens (the luminogens with AIE properties) during the co-assembly process; (3) formation of helical aggregates with excess in the right- or left-handedness (*P* or *M*) due to symmetry breaking of achiral AIEgens with latent chirality in the aggregation process. These strategies are in accordance with the common strategies to produce CPL-active luminescent materials (Figure 1).

The selected AIE systems with CPL property are shown in Figure 6 and corresponding CPL parameters are summarized in Table 2. These AIE-CPL systems contain typical AIE moieties, *e.g.*, hexaphenylsilole (HPS), tetraphenylethene (TPE), and cyano-substituted stilbene (CNSB). Molecules **16**–**19** were synthesized by incorporating a tetraphenylsilole backbone with a chiral mannose unit [50], *L*-leucine pendants [51], *L*-valine [52], and phenylethanamine, respectively [53]. All of these silole derivatives exhibited obvious AIE characteristics as well as good CPL property when aggregating into chiral superstructures. Molecules **20**–**23** are chiral TPE derivatives bearing an *L*-leucine methyl ester moiety [54], cholesterol periphery [55], BINOL-based boronic ester [56], and BINOL-based dihexyl diether [57], respectively. These TPE-derivated AIE-CPL systems with various point, axial and planar chirality have the advantages of facile synthesis, high emission efficiency. Molecule **24** is a CNSB derivative conjugated with a universal gelator moiety *N*,*N*′-bis(dodecyl)-*L*(*D*)-glutamic diamide. During the cooling process from the hot solution, the chiral molecule can self-assemble into nanohelix structures with strong AIE and CPL properties [58]. Molecule **25** was used to realize multicolor tunable CPL in a single AIE molecule by attaching pyridine-modified cyanostilbene to a chiral unit. By virtue of the gelation caused chirality transfer and application, both the gel and xerogel film exhibited AIE and CPL with a large g_{lum} value (Table 2) [59].

Some achiral AIEgens can exhibit latent chirality. For example, the four phenyl rings of TPE could rotate either in the clockwise or the anticlockwise direction. Thus, no chirality was observed in the solution state due to the rapid and reversible conformational change. However, chirality could be achieved upon aggregation to break the mirror symmetry. Typically, in the TPE-based teracycle molecule **26**, the phenyl rings of TPE were locked through a covalent bond connection [60]. Due to the rotation fixation, a dynamically stable single helical propeller-like structure can be resolved from their racemic forms. These resolved (*M*)-**26** and (*P*)-**26** enantiomers exhibited AIE effect and a mirror and large CPL dissymmetric factor when they formed aggregates in H_2O/tetrahydrofuran (THF) mixed solvents.

For achiral AIEgens, chirality transfer can be realized by co-assembling with chiral molecules through non-covalent bonding interactions to achieve AIE-CPL property. This strategy was used to prepare several AIE-CPL systems with potential applications in biosensing and photoelectronics. As shown in Figure 7a, a chiral tetraphenylpyrazine (TPP)-based cage compound (TPP-Cage) can encapsulate achiral diketopyrrolopyrrole (DPP), forming the DPP@TPP-Cage complexes, which achieves white-light emission with CPL property as a combination of the yellow emission from the host (TTP-Cage) and the blue emission from the guest (DPP) [61]. The DPP@TPP-Cage complex introduces a promising strategy for developing chiral materials through host-guest interaction-induced chirality transfer and provides a prospective pathway for white-light emission based on supramolecular assembly. Tang's group [62] also developed a novel strategy for constructing white-light emission and tunable CPL by interacting achiral AIEgens with host polymers. As shown in Figure 7b, when slowly evaporating the mixed solution of helical polymer (PLLA) and achiral

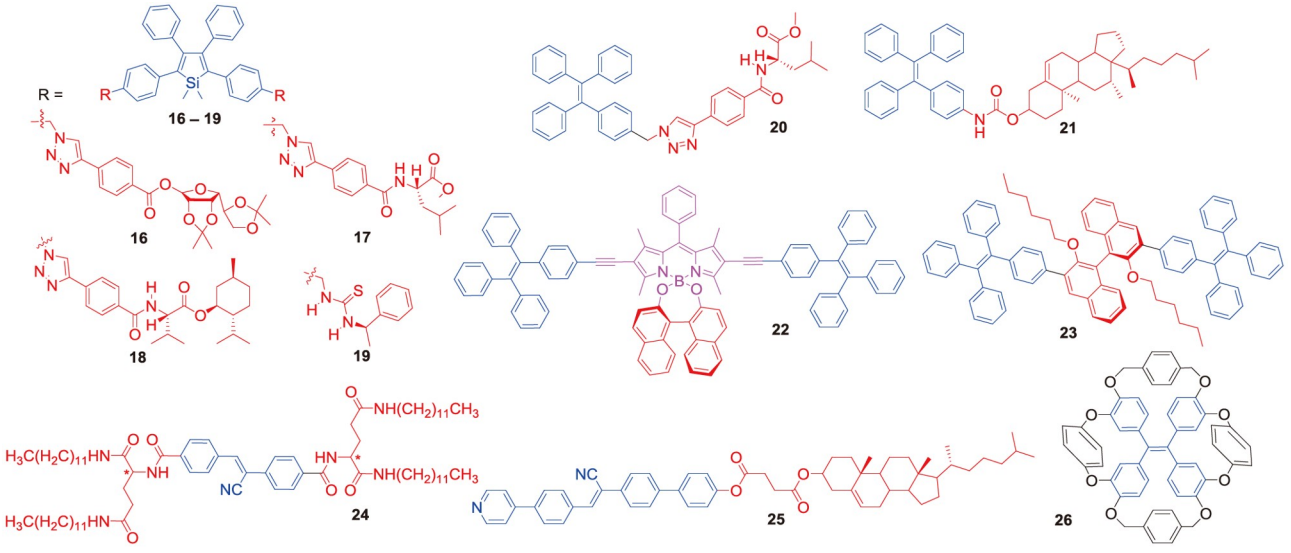

Figure 6 Examples of AIE systems with CPL originated from helical aggregation (**16**–**25**) and symmetry breaking (**26**) (color online).

Table 2 CPL parameters of AIE-active aggregates [a)]

Compound	λ_{em} (nm)	Φ	g_{lum}	Ref.
(*D*)-**16** [b)]	490	0.30	−0.12	[50]
(*L*)-**17** [c)]	416	NR	−0.016	[51]
(*L*,+)-**18** [d)]	487	0.80	−0.05	[52]
(*R*,*R*)-**19** [e)]	505	0.95	−0.01	[53]
(*L*)-**20** [d)]	456	NR	+0.05	[54]
(−)-**21** [f)]	400	NR	−0.37	[55]
(*R*)-**22** [b)]	630	0.58	-2.0×10^{-3}	[56]
(*R*)-**23** [b)]	476	0.28	NR	[57]
(*L*)-**24** [g)]	425	NR	−0.011	[58]
(−)-**25** [g)]	485	0.61	−0.03	[59]
(*M*)-**26** [b)]	495	0.85	$+6.2\times10^{-3}$	[60]

a) NR = not reported; b) suspension in mixed solvents; c) as a fabricated micropattern; d) solid film; e) solid complexed with (*R*)-mandelic acid; f) as a dopant (3 wt%) in liquid crystalline 4-cyano-4′-*n*-pentylbiphenyl (5CB); g) measured in gelation state.

AIEgen, the polymer chains transformed into crystalline lamellae and meanwhile blue-emissive crystalline and yellow-emissive amorphous nano-aggregates were formed. Subsequently, white CPL with a g_{lum} of -2×10^{-3} was produced.

Chiral materials with multiple switchable emission states and high g_{lum} have attracted increasing attention due to their broad applications in diverse fields such as intelligent devices and sensors. Recently, a switchable CPL system **27** was presented by assembling a chiral rotaxane with achiral AIEgen 9,10-distyrylanthracene unit based on the controlled motions of the chiral pillar arene macrocycles along the axle by the addition or removal of the acetate anions (Figure 7c) [63]. As a result, two CPL emission states of the chiral [3]rotaxane **27** with g_{lum} values of $\pm1.36\times10^{-2}$ and $\pm2.14\times10^{-3}$ can be realized by adding or removing acetate anions. In addition to these applications, AIEgens have also been used to prepare CPL-active polymers [4,64,65], metal-organic frameworks (MOFs) [66], and thermally-activated delayed fluorescence (TADF) [67] materials, which will be further discussed in the following sections (Sections 2.5, 2.6, and 3.2).

2.3 CPL-active supramolecular assemblies

Developing excellent CPL-active materials with both high g_{lum} and Φ is of great significance [68,69]. With the rapid development of supramolecular chemistry in the past several decades, chiral supramolecular self-assemblies and co-assemblies have been assigned to be one of the most suitable and promising CPL-active materials [70–73]. These chiral self-assemblies and co-assemblies with designable microstructures could provide a powerful approach to precisely regulate the arrangement of building blocks and promote the amplified CPL signals during assembly process *via* non-covalent interactions (π-π stacking, hydrogen bonds, hydrophobic interactions, van der Waals interactions, and host-guest interactions) [10,14,43,74–79]. Several advantages of the supramolecular assemblies are provided. First, through the self-assembly, the luminophores and the chiral units can be combined together without tedious syntheses. Second, even for those of the molecules containing the luminophores and chiral units, it is not necessary to display CPL activity if the chiral centre is far from the luminophores or the chiral molecules are flexible. However, self-assembly can bring these molecules together to form diverse supramolecular aggregates or nanoarchitectures, in which the confinement of the molecules facilitates efficient chirality transfer and consequently makes the assemblies CPL-active. More importantly, the molecular rotation can be restricted and orderly arranged in supramolecular self-assembly, and thus the g_{lum} can be significantly boosted. Third, through the self-assem-

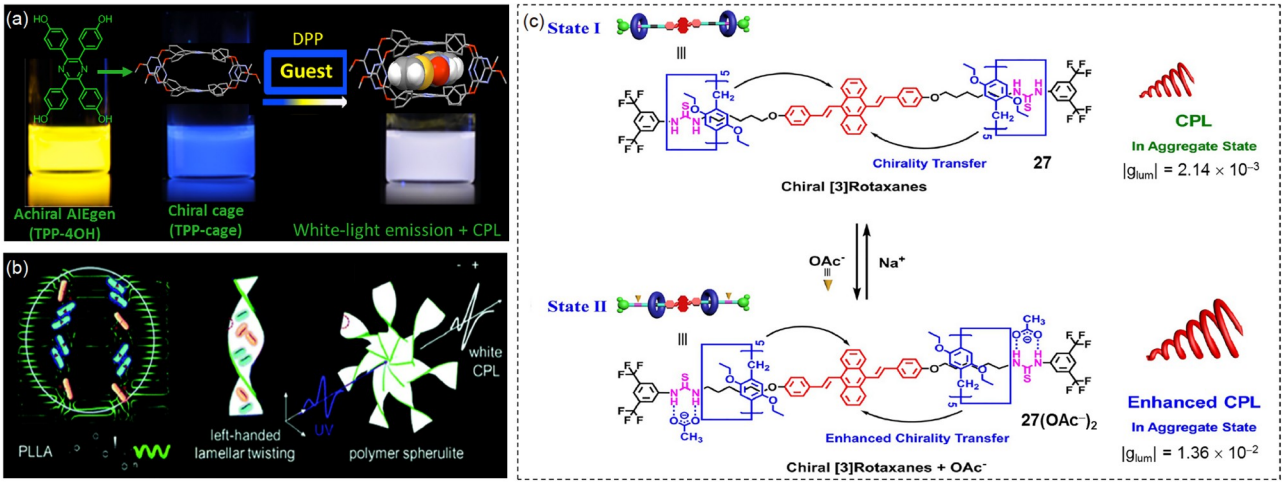

Figure 7 White light emissions from (a) host-guest supramolecular assembly [61] and (b) semi-crystalline polymer doped with AIEgen [62]. (c) Switchable CPL system based on AIE-active chiral [3]rotaxane with chirality transfer property [63] (color online).

bly, the system of single-component achiral molecules can generate CPL *via* symmetry breaking to form chiral supramolecular nanostructures. In addition, by the convenient regulation of the components, nanostructures, supramolecular and nanoscale chirality of the supramolecular systems, the tuning of CPL colour and sign can be handily realized in supramolecular assemblies. Following shows some examples to demonstrate how supramolecular self-assembly can regulate the CPL performance of small molecules.

2.3.1 Emergence of CPL from achiral luminophores assembled with chiral matrices

An important step in fabricating CPL active materials is the control of the coupling between the achiral luminophores and the chiral units. Such coupling can be easily realized through the self-assembly if the chiral unit is appropriately designed. For example, a general approach has been developed to evolve achiral luminophores into CPL active materials (Figure 8) [80]. A C_3-symmetric molecule **28** was found to form nanotube through an instant gelation method at room temperature [81]. The molecular chirality of the gelator controlled the handedness of the resulting nanotube. When achiral AIEgen molecules (TPE to BuCNS in Figure 8a) were doped into the helical nanotube, CPL can be generated. The emission colour follows that of the AIEgen, while the sign of the CPL signals follows the handedness of the nanotube. Similarly, Ihara *et al*. [82] reported the generation of CPL from a series of achiral dye molecules upon doping them into the chiral nanofibers self-assembled from enantiomeric *L*- or *D*-glutamides. Thus, either helical nanotube or fibre can serve as good matrix to induce the supramolecular chirality of achiral dyes and generate CPL activities. With such method, not only the emission colour but also the polarization direction of CPL can be controlled by the elegant combination of achiral dyes and chiral matrix. This approach is not only useful for one kind of dye but also for the mixed dyes, thus providing the possibility to produce white CPL materials by doping red/green/blue (RGB) dyes. For example, mixtures of achiral dyes (**D1**–**D4** in Figure 8b) have been doped into a nanohelix of **29** to afford white CPL materials [83]. Moreover, such method is also effective when achiral quantum dots (QDs) were doped into the chiral matrix. Various QDs have been doped into the chiral nanotube to obtain CPL based on QDs [84,85]. Recently, Lu *et al*. [86] have doped carbon dots into the chiral gel matrix and also obtained the coloured and white CPL hybrid materials.

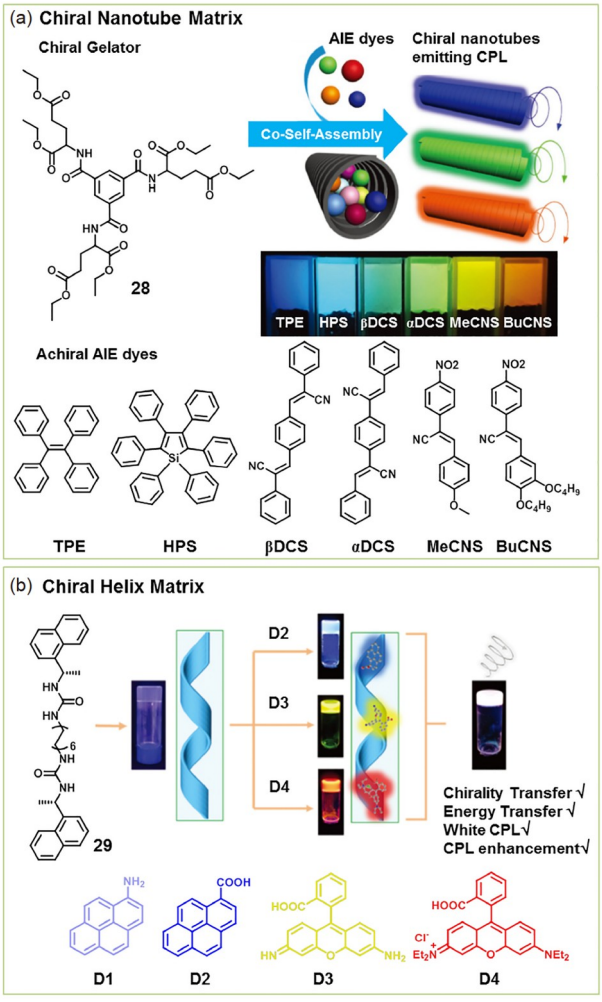

Figure 8 Emergence of CPL from achiral luminophores assembled with chiral (a) nanotube or (b) helix matrices [82,83] (color online).

2.3.2 Amplification of CPL through supramolecular self-assembly of chiral molecules

In order to increase the dissymmetry factors g_{lum} of the CPL materials, both the design of molecules and their assembly manner is vitally important. Liu and co-workers [87] have designed a series of symmetric and asymmetric chiral V-shaped pyrene derivatives by linking achiral pyrenes to chiral *trans*-1,2-cyclohexanediamine scaffolds with varied spacers and investigated the CPL in their assembles in comparison with the molecular states (Figure 9). The compounds were designed for three purposes. First, pyrene is one of the most important units showing excimer emission. Since CPL is connected with the chirality at the excited state, pyrene can be one of the best candidates. Second, the spacers between the chiral *trans*-1,2-cyclohexanediamine and the pyrene were changed to see the efficiency of their chirality transfer since the chiral unit lies at the diamine, while the pyrene is away from the chiral centre. The design of the spacers can help understand the chirality transfer in the assemblies. Third, V-shape molecules were designed to understand the packing effect on the producing of CPL. In true molecular solution, the symmetric V-shaped molecules (**30** and **31**) displayed spacer-dependent CD and CPL activities originating from the intramolecular excimers. Their g_{lum} is strongly dependent on the spacer length. In addition, for the asymmetric V-shaped molecule **32**, which has only one

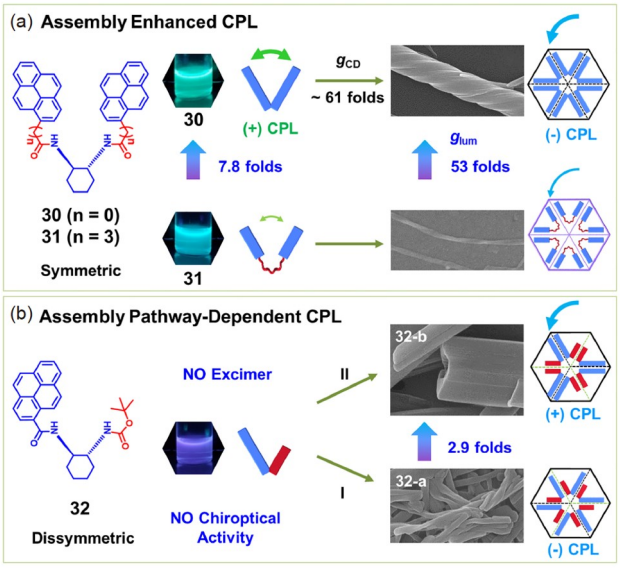

Figure 9 The amplification of CPL of chiral molecules through supramolecular self-assembly. (a) The symmetric molecules with different molecular rigidity showed assembly enhanced CPL performance. (b) The dissymmetric molecule displayed the assembly pathway-dependent CPL properties [87] (color online).

pyrene group, neither CD nor CPL signals could be detected. Upon self-assembly, the V-shaped molecules favoured a helical hexagonal packing and formed various kinds of chiral nanostructures. The compound without any spacer (**30**) formed superhelix, which exhibited the largest g_{abs} (3.59×10^{-2}) for pyrene derivatives to date. The assemblies from the rigid molecule **30** also showed the strongest g_{lum} (2.64×10^{-2}) in comparison with those from the molecules with a spacer. The asymmetric molecules formed two distinct hexagonal aggregates as twists and rectangular nanotubes due to the different packing modes. They all showed significantly enhanced g_{lum}. Through the self-assembly not only the inner rotation of the molecules will be limited, which will reduce the non-radiative transition, but also the intermolecular interaction can be enhanced. All these factors will contribute to the improvement of g_{lum}.

Besides the self-assembly of chiral molecules, the assistance of the achiral unit also plays an important role in developing the CPL materials with good performance. In 2018, Liu and co-workers [88] used the naphthalene-based backbone structure substituted with *L*-histidine moiety to form CPL-active organogel materials, and the CPL signals were efficiently enlarged *via* non-covalent interactions upon the addition of non-fluorescent achiral benzoic acids. Xing's group [89–93] prepared a series of novel CPL-active materials by evolving the molecular chirality to the supramolecular level or the macroscopic level through supramolecular self-assembly process. In 2021, they observed the universal existence of supramolecular tilt helical superstructures in self-assembled π-conjugated amino acid derivatives and unveiled the manipulation mechanism of CPL emission wavelengths and handedness based on charge-transfer complexation [93]. Recently, Duan's group [94] investigated CPL-active materials of the supramolecular self-assembled system ($g_{lum} = -1.1 \times 10^{-2}$, $\Phi_F = 0.80$) driven by arene-perfluoroarene interactions between chiral polycyclic aromatic hydrocarbons and octafluoronaphthalene. This kind of the highly ordered self-assembly can suppress the excimer formation and luminescence quenching, leading to chirality amplification not only in the excited state but also in the ground state. These studies provide excellent examples of the utility of noncovalent interactions on improving the supramolecular chiroptical properties.

2.3.3 CPL generated from symmetry breaking of supramolecular assemblies

Although most of the CPL materials are performed by chiral molecules, through self-assembly, it is also possible to obtain the CPL active supramolecular assemblies exclusively from achiral molecules. Liu's group [95] reported the first CPL active supramolecular gels from a simple achiral C_3-symmetric molecule. It was found that achiral tris(ethyl cinnamate) benzene-1,3,5-tricarboxamides can self-assemble into twist in a DMF/H_2O mixture (5/2, *v*:*v*). An intense CD and CPL could be observed although no chiral species was added. In particular, for the CPL performance, the g_{lum} can be as high as the order of 10^{-2}. Moreover, the g_{lum} can be enhanced simply by mechanical stirring. The generation of the CPL in such system is due to the symmetry breaking in the self-assembled gelation system. Later, several other systems showing the similar phenomenon are observed. Of course, in these systems, the polarization direction of the CPL cannot be determined, which is produced by chance. Even with the controlled stirring, no CPL with determined signs could be obtained.

Recently, Liu's group [96] developed a vortex mixing-accompanied self-assembly strategy and obtained near-unity homochiral entities with controlled handedness from achiral molecules. It was found that if vortex mixing is applied during the self-assembly, near-unity homochiral assemblies with uncontrolled handedness were obtained. Upon measuring the CD spectra, the sign of this batch of assemblies could be known. Then a small amount of the assemblies was added as chiral seeds into the racemic gels, the racemic gels turned into near-unity homochiral suspensions with controlled handedness *via* a ripening process. With such method, CPL with controlled sign can not only be produced but also amplified in co-assembled systems ($g_{lum} > 0.1$) as exemplified by the achiral C_3-symmetric molecule **33** (Figure 10a) [97].

A very interesting example of the CPL materials based on the biased symmetry breaking of self-assembly from achiral molecules was reported by Yang, Zhang and Luo *et al.*

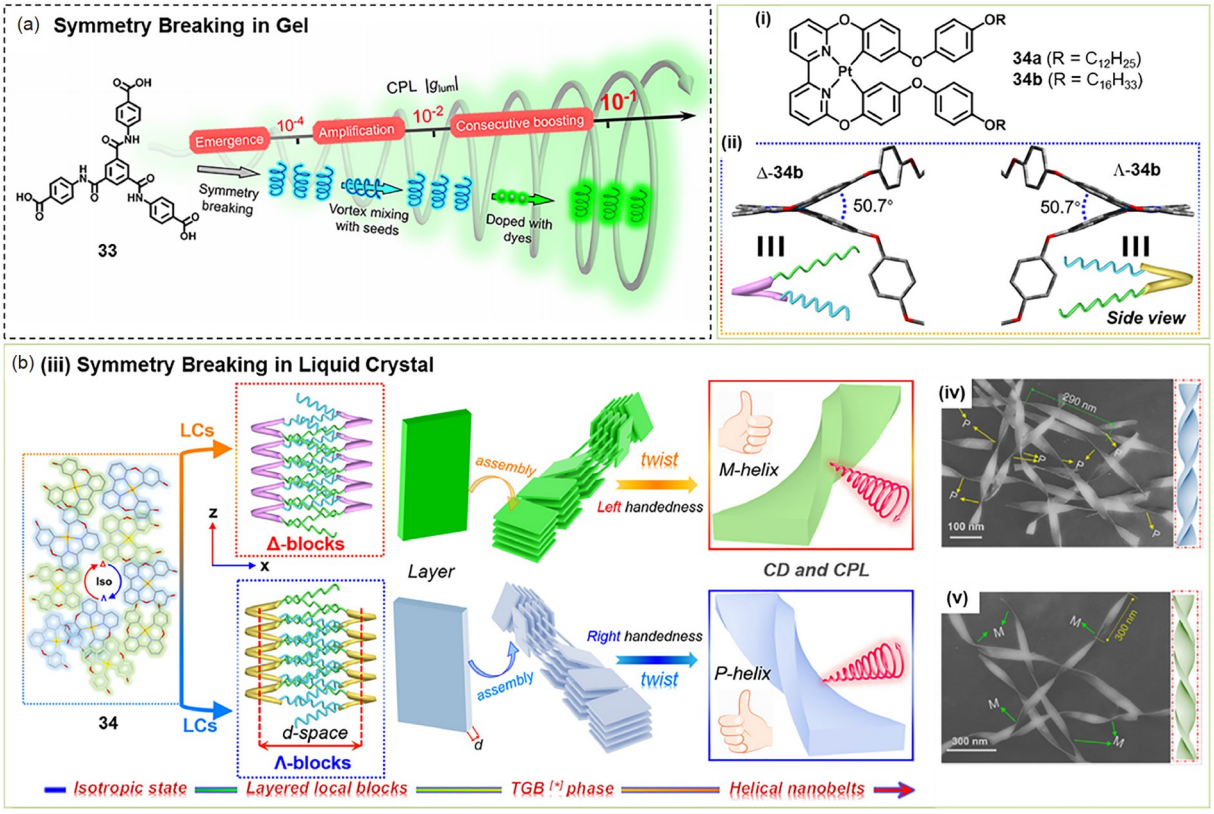

Figure 10 The symmetry breaking of achiral molecules displayed CPL activities in different supramolecular assemblies. (a) Symmetry breaking of **33** in organic gels [97]. (b) Symmetry breaking of **34** in liquid crystals. (i) Structures of **34a** and **34b**; (ii) stereochiral conformations of **34b**; (iii) schematic diagram of chiral self-organization by symmetry breaking of **34**; (iv, v) scanning electron microscopy (SEM) images of **34b** with *P*- or *M*-superhelix handedness [98] (color online).

(Figure 10b) [98]. They developed an achiral platinum (II) complex **34**, which could form LCs and self-organize into an enantiomerically enriched single domain without selection of handedness in twist grain boundary (TGB) phase. The chirality control can be achieved by using homochiral liquid crystal films with determined handedness as a template. Remarkably, the compound self-assembly into chiral twist in the liquid crystal phase and exhibit prominent CPL with higher g_{lum}.

2.3.4 *Sign inversion of CPL in supramolecular assemblies*

The sign of CPL is an important issue in the CPL active materials. In most cases, the sign is determined by the molecular chirality of the component molecules. However, in some cases, it can be tuned by external stimuli in supramolecular system. For example, Liu and co-workers [99] have developed a cinnamic acid conjugated glutamide **35**, which can self-assembly into nanofiber structures in MeOH, THF, and DMF (Figure 11a). The *L*-enantiomer self-assembled into left-handed nanohelix, while *D*-enantiomer formed right-handed nanohelix in DMF and THF. In methanol, the left-handed superhelices could be switched into nanokebabs with opposite helicity upon UV irradiation. The chiral nanostructures could serve as a template to generate the CPL upon doping luminescent dye molecules. It was found that the CPL of dye/nanohelix assemblies followed the helicity of

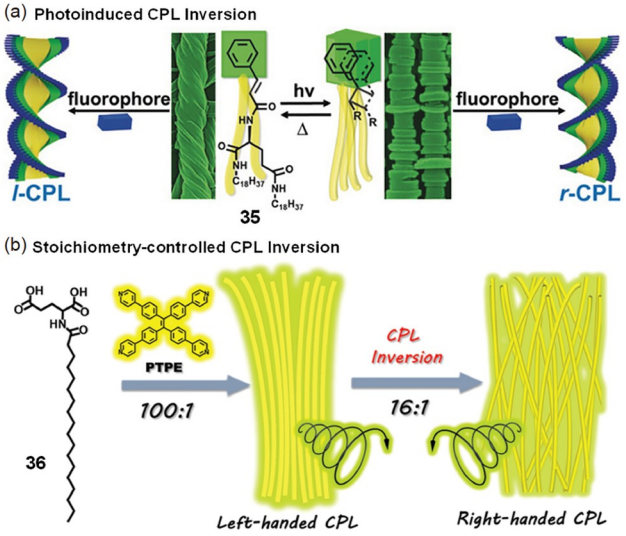

Figure 11 Sign inversion of CPL in supramolecular assemblies. (a) Photoinduced the chirality of supramolecular nanostructures enabled the induced CPL sign inversion of the achiral luminophore [99]. (b) Stoichiometry-controlled CPL sign inversion of the supramolecular co-gel of achiral AIEgen and chiral gelator [100] (color online).

the chiral nanostructure rather than the inherent molecular chirality. Thus, through simple solvent regulation and UV-irradiation, CPL with opposite sign can be obtained, while the molecular chirality was not changed.

Yin and Liu *et al*. [100] have also showed an opposite CPL using the combination of chiral gelator and achiral luminophore (Figure 11b). It was found that in a two-component supramolecular gel composed of a chiral amphiphilic *D*-glutamic acid gelator (**36**) and an achiral AIEgen (pyridine-functionalized tetraphenylethylene, PTPE), the produced co-gel could show opposite CD and CPL depending on the mixing ratios of **36** to PTPE. At PTPE/**36** = 1:16, a negative Cotton effect and R-CPL signal are obtained, while it changed into the opposite one when PTPE/**36** = 1:100. It was suggested that a delicate balance between the different types of hydrogen bonding interactions and different molecular packing modes was responsible for the sign inversion of the supramolecular chirality and CPL.

2.4 CPL-active liquid crystals and liquids

Liquid crystals (LCs), as the specific intermediate phase state between solid crystal and isotropic fluid, have been assigned to be one of the most important soft materials and widely applied for both optoelectronic and biological areas. In the above section, symmetry breaking properties of liquid crystal **34** have been discussed (Figure 10b). In the past several years, there have been more and more reports on chiral emissive liquid crystals (N*-LCs) as CPL-active materials. These materials can self-assemble as highly regular helical arrangement in LC medium after annealing treatment as a result of the LC-templated molecular reorientation, which is beneficial for the enlarged effect of the induced CPL signals [101–107]. In 2020, Cheng's group [101] realized the recyclable CPL response behavior in N*-LCs doped with the axially chiral molecules (*R*/*S*)-**37** (Figure 12a). The obvious texture change from the planar texture into focal conic texture, and then the uniformly-lying helical texture (ULH state) could be observed by using the applied direct current electric field with electric phase transition effect. This work could provide a novel strategy for developing the CPL devices on N*-LCs through the applied DC electric field. In 2021, Cheng's group [102] also achieved the standard white-light-emitting N*-LCs by the co-assembly of the color-matched blue and red emissive chiral naphthalimide dyes at the appropriate ratio. In 2020, Akagi's group [103] fabricated a photoinvertible N*-LCs by adding the photoconductive chiral compounds (*R*/*S*-**38**) as a chiral dopant into liquid crystal 5CB (Figure 12b). The resulting N*-LCs could not only exhibit the reversible chirality photoinversion by virtue of photoisomerization between the open and closed forms of **38** (**38(o)** and **38(c)**), but also high fatigue resistance upon UV and visible light irradiation. Interestingly, this kind of

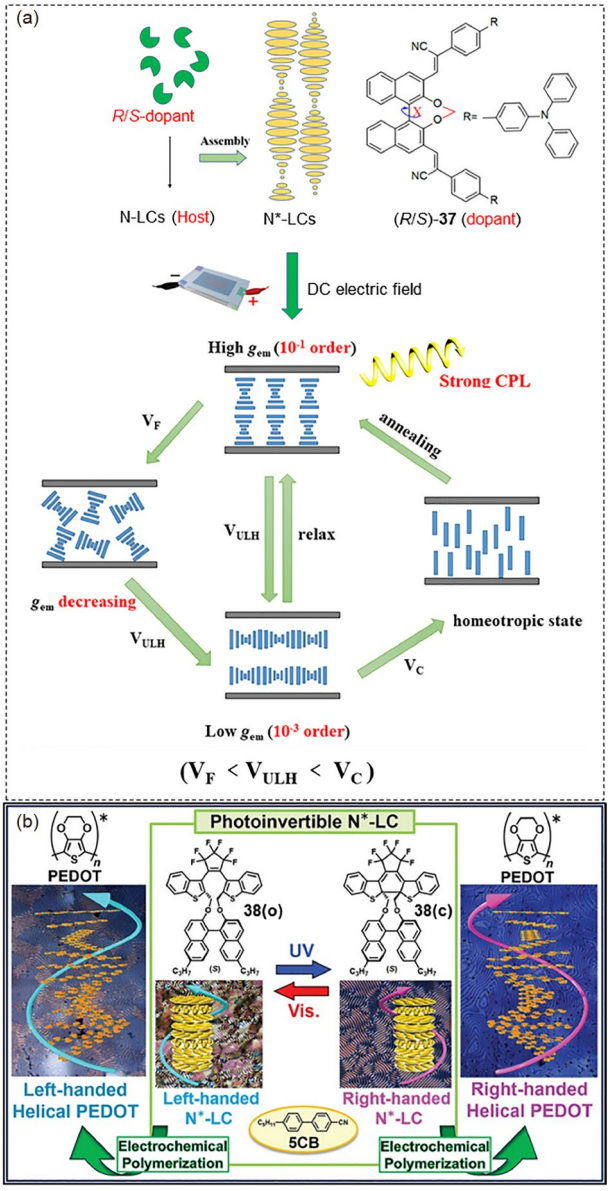

Figure 12 (a) The CPL device on N*-LCs doped with **37** through the applied DC electric field [101]. (b) Photoinvertible N*-LCs with different CPL signals induced by the photoisomerization of chiral **38** [103] (color online).

N*-LC could serve as an asymmetric media for electrochemical polymerization and control the dynamic helicity of the conjugated polymers. In addition to these advances, LCs have also been used to fabricate other CPL-active aggregate materials, which will be further discussed in Sections 2.5, 2.8, and 2.9.

Compared with CPL-active LCs, liquid materials with CPL have rarely been reported. Recently, Liu *et al*. [71] studied the influence of the position of the alkyl chain substituents on the CPL behavior of chiral naphthalene derivatives **Nap1**–**Nap4** as solvent-free chiral organic π-liquids (Figure 13). Among them, **Nap4** is an emissive solid; while **Nap1**–**Nap3** are organic liquids, in which 2,3-subsituted

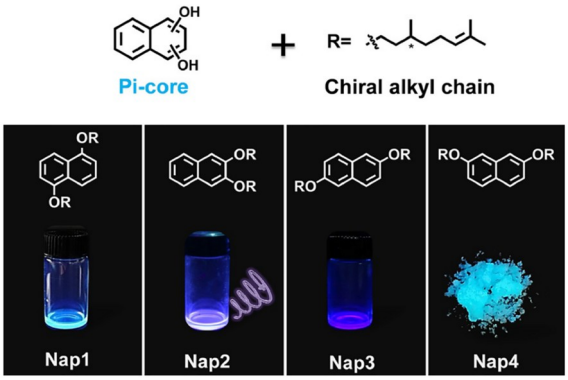

Figure 13 Chemical structures and fluorescent images of **Nap1**–**Nap4** under UV light (365 nm) [71] (color online).

Nap2 shows distinct CPL activity. When achiral anthracene or pyrene was dissolved in chiral **Nap2** liquid, this kind of π-liquids could act as chiral inducer and energy transfer media. The g_{lum} value could be enlarged up to 5.2×10^{-2} which was nearly two orders of magnitude higher than that of the pure **Nap2** π-liquids.

2.5 CPL-active polymers

Polymer-based CPL-active materials have attracted ever-increasing interest, partially due to the merits of high stablity and good processability of polymers. According to the different combination modes of chirality and fluorescence, CPL-active polymeric materials are generally prepared by two strategies: (1) covalent bonding method, in which chiral component and fluorescent component can be chemically bonded at different locations in polymer chains (polymer backbones and/or pendants); and (2) physical blending method, in which chirality transfer can be realized through non-covalent interactions of chiral and fluorescent components or by taking chiral polymers as CPL filters without any non-covalent interactions.

2.5.1 Constructing CPL-active polymers via covalently bonding

Covalently bonding chiral component and fluorescent component in polymer main-chains is an effective strategy for constructing CPL-active polymeric materials, in which chiral and fluorescent components generally possess two or more reaction sites [108,109]. For example, Cheng and co-workers [110,111] reported a series of CPL-active chiral fluorescent conjugated polymers with BINOL units in the main chain. Besides, since the concept of AIE was first proposed by Tang's team [112] in 2001, introducing AIE-active groups into chiral polymers for constructing CPL polymers with high solid-state luminescence efficiency has aroused wide interest. The as-obtained polymers often show no or weak fluorescence emission in solution, but can exhibit strong fluorescence and CPL after forming aggregates [113–116]. Cheng, Zhu and co-workers [117] used Sonogashira coupling reaction to synthesize chiral conjugated polymer **39** with binaphthyl and TPE units in the main-chain, and the resulting polymer exhibits remarkable CPL after aggregating into helical nanofibers (Figure 14a).

Copolymerization of chiral and fluorescent monomers can lead to CPL-active polymers with chiral component and fluorescent component both bonded in pendant chains. Deng and co-workers [118] prepared a series of fluorescent chiral helical monosubstituted polyacetylenes **40** by copolymerizing an achiral fluorescent acetylenic monomer and a chiral monomer (Figure 14b). The presence of helical chirality in

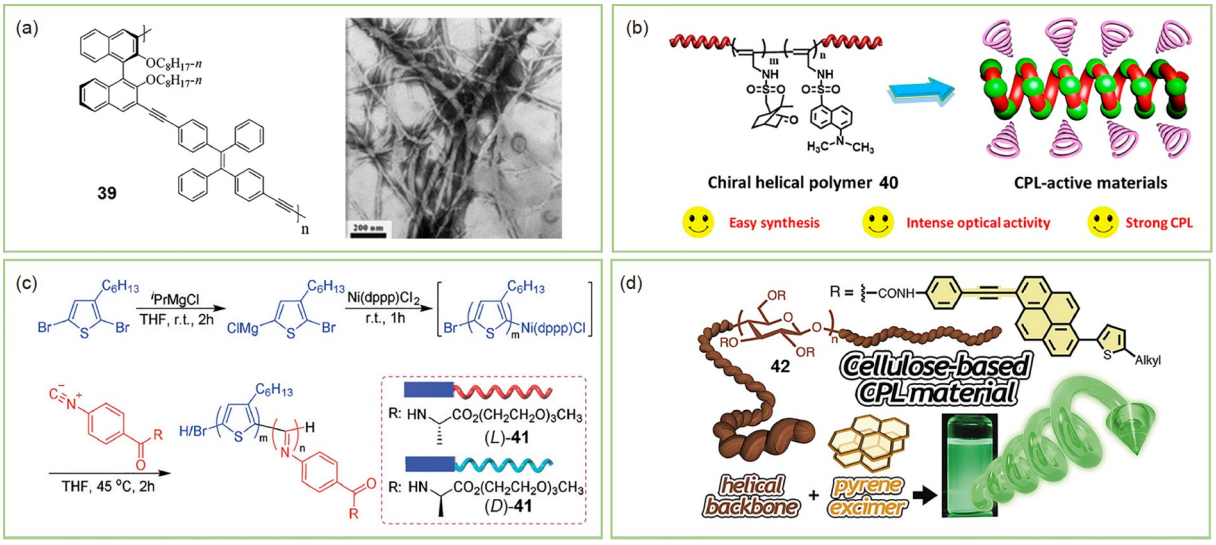

Figure 14 (a) Structure of chiral conjugated polymer **39** with binaphthyl and TPE units in the main-chain and its aggregate structure [117]. (b) Schematic illustration for preparing CPL-active fluorescent chiral helical monosubstituted polyacetylenes [118]. (c) Synthesis routine of P3HT-*b*-PPI copolymers [126]. (d) Schematic illustration for preparing cellulose-based CPL material [127] (color online).

polymer backbones facilitates the polymers to show intense CPL with the highest g_{lum} of +0.136 and –0.264. Following the same idea, Zhao and Deng *et al*. [64] further achieved CPLs in chiral helical substituted polyacetylenes bearing TPE pendants. More recently, the same group [119] reported pyrene-functionalized chiral helical polyacetylenes, in which handedness inversion and amplification of CPL were simultaneously realized in helical polymer systems. The studies demonstrate that helical polymers offer one of the competent candidates for constructing CPL materials with high g_{lum} value.

CPL polymers can also be constructed *via* introducing chiral factors into the side chains of fluorescent conjugated polymers, such as polysilane [120], polyquinoxaline [121], polyfluorene [122], polyisocyanide [123], polytriazole [65], polythiophene [124], and polycarbazole [125]. For example, Wu and co-workers [126] synthesized amphiphilic poly(3-hexylthiophene)-block-poly(phenyl isocyanide)s (P3HT-*b*-PPI) copolymers **41**, which further self-assembled into single-handed helical nanofibers (Figure 14c). By adjusting the proportion of the main-chain components and the solvent ratio, the authors realized white-light CPL with $|g_{lum}|$ of 3.7×10^{-3}.

Besides synthetic polymers, natural bio-molecules such as cellulose are good candidates for constructing CPL materials because of the advantages of low cost, abundant sources and in particular multilevel chirality. By introducing pyrene group onto microcrystalline cellulose, Ikai *et al*. [127] prepared CPL-active cellulose derivatives **42** with maximum g_{lum} of 3.0×10^{-3} (Figure 14d). In other studies, taking *D*-glucose as chiral pendants, Ikai *et al*. [128–130] have prepared a series of CPL-active π-conjugated polymers. Nowadays, biobased CPL materials are mostly realized by physical blends through non-covalent interactions or circular polarization reflection, as to be introduced in more detail below.

2.5.2 Constructing CPL-active polymers via physically blending

Chirality transfer through covalent bonds usually needs tedious synthesis routes which are disadvantageous for industrialization and practical applications. To address this issue, physically mixing chiral component and fluorescent component for constructing CPL-active polymers provides an effective alternative. Using chiral polymers as a template for co-assembly with fluorescent components *via* non-covalent interactions has proved to be powerful and promising towards CPL emission [131–133]. For instance, Lu and co-workers [134] fabricated solid CPL materials through co-assembly of achiral fluorescent molecules and chiral block copolymer (Figure 15a). The g_{lum} values of the fabricated materials were as high as 2.3×10^{-2}. In this case, biopolymers also can be used as chiral templates [135]. Based on intermolecular interactions, Fujiki *et al*. [136] achieved chirality induction and CPL from racemic polyfluorene using cellulose derivatives as template. Some studies have further demonstrated that CPL-active hybrids can be fabricated when luminescent metal ions are coordinated with chiral polymers [137–140].

CPL-active polymers have been constructed through intermolecular interactions of chiral small molecules and racemic fluorescent polymers [141–145]. Maeda *et al*. [146] prepared optically active and CPL-active poly(diphenylacetylene) by helix-sense-selective synthesis using chiral amines as inducers (Figure 15b). Nowadays, chiral induction for preparing CPL materials is mainly limited to post-induction method from racemic conjugated fluorescent polymers. In theory, CPL can be realized directly through helix-sense-selective polymerization (HSSP) of achiral fluorescent monomers; if so, the studies along the direction will certainly promote further development of CPL materials.

Inspired by the circularly polarized reflection in nature and living organisms involving the formation of self-organizing chiral nematic photonic structures [147–149], CPL-active polymers were prepared by taking chiral LCs and crystalline polymers as CPL filters [150–155]. In these systems, inter- and intra-molecular interactions between chiral and fluorescent substances are no longer indispensable, and the obtained materials generally possess high g_{lum} values. Akagi *et al*. [156] realized dynamic switching CPLs with the highest g_{lum} values of −1.79 and +1.77 by combining a CPL-emitting disubstituted liquid-crystalline polyacetylene and thermotropic chiral nematic liquid crystal. Recently, Cheng, Zhu, Tang and co-workers [157] reported full-color CPLs by incorporating various AIEgens into a polylactide based crystalline chiral polymer film. The handedness and magnitude of CPL could be tuned by simple film tilting, demonstrating a maximum $|g_{lum}|$ of 10^{-2}.

Natural bio-architectures such as cellulose nanocrystals can self-assemble into chiral LCs for preparing CPL materials. Zhang and Xu *et al*. [158] synthesized left-handed chiral photonic cellulose films through evaporation-induced self-assembly process. By incorporating achiral luminophores into the photonic cellulose films and precisely regulating the photonic bandgaps, multicolor CPL materials with high g_{lum} values were fabricated (Figure 15c). Owing to the merits of low-cost, easy preparation, low toxicity, and good product performance, cellulose crystal films have become a versatile platform for exploring multifarious CPLs through combination with a variety of luminophores [159–162].

Synthetic non-crystalline polymers may serve as chiral filters for CPL generation. Deng and co-workers [163] have proposed a “Matching Rule” for constructing CPL materials, in which CPL can be generated in the overlapping area of CD spectra and PL spectra even without any interaction between

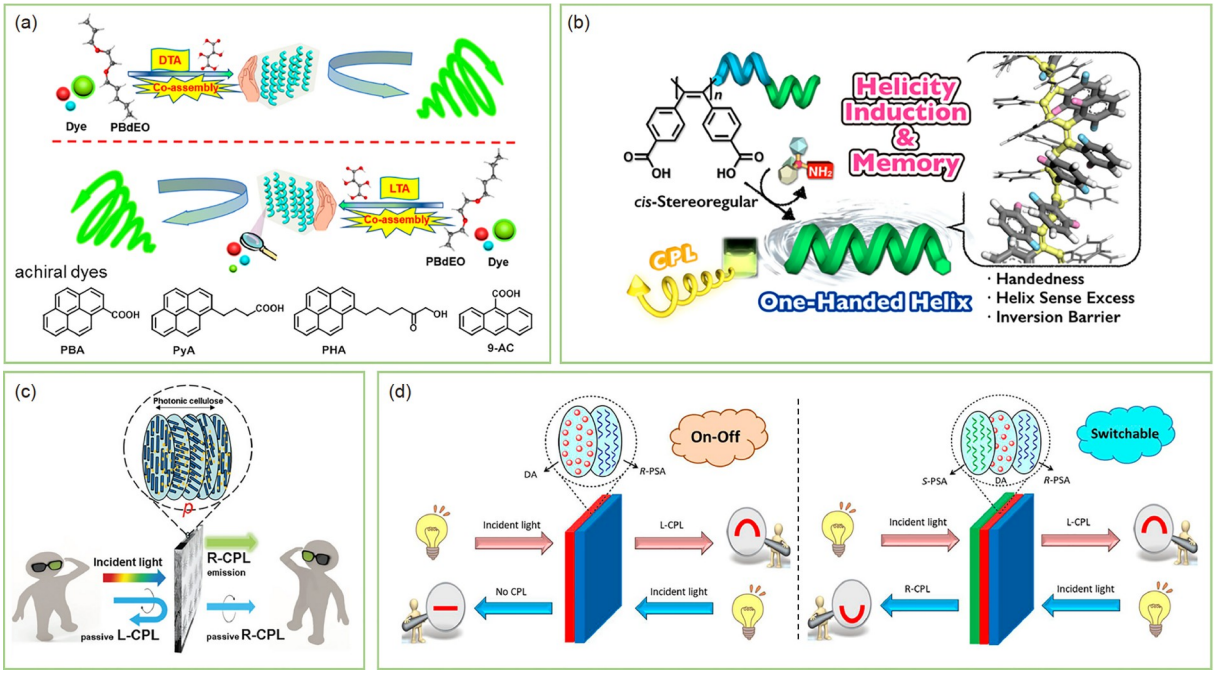

Figure 15 (a) Scheme of co-assembly of achiral fluorescent molecules using chiral block copolymer as a template [134]. (b) Schematic illustration for helix-sense-selective synthesis of CPL-active poly(diphenylacetylene)s [146]. (c) Illustration of the intrinsic CPL ability of chiral photonic cellulose films [158]. (d) Schematic illustration for preparing "on-off" and switchable CPL by taking chiral helical polyacetylenes as CPL filters [163] (color online).

chiral component and fluorescent component. Following this idea, "on-off" and switchable CPL devices have been easily realized by taking chiral helical polyacetylenes as CPL filter with high g_{lum} up to 10^{-1} (Figure 15d). Moreover, Zhao *et al.* [164–166] and Ma *et al.* [167] have further demonstrated the "Matching Rule" is potentially applicable to numerous chiral matters and achiral fluorophores, clearly confirming the wide universality and superiority of the strategy.

Although striking advancements have been and are being achieved continuously, the development of polymer-based CPL materials is still at the infant state. More efforts are still required to construct high-performance CPL-active chiral polymers with large g_{lum} values and high luminescence efficiency, for which chiral helical polymers seem to be good candidates due to "chiral amplification" effect. Besides, the essential mechanism of CPL generation is still open to discussion. In particular, only sporadic examples concerning the application of polymer-based CPL materials have been reported so far [168–170]; and so how to promote their practical applications is of significant importance and needs more efforts.

2.6 CPL-active metal-ligand coordination materials

The exploitation of CPL-active metal-ligand coordination materials, including discrete small-molecular metal complexes, metal-organic coordination polymers (MOPs), and MOFs, has received increasing attention in view of their diverse coordination modes, rich metal-involving excited states, high Φ and g_{lum} values, as well as potential applications in optoelectronic devices and cell imaging [9,12,20,171].

2.6.1 *CPL-active small molecular metal complexes*

The majority of CPL-active coordination materials reported to date are discrete small metal complexes benefited from their explicit molecular structures and tunable luminescence [9,171]. In the early stage, researches in this area mainly focused on chiral lanthanide (Ln) complexes due to their generally high $|g_{lum}|$ originating from the magnetic dipole-allowed and electronic dipole-forbidden Ln-centered f-f transitions. Up to now, the highest $|g_{lum}|$ value of 1.38 has been achieved by complex Cs[Eu(+)-(hfbc)$_4$] (hfbc = 3-heptafluoro-butylryl-(+)-camphorato) [172]. Unfortunately, these Ln complexes usually have low Φ due to their low molar absorptivity of Ln-centered f-f transitions. In order to enhance the emission efficiency, a classical strategy is introducing organic chromophores as light-harvesting antennas into these complexes. Nevertheless, how to effectively obtain Ln complexes with strong CPL still remains a question [171,173].

Recently, Di Bari [174,175], Yan [176,177], Law [178,179], and Sun [180] have made impressive progress in the exploration of CPL-active Ln complexes (Figure 16 and Table 3). Using diketonate as an efficient antenna, Di Bari and co-workers [174] prepared in 2019 a pair of the CPL-active Yb diketonate complex (*R*,*R*/*S*,*S*)-**43** with a chiral pyridine bisoxazoline as the chiral inducer, which displayed

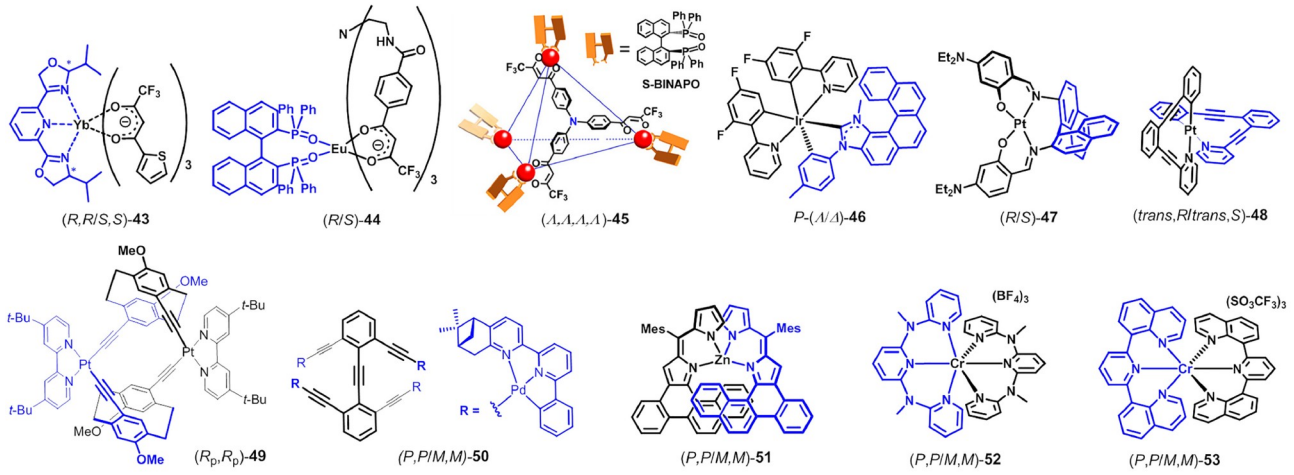

Figure 16 CPL-active discrete chiral metal complexes (color online).

Table 3 CPL parameters of coordination materials [a)]

Material	λ_{em} (nm)	Φ	g_{lum}	Ref.
(*S*,*S*)-**43**	972	0.69	+0.029	[174]
(*R*)-**44**	593/611	0.32	+0.072/−5.0 × 10^{-3}	[176]
(*Λ*,*Λ*,*Λ*,*Λ*)-**45**	592/612	0.81	−0.204/+8.0 × 10^{-3}	[177]
(*P*,*Λ*$_{Ir}$)-**46**	530	0.13	+3.7 × 10^{-3}	[182]
(*P*,*Δ*$_{Ir}$)-**46**	530	0.13	+1.5 × 10^{-3}	[182]
(*R*)-**47**[b)]	655	0.05	+3.0 × 10^{-3}	[184]
(*trans*,*R*)-**48**	519	0.07	−1 × 10^{-3}	[186]
(R_p,R_p)-**49**	656	0.1	+1 × 10^{-3}	[187]
(*M*,*M*)-**50**	640	0.40	+2 × 10^{-3}	[188]
(*M*,*M*)-**51**	660	0.23	+0.022	[189]
(*M*,*M*)-**52**	775	0.031	−0.093	[192]
(*M*,*M*)-**53**	728/749	0.052	+0.1/−0.2	[193]

a) Measured in diluted solution unless other noted; b) measured in solid film state.

near-infrared (NIR) CPL with Φ of 0.62%–0.69% and $|g_{lum}|$ of 0.025–0.029 at 972 nm associated with the Yb(III) $^2F_{5/2}\rightarrow{}^2F_{7/2}$ transition in CH_2Cl_2. Yan and co-workers reported a pair of homochiral Eu diketonate complexes (*R*/*S*)-**44** consisting of an achiral tris[4-(4,4,4-trifluoro-1,3-dioxobutyl)-benzamidoethylamine] (TTEA) and a chiral ancillary ligand of 2,2′-bis-(diphenylphosphoryl)-1,1′-binaphthyl (BINAPO). These triple-helical podates exhibited intense CPL with a total Φ of 32% and $|g_{lum}|$ of 0.072 at 593 nm originating from the Eu(III) $^5D_0\rightarrow{}^7F_1$ transitions in $CHCl_3$ [176]. Subsequently, when the TTEA ligand of **44** was replaced by another C_3-symmeric achiral ligand 4,4′,4″-tris-(4,4,4-trifluoro-1,3-dioxobutyl)-triphenylamine, the enantiopure tetrahedral Eu cage **45** was fabricated by the same group [177]. This chiral cage displayed stronger CPL with $|g_{lum}|$ of 0.20 at 592 nm and a high Φ of 81% in $CHCl_3$, representing one of the best results reported for CPL-active chiral Ln complexes.

In comparison with Ln complexes, other transition metal complexes are typically characterized by a high Φ, more stable molecular structures and tunable luminescence. Therefore, various CPL-active transition metal complexes have been designed in the past few years, mainly including octahedral Ir(III) and square planar Pt(II) complexes [9,12,20,171]. For instance, Crassous and co-workers [181–183] reported in 2017 a series of CPL-active stereoisomeric organometallic helicenes, including a pair of enantiomeric [5]helicene Ir complexes *P*-(Λ/Δ)-**46** with g_{lum} of +0.0015–+0.0037 at 530 nm and Φ_P of 9%–13% in CH_2Cl_2. The CPL sign was found to be dominated by the helical carbene ligand. Xiang and co-workers [184,185] have synthesized a series of enantiopure mono-/binuclear Pt(II) complexes with an axially chiral binaphthyl linker, *e.g.*, (*R*/*S*)-**47**, and these complexes showed unusual aggregated-induced NIR CPL at 650–680 nm with moderate $|g_{lum}|$ of 0.003–0.01 yet low Φ_P (≤5%). Clever and co-workers [186] have prepared two en-

antiomeric Pt(II) complexes (*trans*,*R*/*trans*,*S*)-**48** with a chiral metal center through the coordination of two achiral bidentate ligands and the Pt ion, showing CPL with Φ_P of 7% and $|g_{lum}|$ of about 10^{-3} in CH_2Cl_2. In addition, another weakly CPL-active di-Pt(II) helicate **49** (Φ < 1% , $|g_{lum}|$ = 10^{-3}) containing two planar chiral [2.2]paracyclophane ligands has been reported [187]. More recently, Lu and co-workers [188] prepared a pair of chiral tetranuclear Pd(II) arylacetylide helicates (*P*,*P*/*M*,*M*)-**50**. These enantiomers showed intense CPL at 647 nm with Φ of up to 50% and $|g_{lum}|$ of 10^{-3} originating from the triplet metal–metal-to-ligand charge-transfer (^{3}MMLCT) excited states in CH_2Cl_2, representing the first CPL-active molecular Pd(II) complexes.

Apart from the aforementioned chiral Ir(III), Pt(II) and Pd(II) complexes, a few of CPL-active Zn(II) complexes have been reported [189–191]. One representative sample is molecular helicates (*P*,*P*/*M*,*M*)-**51** reported by Hasobe and co-workers [189] in 2018, which display intense NIR CPL at 700–850 nm with Φ of 23% and $|g_{lum}|$ of 0.022 in toluene. Theoretical calculations revealed that this large $|g_{lum}|$ benefited from the formation of exciplex between two dipyrromethene ligands. Additionally, enantiomeric octahedral Cr(III) complexes comprising two six-membered tridentate ligands represent another new emerging CPL-active materials. These enantiomers usually display relative high $|g_{lum}|$ (≥ 0.05) because their CPLs originating from characteristic metal-centered spin-flip $^2E/^2T_1 \rightarrow {}^4A_2$ transitions of the Cr(III) ion [192–194]. For example, Seitz and co-workers [192] have resolved in 2019 two enantiomers (*P*,*P*/*M*,*M*)-**52** from corresponding racemic Cr(III) complex through chiral high performance liquid chromatography (HPLC). Spectral experiments revealed that enantiomers (*P*,*P*/*M*,*M*)-**52** displayed acceptable NIR CPL with Φ of 3.1% in oxygen-saturated water (30% in deoxygenated CD_3CN) and $|g_{lum}|$ of 0.093 at 775 nm in D_2O. Piguet and co-workers prepared another two enantiomeric Cr(III) complexes (*P*,*P*/*M*,*M*)-**53**, showing excellent NIR CPLs with total Φ of 5.2% and $|g_{lum}|$ of 0.2 at 749 nm ($^2E \rightarrow {}^4A_2$ transition) [193]. Subsequently, a series of similar enantiomeric Cr(III) complexes decorated with different substituents were fabricated by the same group, with the best CPL with a Φ up to 17% and $|g_{lum}|$ of 0.2 in H_2O being achieved [194]. Thus, the high $|g_{lum}|$ values of chiral Cr(III) complexes are comparable to those of Ln complexes ever reported. Furthermore, other CPL-active metal complexes, *e.g.*, chiral Cu(I) complex (Φ = 1.8%, $|g_{lum}|$ = 0.0012) [195] and Al(III) complex (Φ = 54%, $|g_{lum}|$ = 10^{-3}) [196] have also been reported.

2.6.2 *Molecular assemblies of transition metal complexes*

As has been discussed in the previous sections of organic chromophores (Sections 2.2 and 2.3), supramolecular assembly was an effective method to enhance the CPLs of chromophores. This also applies to chiral metal complexes, in particular square planar Pt(II) complexes with the tendency to form ordered aggregates due to rich Pt/Pt and π/π intermolecular interactions (Figure 17) [12,197,198]. For instance, Haino and co-workers [199] reported in 2018 the gel materials in decanol of the chiral Pt(II) complex (*S*)-**54**, which showed strong aggregation-enhanced emission (AEE) CPL with the maximum g_{lum} of +0.011 (Figure 17a). Based on the single enantiomer of the chiral Pt(II) complex (*R*)-**55**, single-component assemblies with an opposite helical chirality were demonstrated by Zhong and co-workers [200] to exhibit yellow (Φ = 33%–36%, $|g_{lum}|$ = 0.022 at 555 nm) and red (Φ = 25%–27%, $|g_{lum}|$ = 0.027 at 660 nm) AEE CPL, respectively (Figure 17b). Luo and co-workers [201] reported in 2020 the CPL-active liquid crystalline materials based on the chiral Pt(II) complexes (*R*,*S*)-**56** *via* straightforward self-assembly. In the high-temperature $S_mC_h^*$ phase, enhanced CPL (Φ = 46%) with a high $|g_{lum}|$ value of 0.04 was detected, induced by effective chirality transfer from the molecule to the liquid crystal assemblies (Figure 17c).

Furthermore, CPL-active two-component co-assemblies were prepared by doping achiral aggregates with a chiral emitter or by doping helical assemblies with an achiral emitter. For example, in 2019 You and co-workers [202] reported the CPL-active co-assemblies consisting of the achiral Pt(II) complex **57** and a small fraction of the chiral Pt(II) complexes (*R*,*S*)-**58**, which displayed enhanced $|g_{lum}|$ of 0.05–0.064 (Figure 17d). Tang and co-workers [203] constructed helical structures *via* the hierarchical self-assembly of the chiral di-Au(I) complexes (*R*,*S*)-**59**, which served as the chiral templates to co-assemble with other achiral dyes, *e.g.*, 9,10-bis(phenylethynyl)anthracene (BPEA) and TPE, to realize CPL-active coassemblies with $|g_{lum}|$ of 0.001–0.005 (Figure 17e).

2.6.3 *CPL-active coordination polymers and frameworks*

Besides discrete small-molecular complexes and assemblies, an increasing number of CPL-active MOPs have been fabricated recently (Figure 18) [140,204–206]. In 2018, Hasegawa and co-workers [140] prepared the spiral-type chiral Eu(III) MOPs (+/−)-**60**, which displayed stronger CPLs with Φ of 57% and $|g_{lum}|$ of 0.17 at 586 nm in comparison with those of the mononuclear chiral Eu(III) complex (Eu(+/-tfac)$_3$-(tppo)$_2$; Φ of 36%; $|g_{lum}|$ of 0.09 at 586 nm) (Figure 18a). Cheng and co-workers [204] have recently fabricated a pair of the binaphthyl-based dipyrrin zinc(II) chiral MOPs (+/−)-**61**. Enhanced CPLs of (+/−)-**61** with Φ of 39% and $|g_{lum}|$ of 0.009 at 560 nm were demonstrated compared with those of corresponding chiral monomers (Φ =30%, $|g_{lum}|$ = 0.002 at 570 nm) (Figure 18b).

CPL-active MOFs are promising functional materials in light of their potential applications in enantiomeric separation, chiral sensors, and asymmetric catalysis [207–211]. In the past few years, two kinds of CPL-active MOFs have been

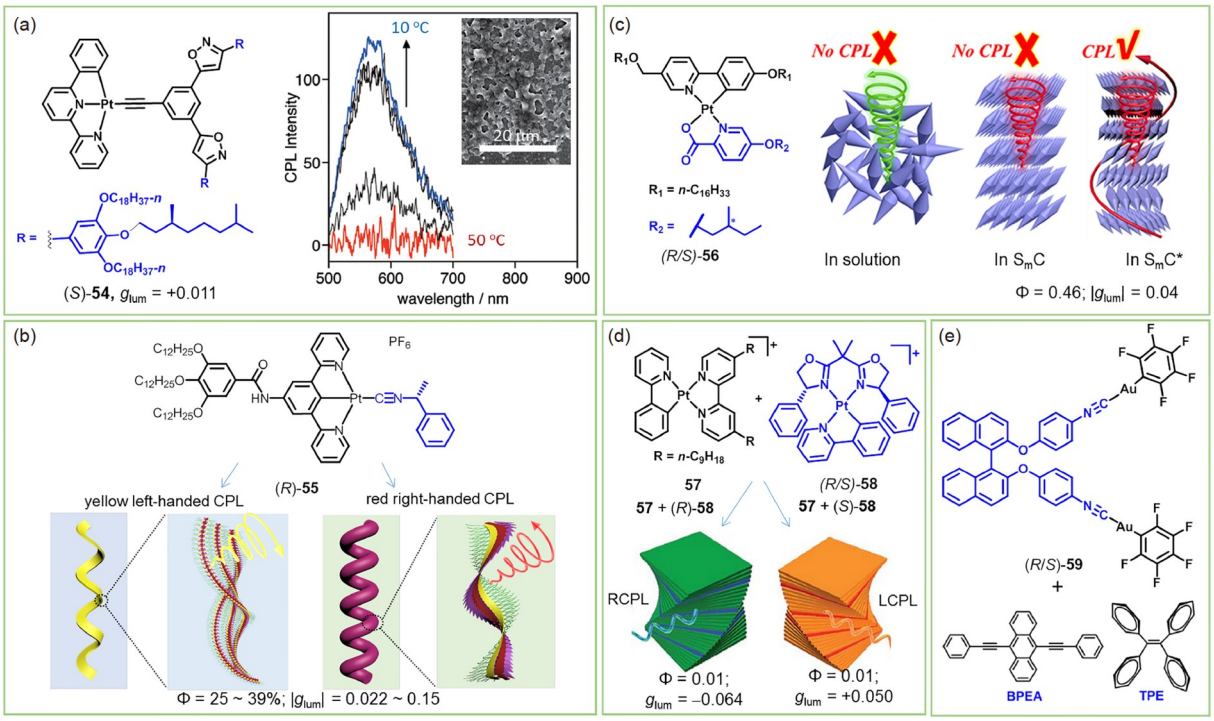

Figure 17 (a) Chiral Pt complex (*S*)-**54** and the CPL spectral changes of the gel of (*S*)-**54** in 1-decanol upon cooling from 50 to 10 °C. Inset shows the SEM picture of the gel of (*S*)-**54** in 1-decanol [199]. (b) Chiral Pt complex (*R*)-**55** and the schematic representation of the chirality-inversed assembly [200]. (c) Chiral Pt complexes (*R*/*S*)-**56** and the CPL properties in different states [201]. (d) Schematic representation of the co-assembly of **57** with (*R*)- or (*S*)-**58** [202]. (e) Chiral gold(I) complexes (*R*/*S*)-**59** and AIEgens BPEA and TPE [203] (color online).

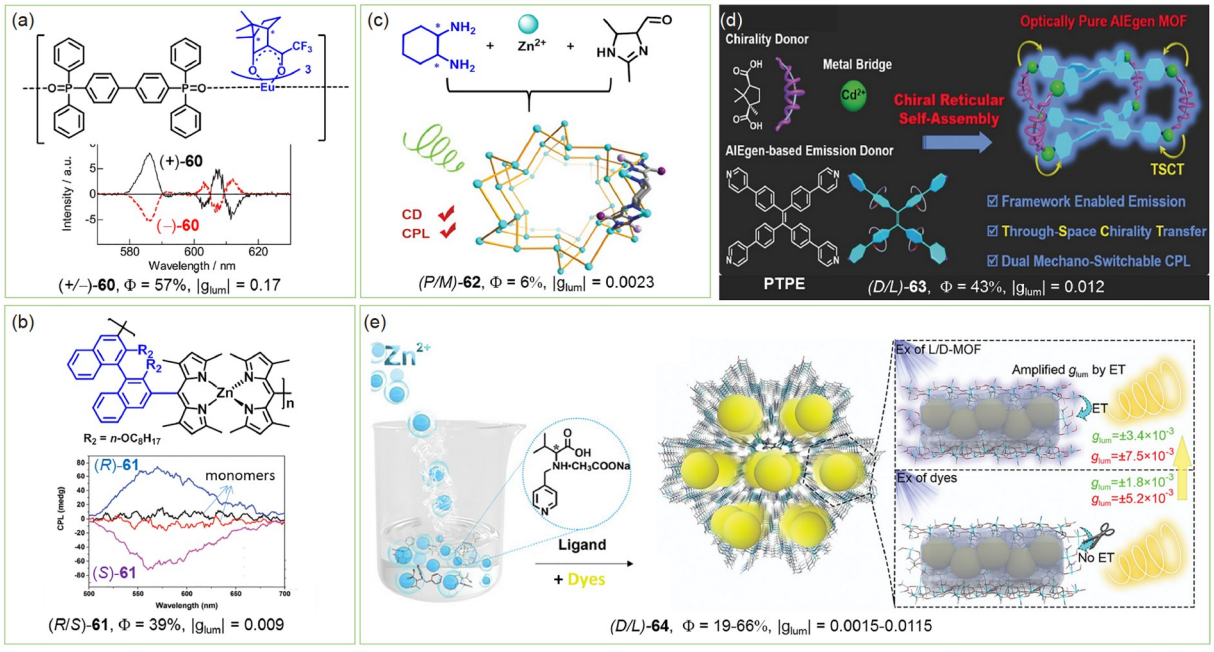

Figure 18 (a) Chiral MOPs (+/−)-**60** and CPL spectra [140]. (b) Chiral MOPs (*R*/*S*)-**61** and CPL spectra [204]. (c) Formation of chiral 3D MOF **62** [207]. (d) Scheme illustration of the coordination assembly to form chiral MOF **63** [208]. (e) Graphical representation of the formation and FRET-amplified CPLs of dye-doped chiral MOF **64** [209] (color online).

fabricated. The first one is formed by the coordination assembly of chiral and/or achiral ligands/dyes with metal nodes; the second one is fabricated by doping emissive chromophores into the chiral pores or channels of frameworks. For instance, a series of chiral emissive Zn-imidazolate MOFs, *e.g.*, (*P*,*M*)-**62**, were reported by Li and co-

workers [207] recently to feature satisfactory CPL with Φ of 4.9–56.4% and $|g_{lum}|$ of 0.001–0.0023 at 488–520 nm (Figure 18c). The achiral AIEgen PTPE and chiral camphoric acid with Cd^{2+} ions could assemble to form optically pure MOFs (*D*,*L*)-**63** (Figure 18d) [208]. These MOFs show both AIE characteristics and CPL by effective through-space chirality transfer, with $|g_{lum}|$ of 0.012 at 452 nm being detected. More interestingly, under external mechano stimuli, *i.e.*, grinding and ultrasound, the red (512 nm) and blue (432 nm) CPLs of (*D*,*L*)-**63** could be reversibly switched as a result of the rotation and stacking change of AIEgen rotors within the intact homochiral framework [208]. Meanwhile, Zang and co-workers [209] have prepared a kind of intrinsically chiral MOFs (*D*,*L*)-**64** containing helical channels as the host (Figure 18e). When achiral emissive guest chromophores were incorporated into the chiral channels *via* hydrogen bonding, amplified multi-color and white CPLs were observed with or without energy transfer.

Great progress has been made in the development of CPL-active metal-ligand coordination materials in the past few years. As was discussed above, an increasing number of CPL-active coordination materials, *e.g.*, small-molecular metal complexes, supramolecular assemblies, and MOPs and MOFs, have been prepared. Several strategies have been employed to develop efficient CPL materials, including the utilization of the magnetic dipole-allowed transitions of Ln and Cr(III) complexes, the exploitation of supramolecular chirality based on helical assemblies or chiral liquid crystalline materials, and the exploration of large and supramolecular structures for chirality amplification (*e.g.*, molecular helicates, twisted MOPs, and MOFs [212]. In spite of these advances, the g_{lum} values of most of these reported materials are still low (in the order of 10^{-2} or less), and only a few of examples have achieved the value of more than 0.1 for practical optoelectronic applications. Efficient CPL materials with high g_{lum} and Φ remain in greed demand in the future.

2.7 CPL-active metal clusters

Metal clusters bridging molecules and nanoparticles have attracted increasing attention for the remarkable structures and fascinating chemical/physical properties [213–218]. Chiral metal clusters that have discrete energy level for promising emission properties are potential candidates for CPL materials [10,46,219–226]. In this section, we will highlight the recent advances in this emerging research area.

The chiral ligand induction synthesis and chiral assembly are the effective strategies to design and prepare the CPL-active metal clusters, including single-valence and mixed-valence metal clusters (Figure 19). In 2019, using (*S*) or (*R*)-4-phenylthiazolidine-2-thione (denoted as PL or PD) and (*S*) or (*R*)-4-isopropylthiazolidine-2-thione (denoted as L or D)

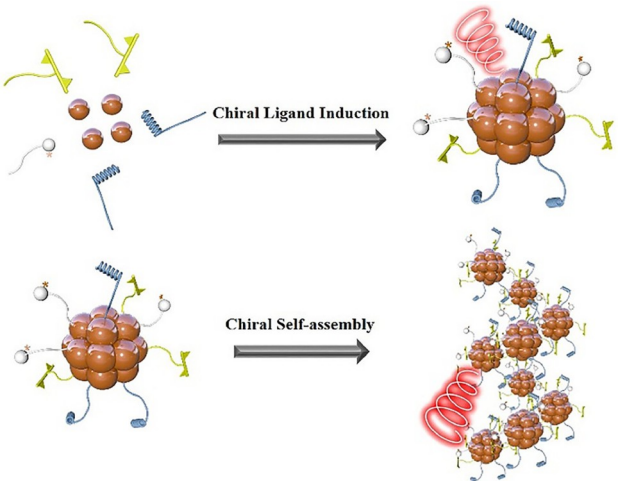

Figure 19 Schematic diagram for asymmetric synthesis and chiral self-assembly of chiral coinage metal clusters with CPL (color online).

chiral ligands, respectively, Zang and co-workers [227] reported two pairs of chiral octahedral Ag_6 cluster featuring TADF properties with the highest quantum yield of 95.0% for Ag_6PL_6/PD_6, which achieved ground-breaking progress in monolayer-protected silver cluster systems. The bright luminescence combines chirality in excited states to generate strong CPL signals with g_{lum} of $\pm 4.42 \times 10^{-3}$.

Analogous to chiral silver clusters, some copper clusters also exhibited CPL response induced by chiral ligands. In 2020, chiral ligands (*R*)- or (*S*)-2,2′-bis(di-*p*-tolylphosphino)-1,1′-binaphthyl (denoted as *R*-BINAP or *S*-BINAP) were used to construct a pair of enantiomeric Cu_3 clusters *via* one-step synthesis [228]. The propeller-like chiral copper clusters exhibited unique photoinduced fluorescence enhancement properties and AIE characteristics. In the aggregated state, the chiral clusters showed remarkable CPL responses with a g_{lum} of $\pm 2 \times 10^{-2}$. Moreover, chiral alkynyl ligands with massive phenyl functional groups (*R*)- or (*S*)-2-diphenyl-2-hydroxylmethylpyrrolidine-1-propyne (denoted as *R*-DPM or *S*-DPM) were developed to prepare an optically pure enantiomeric pair of copper clusters (*R*/*S*)-Cu_{14} [229]. Isolated monomers that have mirror image CD signals are non-luminescent and CPL inactive in solution, while their aggregated and crystalline states feature bright red emission originating from AIE and crystallization-induced emission (CIE), which correspondingly triggered the CPL signals of the chiral clusters with a g_{lum} of $\pm 1 \times 10^{-2}$.

Compared with CPL-active single-valence coinage metal clusters, mixed-valence metal clusters that contain both M(0) and M(I) centers have much room for development due to the novel functions and high-performance properties. In 2021, CPL-active superatomic coinage metal cluster was presented by Zang *et al.* [230]. They prepared and structurally characterized an enantiomeric pair of superatomic silver clusters with symmetric CPL activities by using designed chiral al-

kynyl ligands (Figure 20a). The Ag framework and the protecting ligand in superatomic silver clusters presented C_3 symmetry and emitted bright NIR luminescence in the solid state with a quantum yield of 8%, resulting in an unprecedented NIR CPL response. More importantly, by a combination of single-crystal X-ray structural analysis, optical experiments and theoretical calculations, it was clearly revealed that the CPL originated from transitions between superatomic *S* and *P* orbitals. In a study by Bürgi *et al*. [231], the synthetic method of $Ag_{24}Au_1$ clusters was modified by the introduction of the second thiol ligands (*R*/*S*)-1,1′-[binaphthalene]-2,2′-dithiol. The chiral $Ag_{24}Au_1$ clusters exhibiting CPL activities were synthesized. The results revealed that combination of chirality and luminescence to understand the origin of electronic transitions of metal clusters has the considerable progress in such molecule-like coinage metal clusters.

Since intrinsically chiral metal clusters constructed by achiral ligands are generally obtained as racemic mixtures, the enantioseparation is required before further chiroptical exploration. And, the helical structures can be achieved by self-assembly of the metal clusters. In 2020, Zang and co-workers [232] developed the chiral resolution of racemic Ag_{30} clusters through conglomerate crystallization method. Recrystallization of the racemic clusters in dimethylacetamide successfully produces single crystals of a pair of enantiomers. The enantiopure clusters adopt a spontaneous double-helical assembly *via* diverse noncovalent interactions. Due to the red-emitting and homochiral structure, the CPL responses of the optically pure Ag_{30} clusters were observed, in which the g_{lum} was $\pm 7 \times 10^{-4}$.

Postmodification synthetic approach allows for tailoring properties through the stepwise modification of the clusters using joint functional ligands. In 2020, by combining both chiral amino acids and luminescent sulfonic-group-containing organic ligands 4,4′-bis(2-sulfonatostyryl)biphenyl disodium salt (denoted as Na_2CF351) and *N*,*N*′-di(ethanesulfonic acid)-3,4,9,10-perylene tetracarboxylic diimide (denoted as $H_2TauPDI$) on the Ag_{20} surface, CPL-active silver clusters are demonstrated [233]. This surface engineering enables the atomically-precise Ag_{20} to exhibit the synergistic effect of chirality and emission due to the chirality transfer from the chiral Ag_{24} cluster to the achiral luminescent ligands, producing CPL with a g_{lum} of 5×10^{-3}.

Chiral supramolecular self-assembly of the coinage metal clusters provides possibility to enlarge CPL response of metal clusters. For example, in 2017, Tang and co-workers [234] reported the chiral Au cluster assemblies with CPL response by chiral ligands *R*-BINAP or *S*-BINAP (Figure 20b). Enantiomeric pair of Au clusters *R*/*S*-Au_3 dispersed in dichloromethane displayed mirror image CD responses but free of luminescent and CPL properties. Strikingly, through adding non-polar *n*-hexane, the chiral Au clusters were self-assembled into ordered structures. Compared with the in-

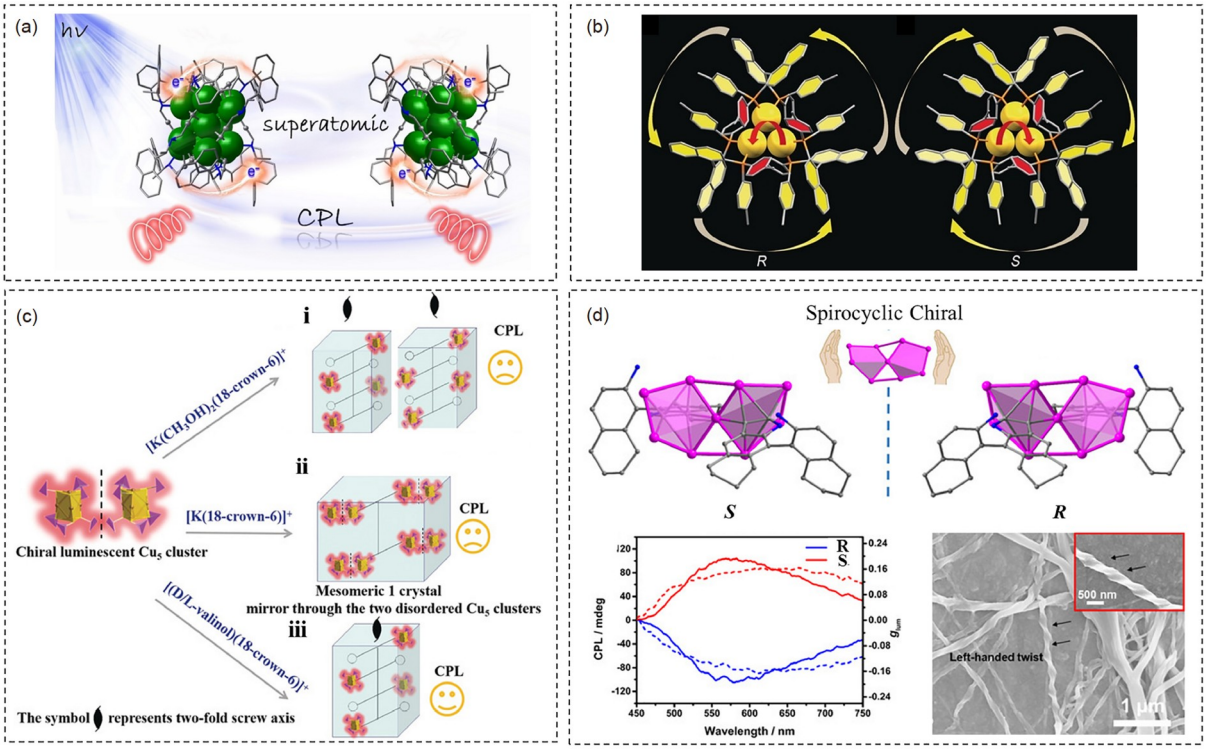

Figure 20 (a) Schematic illustration of CPL-active superatomic silver clusters [230]. (b) The structures of (*R*/*S*)-Au_3 [234]. (c) Schematic diagram of cations manipulating the chiral assembly of copper clusters into the structures with different CPL properties [235]. (d) Upper: the spirocyclic Ag_9 cores of the chiral clusters; Below: CPL spectra for the film samples and SEM images of the assembled structures [237] (color online).

dividual clusters, the chiral gold cluster assemblies showed CPL responses with g_{lum} of $\pm 7 \times 10^{-3}$. In 2019, Zang and co-workers [235] introduced chiral cationic *D*/*L*-valinol into the as-prepared racemic products, and the symmetry of copper cluster was broken by hydrogen bond interactions, eventually resulting in the successful construction of homochiral cluster ensembles with symmetric CD and CPL activities (Figure 20c). The result revealed the chiral assembly of metal clusters induced by counter ions will bring exciting opportunities for their chiroptical properties. Subsequently, Zang and co-workers [236] reported two enantiomeric pairs of gold clusters $Au_4(PL/PD)_4$ and $\{Au_4(L_4/D_4)\}_n$. Intercluster aurophilicity-driven aggregation triggered CPL of chiral gold clusters. For the first time, $\{Au_4(L_4/D_4)\}_n$ was successfully assembled into the circularly polarized organic light-emitting devices (CP-OLEDs) with the dissymmetry factor for electroluminescence $\pm g_{EL}$ nearly equal to $\pm g_{lum}$, implying CPL-active coinage metal clusters hold great promise in the field of chiral lighting materials.

Notably, in 2020, the assemblies of the spirocyclic chiral silver clusters with excellent CPL performance were constructed by Zhao and co-workers [237]. The intrinsically chiral metal clusters were induced by axial chirality ligand (*R*)- or (*S*)-3-ethynyl-5,5′,6,6′,7,7′,8,8′-octahydro-1,1-binaphthyl-2,2′-diamine (Figure 20d). Furthermore, under different assembly conditions, the chiral silver clusters showed AIE characteristic along with fluorescence-to-phosphorescence switched properties. Remarkably, the assembled helical nanofibers were achieved in solution. The assembled film of chiral silver clusters showed strong CPL responses with a remarkably high g_{lum} of ±0.16, which are the highest values reported among metal cluster-based assemblies as for 2021.

Together, chiral metal clusters represent a new class of promising CPL system. The precise structure of chiral metal cluster is helpful to understand the structure-chiroptical activity relationship at the atomic level. However, until now, CPL-active atomically precise metal clusters are very scarce. There remain many difficulties in this field. First, there is a challenge to attain a maximized g_{lum} value in a controllable way in atomically precise metal cluster systems. The helical assembly of luminescent metal clusters driven by diverse non-covalent interactions like van der Waals, electrostatic interactions, C–H···π, π-π and H-bonding is promising for enlarging the g_{lum} value. Second, utilizing the helical polymer structures in combination with the metal clusters may lead to CPL properties with high g_{lum} value. Third, the step-by-step post-modification synthetic approach using custom functional ligands with additional luminescence and chirality may be effective. Fourth, unique coordination assembly of metal clusters into high-dimensional framework could extend applications in CPL sensing, because of their rich and diverse pores. Notably, more synthetic strategies need to be innovated for increasing emission efficiency and asymmetric factor of metal cluster-based materials. Briefly, CPL-active metal clusters act as a type of promising functional materials, which is worthy of further exploration. We believe that the future is bright in this field.

2.8 CPL-active inorganic nanomaterials

The proficient synthetic chemistry has allowed for fabricating tailorable chiral inorganic nanomaterials with intense optical activity and have been extensively studied for various applications in the field of chiral related catalysis [238,239], biosensing [240–242], chiral recognition and bio-interactions [243,244], and biomedicine [245], as well as physicochemical device [246], among others [247,248]. Sophisticated construction techniques for chiral nanostructures have been achieved in individual synthesis of nanocrystals [249,250], two-dimensional (2D) fabrication of either nanosheet [251] or large scale films [252,253] and 3D pyramidal [254], helical and dihedral geometrical [255] assembly of inorganic nanocrystals and so on [256,257]. Now days, the chiral inorganic nanomaterials with CPL have been drawing more and more attention owing to their huge potentials in 3D displays, information security, chiral identification, and optoelectronic devices and so on [1,3,10]. Similar to chiral inorganic nanomaterials, CPL-active inorganic materials can be classified into zero-dimensional (0D) [258] and 1D nanocrystals [259], 2D sheet and film structures [253], and 3D nanostructures, such as helical chiral inorganic nanostructures with CPL activity [166].

Based on recent development of CPL, major efforts have been made to realize the high chiral purity to obtain high CPL signals for solving the problem existing in the field: (1) structural control for highly uniform and ordered CPL-active materials, and (2) strong CPL signals with larger g_{lum}, in which the strong chiral structure can help to induce strong CPL. Different colloidal fabrication systems by synthetic methodology in aqueous and organic phases for 0D and 1D chiral nanocrystals, and their large scale 2D and 3D assembly strategy have been developed for strong CPL active materials including QDs and perovskite nanocrystals.

QDs usually have enhanced photoluminescence quantum yields and display fascinating chiroptical properties for studying CPL signals [10,258,259], in which chirality originating from: (1) dislocations and defects enabled intrinsically chiral nanocrystals, (2) ligand-induced chiral surfaces or chiral interactions between chiral ligands and achiral QDs, and (3) chirally assembled QDs superstructures. Among these, ligand exchange with chiral molecules provides uniform size distribution with known surface chemistry of chiral QDs. It was found that CD signals of a chiral luminescent QD do not ensure the presence of CPL signals, while CPL-active materials usually have chirality with

Cotton effect. For introducing the CPL, the intensive optical activity and fluorescence is necessary. The early reported CPL signals were weak for CdSe QDs with g_{lum} of 4.66 × 10^{-4} (Figure 21a) [258,259]. The individual QD can only generate weak CPL while chiral superstructures, like helical morphology, could give rise to stronger CPL and many attempts have thus been made in chiral assemblies. The reported superstructures included the helical co-gels of CdSe/ZnS core-shell QDs by organic lipid gelator *N*,*N*′-bis(octadecyl)-*L*-/*D*-glutamic diimide [84], the co-gel of QDs by *N*-behenic-1,5-bis(*L*/*D*-glutamic acid)-*L*/*D*-glutamic diamide (*L*-/*D*-BGAc) [28], and chiral FeS_2 quantum dot hydrogels [260] with the highest g_{lum} of 3.26 × 10^{-2} (Figure 21b, c). It is notable that the starting chiral QDs might not be CPL active while the helical co-gel assemblies help to induce CPL signals due to collective enhancement [84,261]. Large scale fabrication of mesoscale QDs structures can even induce stronger CPL signals [262], which aroused great interests for future study.

Chiral semiconductor perovskites have deemed as an emerging topic of interest which were investigated for producing strong CPL signals [263]. CPL-active chiral perovskites have attracted much attention by their facile preparation and great potential applications [264,265]. Chiral perovskites can be facilely prepared using chiral ligand as the capping reagent to generate CPL with chiral origins from: (1) the incorporation of chiral organic moieties that formed metal halide hybrid complex; (2) chiral ligands modified on the surfaces of metal halide nanocrystals; and (3) the metal halide chiral superstructures [266,267]. The first example of perovskite was reported by Duan's group using chiral α-octylamine to prepare cesium lead bromides ($CsPbBr_3$) perovskite nanocrystals, which showed two-photon absorption-based upconverted CPL with g_{lum} of 7.0 ×10^{-3} (see further discussions in Section 2.9) [268]. Generally, for generating strong CPL signals, the chiral ligand involved in synthesis and the uniformity in size of the individual chiral nanocrystal can help to induce stronger CPL. The "ligand-controlled synthesis" strategy has been reported for uniform formamidinium lead bromide ($FAPbBr_3$) nanocrystals by using chiral (*R*)-2-octylamine ligands in the synthetic process that achieved g_{lum} as high as 6.8 × 10^{-2} (Figure 22a–c) [267]. This was about 6 times higher than that of $FAPbBr_3$ nanocrystals prepared through post-synthetic ligand treatment process, which was the highest among reported individual perovskite nanocrystals.

Chiral assemblies of perovskite for helical superstructures could help to induce stronger CPL signals. The helical structure of silica nanohelices assembled perovskite $CsPbBr_3$ nanocrystals [269], chiral helical polymer/perovskite hybrid nanofibers were fabricated for generating and enhancing CPL signals [85,166]. Deng *et al.* [166] reported chiral helical polymer/perovskite hybrid nanofibers through a one-step electrospinning method in which chiral helical polyacetylenes, achiral CsBr and $PbBr_2$ perovskite nanocrystals, and polyacrylonitrile were used as the handed-selective

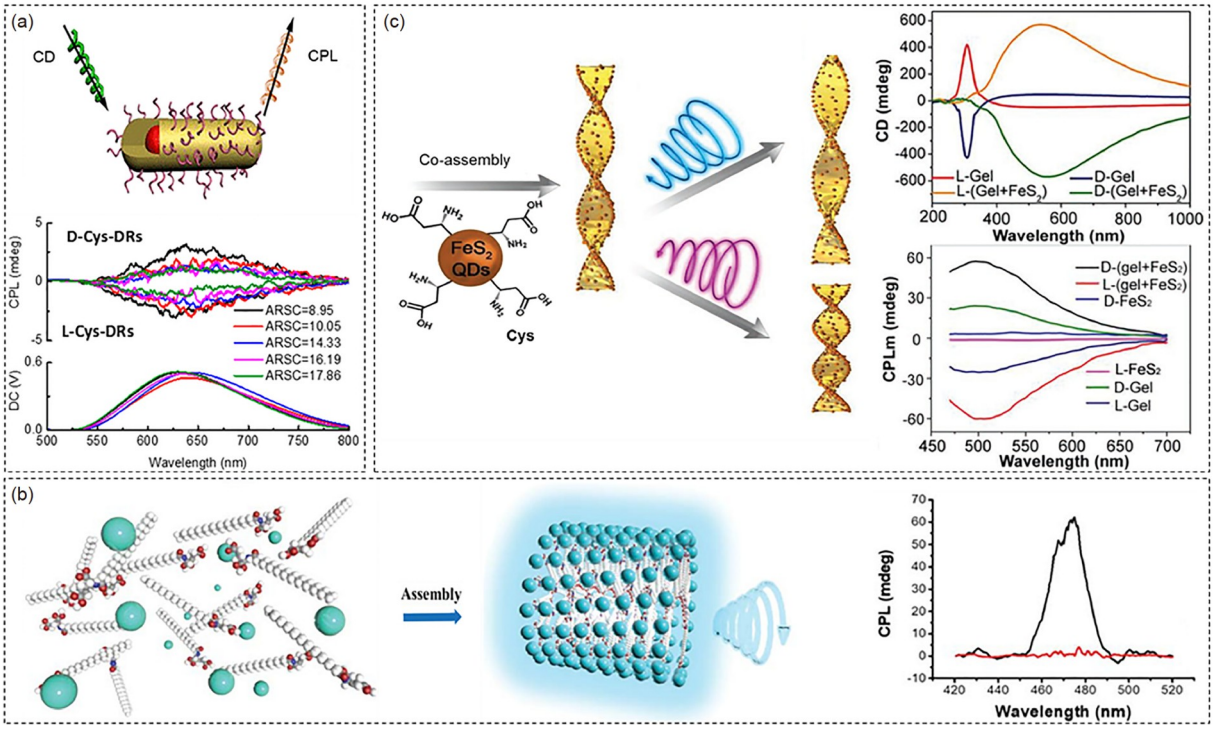

Figure 21 (a) Schematic illustration of the CPL active Cys-CdSe/CdS nanorods and CPL spectra [259]. (b) The cyan-emissive QDs assembled co-gels for the CPL spectra (black line) [260]. (c) Chiral FeS_2 QDs assembled co-gels and corresponding CD and CPL spectra [261] (color online).

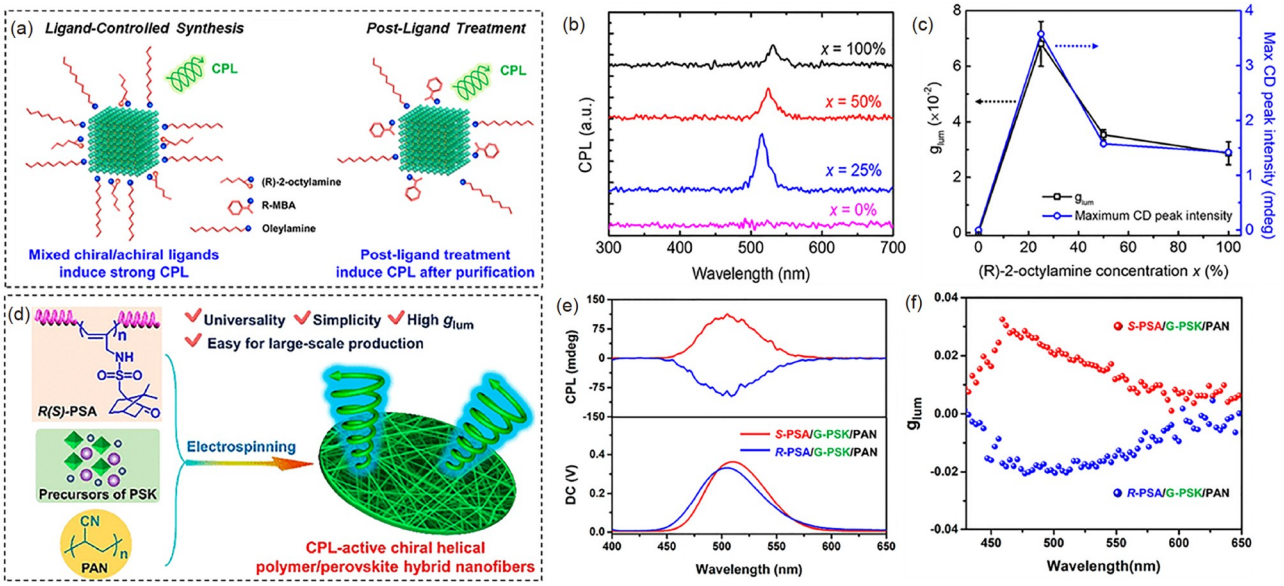

Figure 22 (a) Chiral ligand-controlled synthesis and corresponding (b) CPL and (c) g_{lum} spectra of $FAPbBr_3$ nanocrystals [267]. (d) Preparing CPL-Active chiral helical polymer/perovskite hybrid nanofibers through electrospinning and corresponding (e) CPL and (f) g_{lum} spectra of the hybrid nanofibers [166] (color online).

fluorescence filter, fluorescent source, and electrospinning matrix, and finally, the high g_{lum} value of 3.2×10^{-2} was achieved (Figure 22d–f). Other inorganic nanomaterials, such as the carbon dots, which can be assembled into chiral co-gels using LGAm/DGAm lipid and generated strong CPL with the g_{lum} up to 10^{-2} [86]. This was the first time to successfully prepare circularly polarized white-emitting chiral carbonized polymer dots. Varieties of CPL active inorganic nanomaterials are potentially important to explore with controllable and scalable constructions.

Further large scale assembly of QDs and perovskite into chiral films can help to enhance the CPL signals by either deposition, casting or spin coating that have been reported for chiral ZnS/CdSe QDs film [262], chiral 2D perovskites film [253], and chiral carbon dots film [270]. Semiconductor QDs were co-assembled in cellulose nanocrystal-based left-handed hierarchical photonic films that resulted in full-color tunable CPL with g_{lum} as high as 0.48 (Figure 23a–d) [262]. Using the cholesteric superstructure stack, Li's group [271] assembled $CsPbX_3$ perovskite nanoparticles into chiral cholesteric liquid crystals (CLCs) films with g_{lum} as high as 1.6 (Figure 23e, f). This was the highest value reported for the g_{lum} of CPL from inorganic materials. Similarly, Xu *et al.* [270] reported the hybrid chiral photonic film by co-assembly of carbon dots, cellulose nanocrystals, and poly (vinyl alcohol) with g_{lum} up to 0.27. The future mesoscale construction of chiral semiconductors with strong CPL will be extremely crucial for real applications.

Recent breakthroughs in technological development have led to great progress in the field of CPL-active inorganic materials, in which the majorities focus on chiral structure fabrication, CPL generation and enhancement. Regarding the progress, the future advances of chiral materials can be summarized from different aspects in this field: (1) The further freedom to fabricate advanced and complex chiral structures with fine control in geometry and enantiomeric configuration is still in great demand. The biological, chemical and physical functions should be further designed and assembled for application purpose. (2) The g_{lum} for the reported inorganic materials is still not high. Most of the inorganic materials are in the 10^{-3} to 10^{-2} magnitude, which limits the application of CPL. The strategy for CPL generation and enhancement may rely on multiple technology advance such as supramolecular chemistry, inorganic chemistry, nanoassemblies, lithography techniques, and glancing angle vacuum, and evaporation. These advances would allow us to construct uniform and scalable homochiral systems with strong CPL signals. (3) We are still on the early stage of CPL active materials research, and rarely have demonstrated realistic applications. The CPL-related optical, electrochemical, and physicochemical properties could result in extensive applications. The great opportunities lie in spins-, electrons- and photons-related field for developing photonic, optoelectronic and displaying devices. Perhaps more comprehensive evolution from current field of CPL will be in near future.

2.9 Photon upconversion systems

The term "upconverted circularly polarized luminescence" (UC-CPL) was developed by integrating the concept "photon upconversion" and "circularly polarized luminescence".

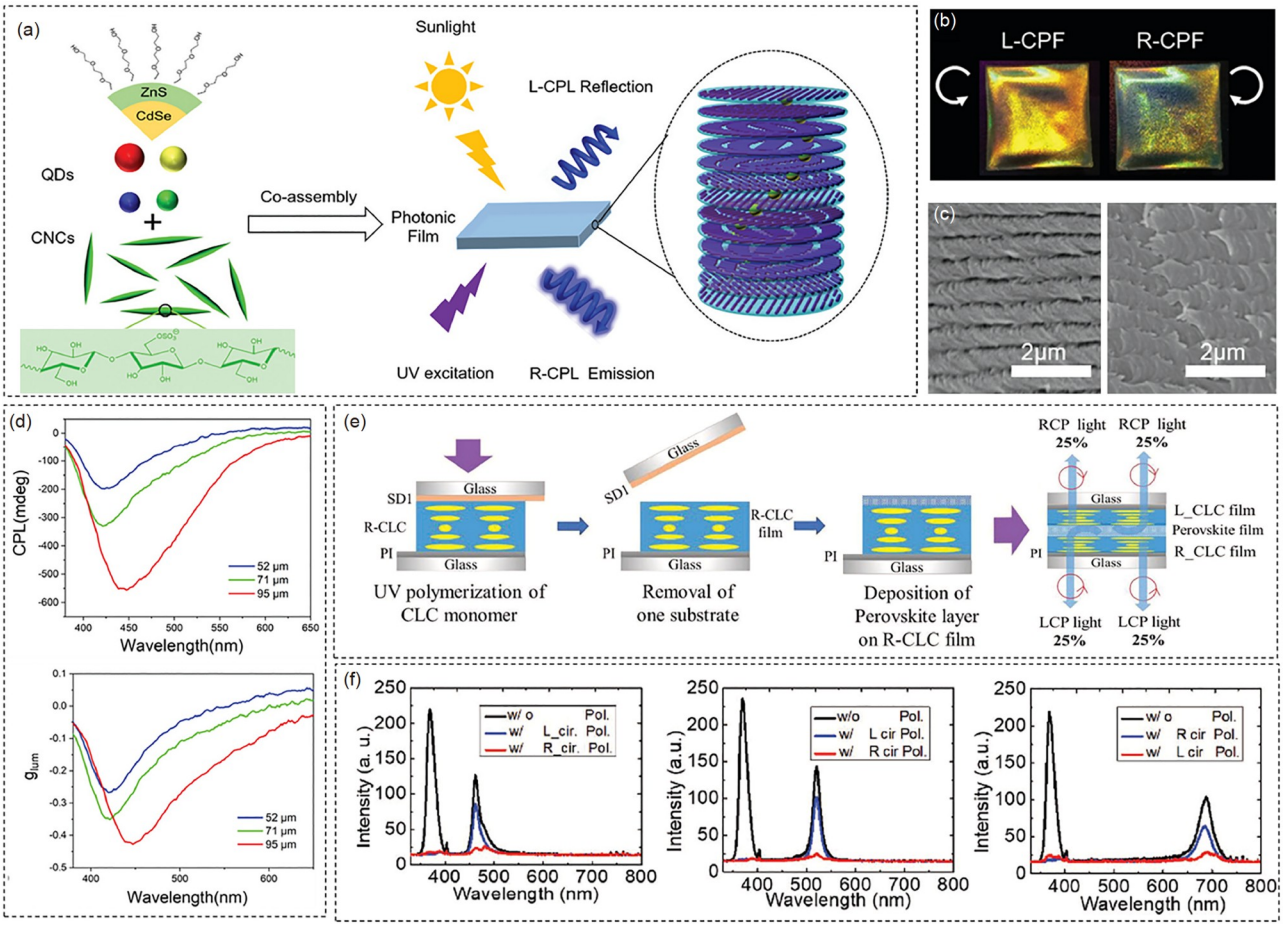

Figure 23 (a) CPL photonic films through the co-assembly of cellulose and semiconductor QDs. (b) Photographs of a photonic film under a left-handed circularly polarized filter (left panel) and a right-handed circularly polarized filter (right panel). (c, d) SEM images and the CPL and g_{lum} spectra for the chiral photonic film [262]. (e) The cholesteric superstructure stack of perovskite nanocrystals for the CPL system. (f) The measured luminescent spectra using the configuration for blue (left), green (medium), and red (right) luminescence probed with and without polarizing filters [271] (color online).

Besides the inherently high dimensional information of CPL, UC-CPL can meet more functional requirements and applications by adjusting the anti-Stokes emission. Meanwhile, since upconversion processes include more photophysical and photochemical processes than the common Stokes emission, UC-CPL should be more flexible to be built. To date, plenty of reports involving various upconversion mechanisms have been presented. We summarize a few noteworthy approaches that have been demonstrated to achieve UC-CPL considerably, which so far can be divided into three categories: two-photon absorption upconversion (TPA-UC), triplet-triplet annihilation-based upconversion (TTA-UC), as well as upconversion of lanthanide-doped nanoparticles (UCNPs) with hybrid mechanisms.

When CPL and TPA-UC are integrated, UC-CPL can be achieved with a significantly large anti-Stokes shift. Chromophore with TPA properties should be incorporated with asymmetric environment as an essential approach to generate CPL based on TPA-UC. In chiral perovskite nanocrystals, Chen *et al*. [268] directly observed the TPA-based UC-CPL phenomenon (Figure 24a). Under the excitation of an 800 nm femtosecond laser, the perovskite nanocrystals modified by chiral ligand showed UC-CPL behavior around 520 nm with g_{lum} at the magnitude of 10^{-3} (Figure 24b, c). Corresponding parameters including TPA cross-section and the power-dependent luminescence curves have been measured to exhibit TPA process, with intensity being proportional to the square of the excitation light intensity.

Currently, direct measuring CPL based on TPA-UC gives the rare case, although some studies have reported several kinds of systems which can exhibit both CPL and TPA-UC [272–275]. Exploration of more systems and corresponding mechanism should be necessary for the improvement of CPL based on TPA-UC. In addition, a plentiful effort should be devoted into the intrinsic defects of TPA-UC for requiring extremely high excitation power density and low upconversion efficiency.

TTA-UC, constructed by sensitizers and acceptors, results in a more interesting effect on CPL. For the CPL through TTA-UC process, to create two excited triplets, two sensi-

tizers absorb an equal quantity of low-energy photons. After that, triplet-triplet energy transfer (TTET) from sensitizer to acceptor will pump the triplet state of acceptor. Finally, TTA of two chiral acceptor triplets generates one acceptor with ground state and one excited singlet state acceptor, which is responsible for the UC-CPL (Figure 25a). Noteworthy, the circular polarization of CPL through TTA-UC process tends to be amplified compared to common downshift CPL from individual acceptors.

UC-CPL systems based on TTA not only require relatively low-intensity excitation light, but also work as potential method to boost the CPL performance. In 2017, Han *et al.* [276] built the CPL system based on TTA-UC process by

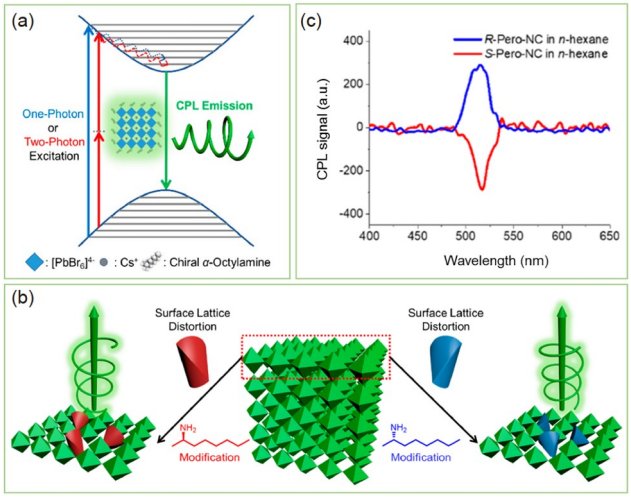

Figure 24 (a) The sketch of TPA-based UC-CPL process. (b) The strategy to endow perovskite with chirality by modification of chiral α-octylamine. (c) Two-photon upconverted CPL spectra of chiral perovskite nanocrystals in *n*-hexane [268] (color online).

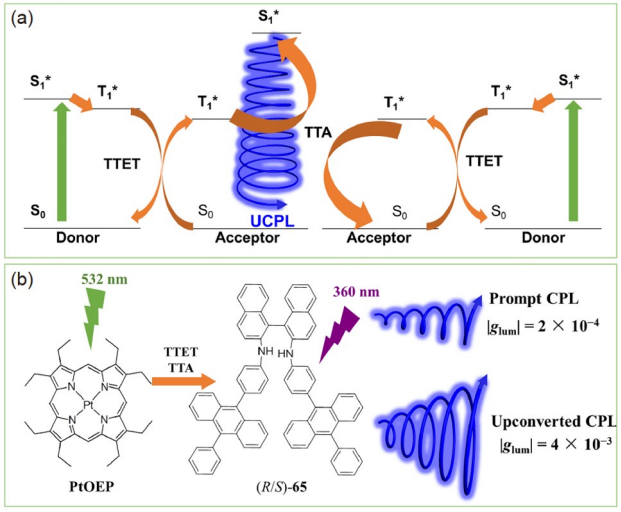

Figure 25 (a) The diagram of the TTA-based UC-CPL mechanism. (b) Boosting CPL of chiral acceptor based on TTA process [276] (color online).

using Pt(II) octaethylporphine (PtOEP) to sensitize chiral chromophore (*R*/*S*)-**65** (Figure 25b). The 20-fold amplification of g_{lum} was observed for UC-CPL in comparison with the normal CPL of acceptors. To further extend the UC-CPL emission region, the generality of various upconversion donor/acceptor pairs were further demonstrated [277]. The efficiency of the TTA process will be reduced due to chirality-induced spin polarization, which is possibly responsible for the enhancement of g_{lum} value. Moreover, CPLs based on TTA mechanism have been widely presented in other systems like liquid crystals [278,279] and supramolecular gels [280,281]. These chiral hosts have received considerable attentions for the flexible controllability of CPL. Recent work has revealed a strategy by using achiral C_3-symmetric molecules to build the chiral nanohelix through symmetry breaking, and then it can load TTA-UC donor/acceptor pairs [280]. Seeded vortex is proven available to control the chirality of assembly and corresponding UC-CPL. In addition, liquid crystal as the common medium can generate a large g_{lum} value, enabling the application in asymmetric catalysis [279]. Yet noteworthy, the measurement of down- and upconverted CPL in the identical materials is necessary to evaluate the amplifying g_{lum} of CPL through the TTA process. Therefore, to evaluate the amplifying CPL effects in the heterogeneous assembly systems ought to carefully avoid potential pitfalls by other factors.

Recent advances in UCNPs were broadly utilized to conduct the UC-CPL study. Advantages of using UCNPs include the following aspects: tunable emission wavelength, stability, and relatively low-power excitation. In 2019, Jin *et al.* [282] reported a chiral supramolecular gel system, which could co-assemble with UCNPs to form hybrid gel system, exhibiting UC-CPL behavior (Figure 26a). Its ultraviolet region has been successfully used for the enantioselective polymerization of diacetylene. In addition, the approach of seeded vortex could be used to adjust chiral assembly, thus UCNPs were successfully blended into the nanohelix, enabling the UC-CPL emission [280]. Other chiral environments were also demonstrated like liquid crystal [282–284] and metal-organic framework [285,286], which built powerful platforms for constructing stimulus responsiveness of UC-CPL.

Afterwards, the UC-CPL phenomenon on the basis of UCNPs has been further extended to the donor-acceptor system involving energy transfer process (Figure 26b). Energy transfer can occur between UCNPs and acceptors in the cases of perovskite nanocrystals [287] or organic dyes [286]. In the asymmetric environment, this kind of acceptors is an important component in achieving functional and tunable CPL. Meanwhile, relying on re-excitation of CPL from donor, this kind of approach is possible for enhancing CPL of acceptor. In the liquid crystal, by matching the photonic bandgap with emission of energy acceptors, the selective

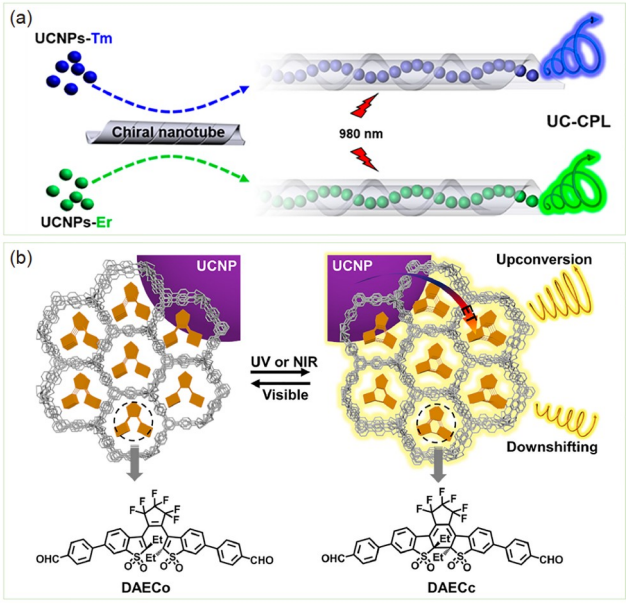

Figure 26 (a) Chiral nanotube wrapping UCNPs to generate the UC-CPL [282]. (b) Energy transfer from UCNPs to DAEs loaded in chiral MOFs with amplified UC-CPL [286] (color online).

reflection will result in a pretty large g_{lum} value of UC-CPL. Particularly, in liquid crystal system, CPL performance is switchable by tuning the electric field due to the electro-optical effect of LCs based on the electric field-responsive molecular rotations [101]. Herein, liquid crystal should be regarded as a good substrate to get high-quality CPL performance.

Basically, based on the three types of photons upconversion mechanisms: TPA, TTA, and UCNPs, in the realm of photochemistry and physics, the proposed UC-CPL concept is a relatively new research area. The design of UC-CPL through TPA-UC process is simple because it is normal to achieve TPA emission from single component. However, the high-power excitation requirement and TPA cross-section should be considered thoroughly. TTA-based UC-CPL has much more design freedom, but it requires the challenge about good combination of donors and acceptors. Furthermore, oxygen quenching of triplets is a critical issue. UC-CPL system built by UCNPs enables more possibility to tune the emission; however, the adjustable chirality and compatibility of UCNPs strongly rely on chiral ligand structure where inappropriate ligands tend to induce phase classification and weak interaction to the target. Exploring effective methods to solve the problems including the low upconversion efficiency, small dissymmetry factor value, and incompatibility with various practical applications, should be the critical issue. Moreover, size effect of the nanostructure on UC-CPL performance needs to be further explored.

For improving the quality of CPL, structure-activity relationships from different chiral materials are still desirable to be researohed. To date, chiral assembly demonstrates dramatically high CPL performance. Especially in liquid crystals, near-completely left or right CPL is possible to be obtained. Designing upconversion in chiral liquid crystal is an alluring choice for achieving excellent UC-CPL performance. Meanwhile, considering that upconversion frequently involves multi-step photophysical or photochemical processes, how to build chiral environment and endow donor/acceptor system with chirality becomes more and more important. Re-excitation by circularly polarized light generated from the donors may raise more possibilities in amplifying CPL. To understand the inherent mechanism of chiral systems, it is encouraged to take in-depth and quantitative research on each step of the photophysical process. The development, amplification, and modulation of UC-CPL will have been instrumental in our understanding of practical applications like sensors, imaging and data transformation applications.

3 Applications of CPL

3.1 Circularly polarized organic light-emitting devices (CP-OLEDs)

Since the first report of the low-voltage driving organic light-emitting device (OLED) in 1987, it became a rapidly expanding field in both industry and academia [288]. By researchers' effort, OLED displays have been widely used in smart phone, television, and laptop and so on because the external quantum efficiencies (EQEs) of OLEDs have already reached the theoretical maxima of 30%–35%. Therefore, it is necessary to develop new technology and materials for next generation display. Compared with using a polarizer and a quarter-wave plate to obtain CP light, chiral CPL material avoids complicated filtering structure and brightness loss. Therefore, the CP-OLED based on chiral luminescent materials can simplify device structure and improve device efficiency for 3D display.

The widely used OLEDs always have "sandwich" structure, characterized by the hole injection from the indium-tin oxide (ITO) anode and electron injection from the metal cathode. Due to the differences of the charge transport property and sublimate ability of the emitters, OLEDs can be fabricated by solution-processed or evaporation process with single, double or multi organic layers including hole injection and transport layers, electron injection and transport layers, and emissive layers (Figure 27). Compared with traditional OLEDs, CP-OLEDs have the similar structures but replacing the normal emitters with chiral luminescent materials.

Solution-processed methods are widely applied to polymers, organic molecules and metal complexes. The first CP-OLED was reported by Meijer *et al.* [289] in 1997 based on a

chiral π-conjugated poly(*p*-phenylenevinylene) (PPV) derivative (**66**), and the g_{EL} factor reached -1.7×10^{-3} at 600 nm (Figure 28 and Table 4). But because the simple single-layer

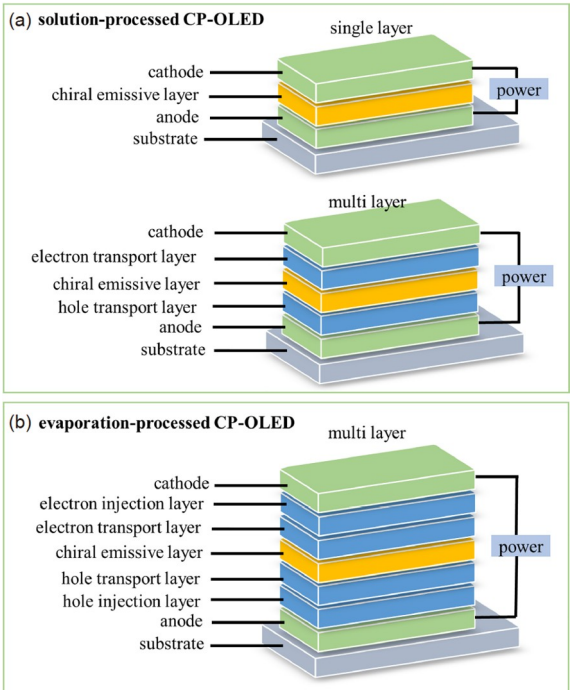

Figure 27 CP-OLED device structures (color online).

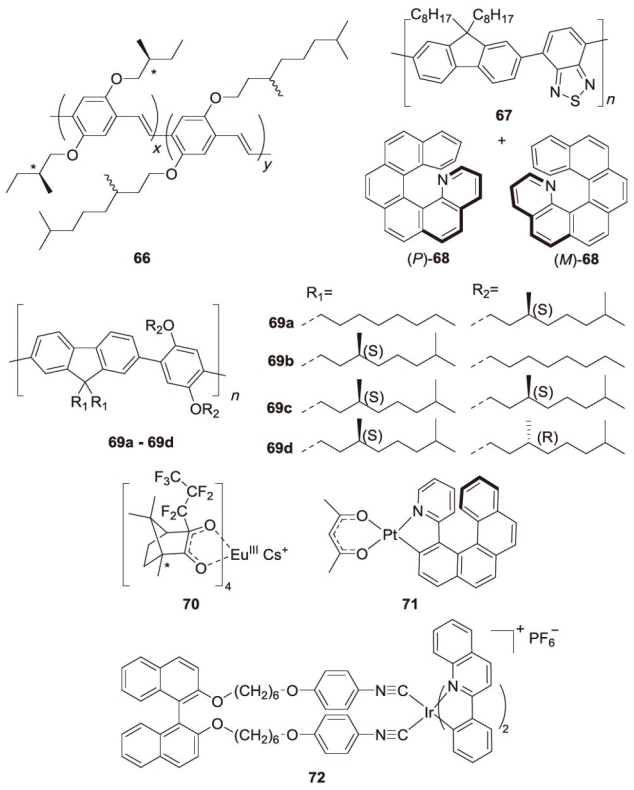

Figure 28 Chiral materials used in solution-processed CP-OLEDs.

Table 4 Parameters of CP-OLEDs [a]

Material	λ_{EL} (nm)	g_{EL}	EQE_{max} (%)	Ref.
(−)-**66** [b]	600	-1.7×10^{-3}	NR	[289]
67 +(*P*)-**68** [b]	575	+0.2	NR	[292]
69a [b]	ND	ND	NR	[293]
69b [b]	425	−0.20	NR	[293]
69c [b]	430	−0.07	NR	[293]
69d [b]	425	−0.04	NR	[293]
(−)-**70** [b]	595/612	−1.0/+0.19	0.005	[297]
(−)-**71** [b]	615	−0.38	NR	[298]
(*R*)-**72** [b]	525/558	-10^{-3}	NR	[299]
(*fac*,*Λ*)-**73** [c]	522	-2.8×10^{-4}	21	[304]
(*Λ*)-**74** [c]	533	-3.1×10^{-4}	25	[304]
(*Λ*)-**75** [c]	470	ND	30	[304]
(*Λ*,*R*)-**76** [c]	500	-2.6×10^{-3}	NR	[304]
(*Λ*,*R*)-**77** [c]	595	$+5\times10^{-4}$	23.7	[305]
(*Λ*,*R*)-**77** [c]	595	NR	NR	[305]
(*Λ*,*R*)-**78** [c]	599	NR	21.7	[305]
(*Λ*,*R*)-**78** [c]	599	NR	21.7	[305]
(*Λ*,*R*)-**79** [c]	466	$+2.4\times10^{-3}$	12.3	[306]
(*Λ*,*R*)-**79** [c]	466	-2.1×10^{-3}	13.3	[306]
(*M*)-**80** [c]	653	$+1.3\times10^{-3}$	4.6	[307]
(*M*)-**81** [c]	650	$+1.4\times10^{-3}$	18.8	[314]
(*Λ*,*R*)-**82** [c]	525	$+7.7\times10^{-3}$	17.1	[315]
(*Λ*,*R*)-**82** [c]	525	-6.6×10^{-3}	11.8	[315]
(*S*,*S*)-**85** [c]	520	-1.7×10^{-3}	19.7	[22]
(*R*,*R*)-**86** [c]	592	NR	12.4	[322]
(*S*)-**87** [c]	537	+0.06	3.5	[323]
(*S*)-**88** [c]	563	+0.054	2.3	[323]
(*S*)-**89** [c]	550	+0.067	2.9	[323]
(*S*)-**90** [c]	597	+0.084	0.6	[323]
(*S*)-**91** [b]	496	-3.7×10^{-4}	10.1	[324]
(*S*)-**91** [c]	492	-5.5×10^{-4}	8.4	[324]
(*S*)-**92** [b]	516	-3.9×10^{-4}	10.6	[324]
(*S*)-**92** [c]	515	-8.6×10^{-4}	12.4	[324]
(*R*)-**93** [c]	550	$+2.3\times10^{-3}$	12.3	[309]
(*R*)-**94** [c]	526	-2.3×10^{-3}	32.6	[308]
(*R*)-**95** [c]	536	-6×10^{-4}	28.3	[311]
(*R*)-**96** [c]	567	-2.4×10^{-3}	20.3	[311]
(*R*)-**97** [c]	604	-4.2×10^{-4}	0.12	[303]
(S_p)-**99** [c]	480	NR	17	[325]
(*S*)-**100** [c]	468	−0.012	12.5	[326]
(*S*)-**101** [c]	537	$+4.5\times10^{-3}$	17.8	[327]
(+)-**103** [c]	500	NR	20.8	[328]
(*S*)-**104** [c]	508	$+1.3\times10^{-3}$	12.5	[329]
(*S*)-**105** [c]	508	$+1.0\times10^{-3}$	23.1	[329]
(*S*)-**106** [c]	472	$+3.1\times10^{-3}$	20	[330]
(*M*)-**107** [c]	585	$+3.0\times10^{-3}$	5.1	[331]
(*S*,*S*)-**108** [c]	536	-1.4×10^{-3}	21.5	[332]

a) NR = Not reported, ND = not determined due to low signals; b) solution-processed OLEDs; c) evaporation-processed OLEDs.

structure and the fluorescence characters of the polymer, the onset voltage of the device was as high as 6–7 V with poor device performances. Then, a series of similar studies were done by Chen's group [290], Nuzzo's group [154] and Cheng's group [291] with improved device efficiencies. In 2013, Campbell *et al*. [292] doped achiral conjugated polymer **67** with chiral 1-aza[6]helicene (*P*/*M*)-**68** acting as one CPL filter and the device exhibited a high g_{EL} of 0.2 with a low power efficiency (PE_{max}) of 1.1 lm/W. More recently, Meijer *et al*. [293] developed a series of alkyl-substituted copolymers, **69a**–**69d**, of which the devices exhibited g_{EL} factors up to −0.2 at 425 nm, but the device still suffered from low efficiency. The presence of chiral groups on the fluorene unit of **69** was found to be crucial for the CPL activity and no CPL was observed for **69a**. In addition, great progress was made by Campbell's group [294], Kim's group [295] and Yu's group [296] in recent years with g_{EL} factors up to 1.13, which is mainly due to the formation of the helical structures after annealing treatment of the polymer emitters.

In 2015 and 2017, Di Bari *et al*. [175,297] blended the ionic europium complex $CsEu(hfbc)_4$ (**70**) with polyvinylcarbazole (PVK) and 1,3-bis[2-(4-tert-butylphenyl)-1,3,4-oxadiazo-5-yl]benzene (OXD7) as the emissive layer. The corresponding devices exhibited high g_{EL} up to 1.0 due to the allowed magnetic dipole transition (g_{lum} = 1.35) of the Eu(III) complex with low EQE_{max} of 5×10^{-3} because of the complex's long excitation state lifetime. In 2016, Fuchter *et al*. [298] also fabricated the similar CP-OLEDs with a platinum helicene emitter **71** achieving a high g_{EL} factor but low device efficiency. In 2017, Zhao *et al*. [299] fabricated the CP-OLEDs with the chiral bis-cyclometalated phosphorescent iridium(III) isocyanide complex **72**, obtaining a current efficiency of 7.50 cd A^{-1} with the g_{EL} factors in the order of 10^{-3}. At the same time, some groups also fabricated the CP-OLEDs with a single layer based on small fluorescence and TADF molecules with similar properties [67,169,300–303].

These CP-OLEDs fabricated with solution process exhibit high g_{EL} factors; however, the relatively simple device structure remains hard to balance the hole-electron injection and transport, and the unsatisfactory performances hinder them for commercial application. Therefore, to improve the CP-OLED performances, most devices were fabricated by evaporation method with multi-functional layers. To meet the requirement of evaporation, chiral luminescent molecules should contain two features, relatively small molecular weight and weak intermolecular π-π interaction. Thus, emissive layers of this type of CP-OLEDs mainly consist of CP-TADF molecules, which will be mainly discussed the following section, and chiral neutral metal complexes. This section mainly focuses on the CP-OLEDs based on chiral metal complexes.

In 2015, Zheng's group [305] reported the CP-OLEDs with

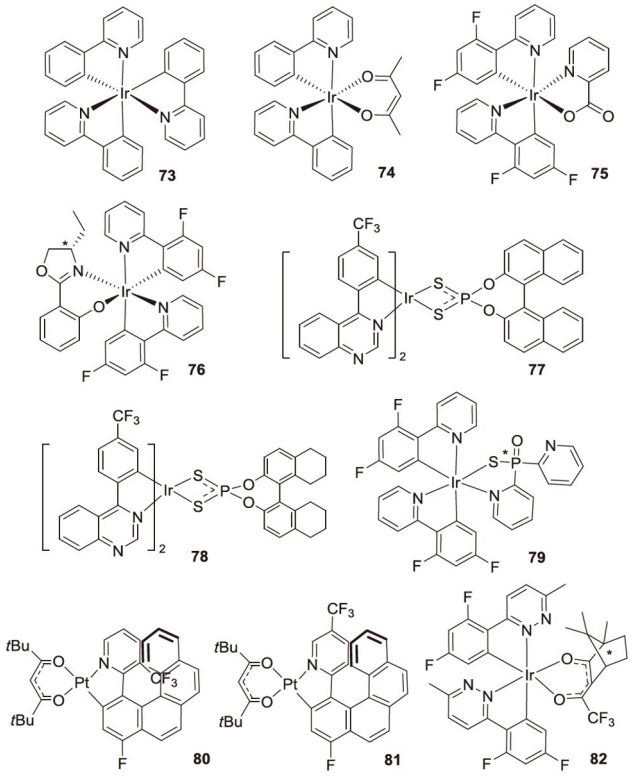

Figure 29 Metal complexes used in evaporation-processed CP-OLEDs.

multi-functional layer based on chiral Ir(III) complexes **73**–**76** for the first time, and the g_{EL} factors are in the order of 10^{-3} with an EQE over 21% (Figure 29 and Table 4) [304]. In 2019, they reported two series of chiral red cyclometalated Ir(III) complexes **77** and **78** based on sulfur atom containing axially chiral derivatives, and the corresponding CP-OLEDs show an EQE of 23.7% with low efficiency roll-off as well as g_{EL} factors around 5×10^{-4}. Recently, they introduced phosphine chirality to the ancillary ligand and the blue Ir(III) complex **79** with double chiral centers was separated into four enantiomers with $|g_{lum}|$ around 1.4×10^{-3} [306]. The CP-OLEDs exhibited an EQE of 13.3% with $|g_{EL}|$ about 2.0×10^{-3}.

To improve the device efficiency, researchers also applied double emissive layers in CP-OLEDs for chiral Pt(II) complexes [307] and TADF materials [308–312]. For example, in 2020 Zheng and co-workers [307] prepared a pair of deep-red platinahelicene enantiomers (*P*/*M*)-**80** peaking at 653 nm, which showed a $|g_{lum}|$ of 6×10^{-3}. Moreover, the evaporated CP-OLEDs displayed an EQE of 4.6% as well as the $|g_{EL}|$ in the order of 10^{-3}.

So far, CP-OLEDs demonstrated by various research groups have exclusively focused on bottom-emission devices. In 2020, Pieters group [313] fabricated the top-emission CP-OLEDs, which meet the requirements of silicon-based high-resolution microdisplay technology, paving the way to other microelectronics-related photonics applications.

To present, most CP-OLEDs show lower g_{EL} than g_{lum} factors, except for the chirality transfer from the guest to host. One main reason is the spiral direction of CP light would reverse after the reflection from cathode, which would impair the degree of circular polarization. For instance, Bari and co-workers measured the CP photoluminescence of the $CsEu(hfbc)_4$ blend film covered with 100 nm Al film (glass/$[CsEu(hfbc)_4$+host]/Al) by exciting and collecting light from the glass side and found that the g_{PL} value was lowered to −0.11 at 595 nm from −1.21 in the uncovered film [297]. In corresponding CP-OLEDs, the g_{EL} values were also found to decrease significantly when a thick layer of Al cathode was used [297]. Therefore, to reduce this effect, devices with aluminum/silver (Al/Ag) as semitransparent cathode were deposited as cathode, and the CP-OLEDs showed equally g_{EL} than g_{PL} factors. For example, in 2019, Zheng and Zhou groups [314] reported a pair of platinahelicene enantiomers (*P*/*M*)-**81** featuring superior configurational stability with $|g_{PL}|$ factors about 4×10^{-3}, and the CP-OLEDs exhibited an EQE of 18.81% with $|g_{EL}|$ factors 0.0011–0.0016. To suppress the effect of reverse CPEL signal from the cathode reflection, the further implementation of semitransparent aluminum/silver cathode successfully boosts up the $|g_{EL}|$ by over three times to 5.1×10^{-3}. Recently, Yang, Zheng and Zhou groups [315] reported two green chiral iridium(III) isomers (Λ/Δ)-**82** containing dual stereogenic centers at iridium and ancillary ligand. The CP-OLEDs showed excellent performances with the EQE of 30.6% and g_{EL} in the 10^{-4} order of magnitude. By using semitransparent cathode, the resulting g_{EL} values are significantly boosted by one order of magnitude, up to 7.70×10^{-3}. Furthermore, this strategy was also applied in CP-OLEDs based on chiral TADF materials [316]. The regular CP-OLEDs showed g_{EL} values at the degree of 10^{-4}, and the semi-transparent devices exhibited $|g_{EL}|$ factors around 4.6×10^{-3}.

To sum up, chiral luminescent molecules and CP-OLEDs have potential application for 3D displays and the device efficiencies have already drawn near to the theoretic limit in some reports. But the main challenge is to realize good device performances with high enough g_{EL} factors (> 1 at least). However, some chiral polymers with helical structures after annealing and Eu(III) complexes based CP-OLEDs showed g_{EL} factors higher than 1 with low efficiency. The chiral phosphorescent materials display excellent device efficiencies, but the $|g_{EL}|$ ranging from 10^{-4} to 10^{-2} is still far from satisfactory. Considering the g_{EL} factors are mainly determined by the g_{PL} factors of chiral luminescent materials, we believe that the helical phosphorescent materials or polymers would be promising candidates for CP-OLEDs with both high efficiency and *g* factors. In addition, chiral TADF materials are another kind of important candidate for highly-efficient CP-OLEDs, which will be discussed in the following section.

3.2 CP-OLEDs based on chiral TADF molecules

TADF emitters have been used as new-generation luminescent materials to fabricate highly efficient OLEDs [316–319]. Owing to the efficient up-conversion process of TADF materials with small singlet-triplet splitting energy (ΔE_{ST}), TADF materials can result in purely organic electroluminescence with theoretically 100% internal quantum efficiency (IQE), and the efficiencies of TADF-based devices are comparable to those of phosphorescent emitters, which have even surpassed 30%. Combination of TADF emitter and chiral unit provides the most effective way to realize the fabrication of high efficiency CP-OLEDs [20].

In 2015, Imagawa *et al.* [320] reported the first chiral TADF molecules (*R*/*S*)-**83** (Figure 30) with CPL properties. The enantiomers showed ΔE_{ST} of 0.19 eV in doped film, and exhibited mirror-image CD signals and CPL ($|g_{lum}|$ were 1.1×10^{-3}) properties in toluene. Unfortunately, the devices based on the enantiomers have not been achieved, and their CPEL properties have not been detected as well. One year later, Pieters *et al.* [321] reported a pair of chiral TADF emitters (*R*/*S*)-**84** with CPL activities, which consisted of a chiral perturbing moiety (binaphthol unit) and a TADF emitter moiety. It was found that the chirality of binaphthol could be well transferred to the TADF emitter, which made the enantiomers emit CP light. The chiral TADF emitters showed high photoluminescence quantum yield (PLQY) of up to 74% and mirror-image CPL activities with the $|g_{PL}|$ value of 1.3×10^{-3}. Furthermore, the devices fabricated with (*S*)-**84** displayed maximum current efficiency (CE_{max}) of 34.7 cd/A, PE_{max} of 16.3 lm/W, and EQE_{max} of 9.1%. However, the CPEL properties of the devices were still not studied.

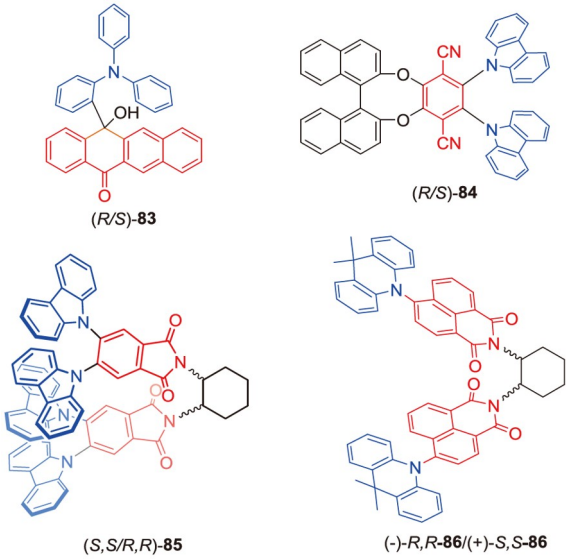

Figure 30 Structures of chiral TADF molecules (*R*/*S*)-**83**, (*R*/*S*)-**84**, (*R*,*R*/*S*,*S*)-**85**, and (*R*,*R*/*S*,*S*)-**86** (color online).

In 2018, Chen's group [22] reported a pair of chiral TADF emitters (*S*,*S*)- and (*R*,*R*)-**85**, which were designed by combining achiral aromatic-imide-based TADF enantiomers with chiral 1,2-diaminocyclohexane. The enantiomers displayed high excellent photophysical properties and mirror-image CD and CPL properties. Notably, the CP-OLEDs based on the enantiomers not only achieved maximum EQE (EQE_{max}) of up to 19.7% and 19.8%, respectively, but also displayed opposite CP electroluminescence (CPEL) signals with g_{EL} values of -1.7×10^{-3} and 2.3×10^{-3}, respectively (Table 4). This represented the first CP-OLEDs based on the enantiomerically pure TADF emitters with both high efficiencies and intense CPEL properties. Recently, Chen *et al.* [322] have conveniently synthesized a couple of 1,8-naphthalimide-based chiral emitters (*R*,*R*)- and (*S*,*S*)-**86**. The enantiomers exhibited high thermal stability with decomposition temperature of 405 °C, excellent electrochemical properties and TADF properties with small ΔE_{ST} of 0.07 eV. Moreover, the emitters also showed obvious mirror-image CD and CPL properties. By using the enantiomers as emitters, the OLEDs with the bands centered at 592 nm achieved high EQE_{max} values of 12.4% and 12.3%, respectively.

Based on the chiral perturbation strategy similar to that of Pieters' work, Tang's group reported a series of chiral AIEgens (*R*/*S*)-**87**–(*R*/*S*)-**90** in 2018 (Figure 31) [323]. These chiral AIEgens with TADF activities emitted light ranging from green to red. Moreover, these emitters displayed good photophysical properties with Φ_F of 0.05–0.38 in neat films and exhibited mirror-image CPL properties with the $|g_{lum}|$ values of 2.0×10^{-2}–4.1×10^{-2} in neat films. The chiral AIEgens were further used as the dopant and neat film to fabricate CP-OLEDs. The multicolour electroluminescence from 493 to 571 nm for doped film-based CP-OLEDs and from 537 to 597 nm for neat film-based CP-OLEDs was achieved. Among them, the obtained doped and nondoped CP-OLEDs based on the enantiomers (*R*/*S*)-**87** exhibited EQE_{max} of 9.3% and 3.5%, respectively, and they also showed large g_{EL} values of +0.026/−0.021 and +0.06/−0.06.

Recently, Huang *et al.* [324] reported two pairs of chiral TADF emitters (*R*/*S*)-**91** and (*R*/*S*)-**92** based on the chiral perturbation strategy and then constructed vacuum-deposited and solution-processed CP-OLEDs. It was found that the emitters exhibited high PLQYs, good TADF properties, good solubility, excellent optical stability, as well as mirror-image CD and CPL properties. Moreover, the sky-blue CP-OLEDs based on (*R*/*S*)-**91** and (*R*/*S*)-**92** displayed EQE_{max} of 8.4%/12.4% and $|g_{EL}|$ values of 4.0×10^{-4}–5.5×10^{-4} and 6.0×10^{-4}–8.6×10^{-4}, respectively, in the vacuum-deposited devices, as well as EQE_{max} of 10.1%/10.6%, and $|g_{EL}|$ values of 2.5×10^{-3}–3.7×10^{-3} and 3.5×10^{-3}–3.9×10^{-3}, respectively, in the solution-processed devices. This work also promoted the development of solution-processed CP-OLEDs based on chiral TADF emitters.

To optimize the efficiencies of CP-OLEDs, Zheng *et al.* [309] reported the diphenylamine-based TADF emitters (*R*/*S*)-**93** based on chiral octahydro-binaphthol (Figure 32). Compared with TADF molecules (*R*/*S*)-**84**, (*R*/*S*)-**93** exhibited slightly better optical property with the PLQY of 84.67% and $|g_{lum}|$ values of about 2.0×10^{-3} in films. Then, non-doped and doped CP-OLEDs based on (*R*/*S*)-**93** were fabricated, which displayed the EQE_{max} of 12.4% and $|g_{EL}|$ value of 2.9×10^{-3}. Using the same strategy, their group also reported carbazole-based chiral TADF emitters (*R*/*S*)-**94** and corresponding CP-OLEDs [308]. These chiral emitters

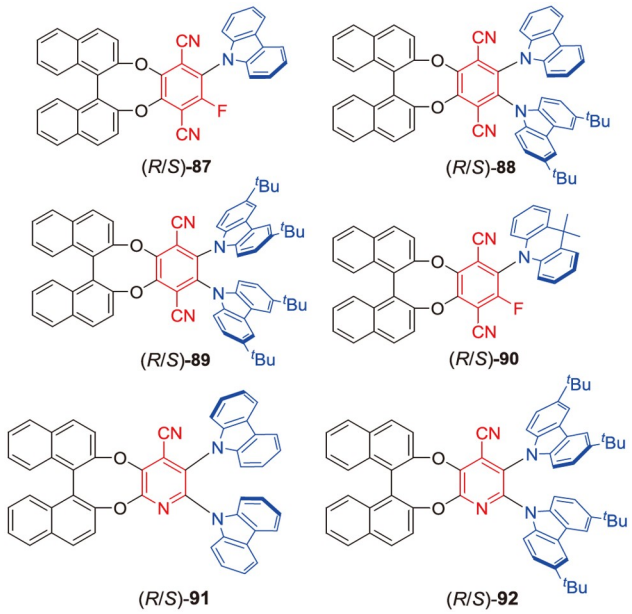

Figure 31 Structures of chiral TADF molecules (*R*/*S*)-**87**–**92** (color online).

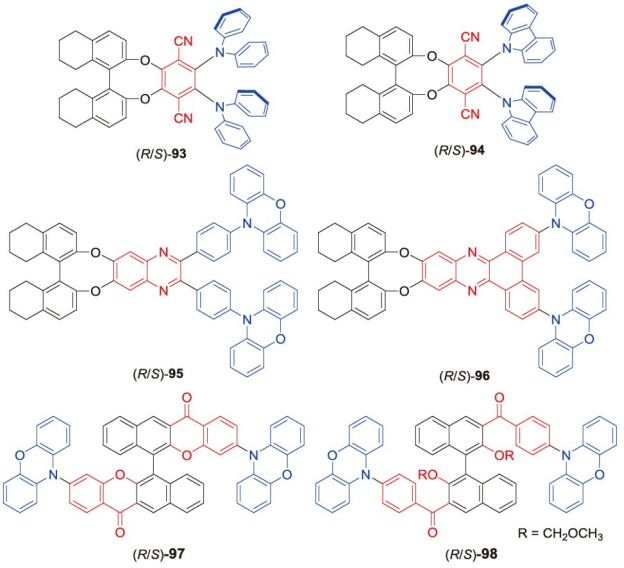

Figure 32 Structures of chiral TADF molecules (*R*/*S*)-**93**–**98** (color online).

exhibited excellent TADF properties with low ΔE_{ST} of 0.037 eV, high PLQY of 92% and $|g_{lum}|$ value of 4.24×10^{-3} in film. When the chiral emitters (*R*/*S*)-**94** were used to fabricate CP-OLEDs with dual emissive layers, the $|g_{EL}|$ value of 2.0×10^{-3} was displayed. Notably, the devices exhibited high EQE_{max} of 32.6% and low efficiency roll-off, which represented the highest efficiency of CP-OLEDs based on chiral TADF materials so far.

Based on the chiral perturbation strategy, Tang *et al*. [311] recently constructed two pairs of red color chiral emitters (*R*/*S*)-**95** and (*R*/*S*)-**96** by combining chiral octahydrobinaphthol and red TADF luminescent subunit. The chiral moiety successfully induced the chirality of the molecules in the ground and excited states, and the two pairs of chiral emitters showed obvious mirror-imaged CPL properties. The g_{lum} values of (*R*/*S*)-**95** and (*R*/*S*)-**96** are $-4.6 \times 10^{-4}/4.0 \times 10^{-4}$ and $-1.4 \times 10^{-3}/1.9 \times 10^{-3}$, respectively. Moreover, **95** and **96** showed obvious TADF properties, in which the ΔE_{ST} values are 0.16 and 0.07 eV, and PLQYs are 92% and 89%, respectively. The planar conjugation degree of the receptor subunit of **96** is greater than that of **95**, which led to the lower LUMO level of **96** and the red shift of the emission wavelength of **96** compared to that of **95**. CP-OLEDs based on (*R*)-**95** and (*R*)-**96** showed yellow and orange emission, respectively. The maximum EQEs of the devices are 28.3% and 20.3%, respectively. Obvious CPEL signals were also detected in the devices based on the chiral emitters. The $|g_{EL}|$ value of CP-OLED based on (*R*/*S*)-**96** is 2.4×10^{-3}, which is higher than that of (*R*/*S*)-**95** device (6.0×10^{-4}).

In 2019, Cheng, *et al*. [303] reported two pairs of chiral TADF molecules (*R*/*S*)-**97** and (*R*/*S*)-**98**. It was found that the chiral molecules all exhibited AIE and TADF properties, while only (*R*/*S*)-**97** showed mirror-imaged CPL properties with g_{lum} values of -0.9×10^{-3} and $+1 \times 10^{-3}$, respectively. Moreover, CP-OLEDs based on (*R*/*S*)-**97** in neat films and doped films were fabricated. Although these devices exhibited high L_{max} of 11,783 cd/m^2, the EQE_{max} of nondoped devices were just 0.12%/0.22% for (*R*/*S*)-**97** and 0.85%/1.8% for (*R*/*S*)-**98**, respectively. The g_{EL} values of the nondoped and doped CP-OLEDs based on (*R*/*S*)-**97** were -0.42×10^{-3}/0.58×10^{-3} and $-0.9 \times 10^{-3}/1.0 \times 10^{-3}$, respectively.

With indolo[2.2]paracyclophane as the chiral donor, Zysman-Colman *et al*. [325] synthesized a pair of chiral TADF emitters (R_p/S_p)-**99** (Figure 33). The emitters (R_p/S_p)-**99** displayed sky-blue CPL (λ_{em} at 480 nm) with g_{lum} values of -1.2×10^{-3} and 1.3×10^{-3}, respectively. Although those emitters were used to fabricate OLEDs and they displayed sky-blue EL with EQE_{max} of 17%, their CPEL properties had not been studied as well probably due to the racemization of the chiral emitters at high temperatures during the fabrication of devices. If problem of the racemization could be solved, the TADF emitters based on planar chirality would be new potential CPL materials for CP-OLEDs.

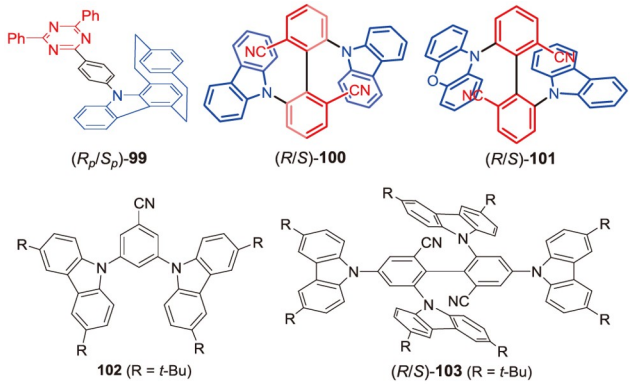

Figure 33 Structures of chiral TADF molecules (R_P/S_P)-**99**, axial TADF enantiomers (*R*/*S*)-**100**, (*R*/*S*)-**101**, **102**, and (*R*/*S*)-**103** (color online).

Recently, Chen's group [326] proposed a chiral emitting skeleton strategy for designing axial TADF enantiomers, and thus fabricating CP-OLEDs with both high EQE_{max} and large g_{EL} values. Consequently, the enantiomers (*R*/*S*)-**100** with rigid chiral axis obtained by coupling two fluorophores exhibited excellent TADF property with small ΔE_{ST} of 0.029 eV, short delayed fluorescence lifetime (12.6 μs) and mirror-image CPL activity with $|g_{lum}|$ of about 5×10^{-3}. Moreover, the axial enantiomer-based CP-OLEDs emitted blue electroluminescence (λ_{EL} = 468 nm) with the EQE_{max} of 12.5% and 12.7%, respectively, and intense CPEL with g_{EL} values of -1.2×10^{-2} and $+1.4 \times 10^{-2}$, respectively. This work not only represented the first blue CP-OLEDs based on TADF enantiomers, but also provided a promising design for chiral luminescent materials with both high efficiencies and large g_{lum} values. A little later Zheng's group [327] reported one pair of axis chiral TADF emitters (*R*/*S*)-**101** with one phenoxazine and one carbazole as the donors. The highly twisted molecular structure gave the emitters excellent TADF properties, and their ΔE_{ST} was only 0.04 eV and fluorescence life was 1.1 μs. Moreover, the PLQY was up to 86.1%, and the g_{lum} of (*R*/*S*)-**101** in the doped film reached -1.72×10^{-2} and 1.85×10^{-2}, respectively. The EQE_{max} value of CP-OLED based on the TADF enantiomer was 16.6%, and it was accompanied by extremely low efficiency roll off. In addition, the devices based on (*R*/*S*)-**101** showed symmetrical CPEL signals, and the value of $|g_{EL}|$ was 4×10^{-3}. More recently, Chen *et al*. [328] also synthesized an axially chiral TADF emitter (*R*/*S*)-**103** with dual emitting core by coupling two identical TADF emitters of **102**. It was found that (*R*/*S*)-**103** with twisted rigid conformation displayed smaller ΔE_{ST} (0.05 eV) and higher PLQY (74%) than those (0.33 eV and 29%) of **102**. Particularly, compared with that (5.3%) of **102**, the devices based on (*R*/*S*)-**103** showed significantly enhanced EQE (20.8%), which was also the highest EQE_{max} based on the dual emitting core strategy so far. Moreover, the enantiomers (*R*/*S*)-**103** also exhibited mirror-imaged CD and CPL properties, and their g_{lum} values

were $+5.4 \times 10^{-3}$ and -5.0×10^{-3} in toluene, respectively. To our knowledge, (*R*/*S*)-**103** were also the first chiral TADF emitter with dual emitting core.

In 2020, Jiang's group [329] designed and synthesized two pairs of TADF enantiomers (*R*/*S*)-**104** and (*R*/*S*)-**105** based on space charge transfer strategy (Figure 34). The asymmetric carbon atoms in the molecules led to their central chirality. The donor and acceptor of the two chiral molecules were connected by the spirofluorene structure, and kept the face-to-face conformation, so that space charge transfer occurred between the donor and the acceptor, and the overlap between the highest occupied molecular orbital (HOMO) and the lowest unoccupied molecular orbital (LUMO) is small, which leads to their TADF properties. The donor units of **104** and **105** contain sulfur and oxygen atoms respectively. It was found that this slight difference has a great influence on their photophysical, PL and electroluminescence characteristics. Due to the high PLQY (90%) and high exciton utilization, **105** showed good electroluminescence performance in the doped devices, and the EQE_{max} was as high as 23.1%. As a comparison, the larger sulfur atoms in **104** introduced the heavy atom effect, which led to the distortion of the main chain of the molecule and the extension of donor-receptor distance. Therefore, **104** has a lower PLQY and a faster non radiation attenuation rate. The results showed that the EQE_{max} value of **104** in doped device is 12.5%, which is far lower than that of the device based on **105**. Because the molecular structure distortion of **104** is higher than that of **105**, the value of $|g_{lum}|$ of (*R*/*S*)-**104** (4.0×10^{-3}) almost twice as much as that of (*R*/*S*)-**105** (2.2×10^{-3}). In addition, the obvious CPEL signals were detected in CP-OLEDs based on (*R*/*S*)-**104** and (*R*/*S*)-**105**. The corresponding g_{EL} values of (*S*)-**104** and (*S*)-**105** were 1.30×10^{-3} and 1.0×10^{-3}, respectively.

More recently, based on the strategy of space charge transfer, Zheng's group [330] reported one pair of blue TADF enantiomers (*R*/*S*)-**106** with central chirality, in which the donor of phenoxazine subunit and the receptor of sulfone moiety was connected by the spiro-carbon centre. It was found that the ΔE_{ST} of the enantiomers was 0.022 eV, and PLQY in the doped film was as high as 81.2%. CP-OLEDs based on (*R*/*S*)-**106** showed obvious CPEL signals, and the value of $|g_{EL}|$ was as high as 3.0×10^{-3}, the maximum EQE was 20.0%. In addition, the device could still maintain 19.3% EQE at 1,000 cd/m^2, suggesting a very low efficiency roll off.

CP-OLEDs based on chiral fluorescent emitters could not only successfully achieve the CPEL, but also have the advantages of long device lifetime, good stability and low efficiency roll-off. Moreover, chiral fluorescent molecules with CPL activities are also cheap and easily available. However, the devices based on fluorescent emitters usually suffer low efficiencies for only 25% exciton utilization of the fluorophores, and the low efficiencies of fluorescent CP-OLEDs inevitably limit their practical applications. Therefore, how to improve the efficiencies of fluorescent CP-OLEDs is a key issue to be solved urgently. Recently, Chen's group [331] proposed a new strategy of TADF material sensitized CPL for improving the efficiencies of fluorescent CP-OLEDs. As a result, one pair of helicene-based enantiomers (*P*/*M*)-**107** were synthesized. The enantiomers with the rigid helical π-skeleton had highly thermal and enantiomeric stabilities, and they also showed excellent photophysical properties, especially, mirror-image CPL activities with large $|g_{lum}|$ value of about 6×10^{-3}. Notably, the CP-OLEDs with the helicene enantiomers as emitters and a TADF molecule as sensitizer not only displayed better performance of lower turn-on voltage (V_T) of 2.6 V, four-fold EQE_{max} of 5.3%, and lower efficiencies roll-off of 1.9% at 1,000 cd/m^2, than those without TADF sensitizer, but also exhibited intense CPEL with the g_{EL} values of -2.3×10^{-3} and $+3.0 \times 10^{-3}$. Meanwhile, this also represents the first thermally activated sensitized fluorescent CP-OLEDs with markedly improved efficiencies and intense CPEL.

More recently, Chen's group [332] reported a couple of fluorescent enantiomers (*R*,*R*/*S*,*S*)-**108**, which are suitable for the emitters of high-efficiency TADF-sensitized CP-OLEDs. It was found that the enantiomers showed configurational stability, high PLQY of 98%, large k_r of 7.8×10^7 s^{-1}, and intense CPL activity with $|g_{lum}|$ value of about 2.5×10^{-3}. Notably, by using matchable TADF sensitizer, the enantiomers were then exploited as emitter to fabricate CP-OLEDs. Consequently, the TADF-sensitized CP-OLEDs not only showed mirror-image CPEL activities with g_{EL} values of $+1.8 \times 10^{-3}$ and -1.4×10^{-3}, but also displayed fast start-up featuring with low V_T of 3.0 V as well as driving voltage of 4.84 V at 10,000 cd/m^2. Meaningfully, the TADF-sensitized fluorescent device showed high EQE_{max} of 21.5% and

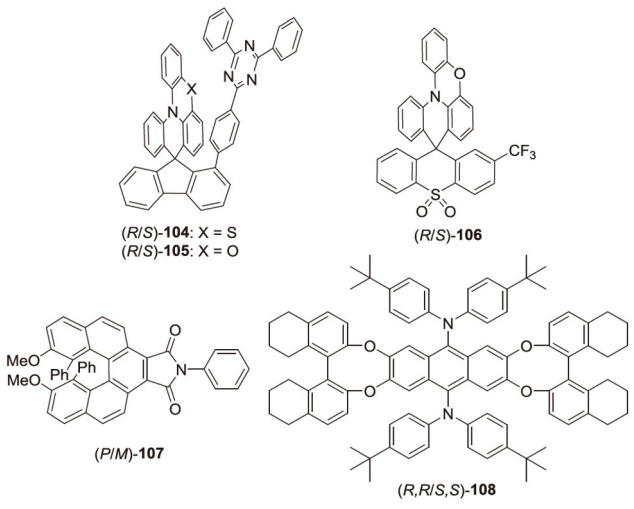

Figure 34 Structures of chiral TADF emitters **104**–**108**.

extremely low efficiency roll-off, whose EQEs were 21.2% and 15.3% at 1,000 and 10,000 cd/m^2, respectively. This result provides a promising perspective to break through the EL efficiency limit of CP-FL emitters.

Although more and more TADF-based chiral materials have been reported for fabricating CP-OLEDs with CPEL properties in the past three years, this research area is still in its infancy. The development of new TADF-based chiral emitters with both high PLQYs and large g values will always be the particular focus and first target of this research area. Moreover, new strategies for the efficient construction of various CPEL materials with high EQE and large g_{EL} values need to be explored. Notably, the strategy for the TADF-sensitized CP-OLEDs with fluorescent materials as the emitters will attract increasing interest and become one of the most important and hot topics in this research areas. Developing new device structures, mechanisms and technologies of CP-OLEDs based on the chiral emitters will also be very important for improving the device performances. More importantly, how to achieve the practical applications of CP-OLEDs in such as 3D displays, optical data storage, and optical spintronics, as well as encryption and anti-counterfeiting will be the challenge and ultimate goal. Undoubtedly, with the development of TADF-based chiral emitting materials, the CPEL researches based on the OLEDs are attracting more and more interest and becoming a frontier and hot topic in the research area of luminescent materials.

3.3 CP light photodetection

Traditionally, to distinguish the information in the CP light, the light should first pass through a quarter-wave plate and be changed to LPL. Then, the obtained LPL passes through a polarizer with the known polarized direction and is detected by an ordinary photodetector. However, this traditional method contains complex optical components, which hinders the miniaturization and integration of CP light detection devices [333].

Chiral materials have a non-centrosymmetric structure different from their mirror image and cannot overlap each other, exhibiting a nonlinear optical response to CP light in the CD spectrum. Chiral materials thus show great potential for application in optoelectronic devices based on the polarization light. In recent years, chiral materials have been attracted the attention of CP light detectors. In this section, the chiral-materials-based CP light photodetectors are summarized, including chiral organic-based CP light photodetectors, patterned inorganic nanostructure (metamaterial) CP light photodetectors, and chiral organic-inorganic perovskite CP light photodetectors. The progress, as well as the strategies for promoting the performance of the CP light photodetectors, are discussed in detail.

3.3.1 Principles for CP light photodetectors

The CP light response of the specific photodetectors comes from the different responses of chiral materials to left-handed CP (L-CP) or right-handed CP (R-CP) light. Usually, chiral materials exhibit a unique optical response to the corresponding CP light, which can be described by CD. Specifically, CD is defined as the difference in the absorption ability for L-CP and R-CP light. Particularly, the anisotropy of CD (g_{CD}) can be derived from Eq. (2) shown in the Introduction section. Therefore, when irradiated by different CP light, the resulting photogenerated photocurrent in the chiral active layer is different. As a result, the CP light can be distinguished as the per difference in the value of the device's output current. And the device performance can be evaluated by the dissymmetry factor (g_{res}), which is defined as Eq. (6):

$$g_{res} = \frac{2(R_L - R_R)}{R_L + R_R} \quad (6)$$

where R_L and R_R are the responsivities for L-CP and R-CP light, respectively.

3.3.2 CP light photodetectors based on chiral organic molecules

Chiral organic semiconductor materials have attracted great attention in light detection applications due to their large absorption coefficient and solution processability [334,335]. In addition, for chiral organic semiconductor materials, electronic energy band structure and photoelectric properties such as carrier transport ability can be adjusted through reasonable chemical synthesis processes, making them promising materials for the active layer of CP light photodetectors. Generally, chiral organic materials used for the active layer of CP light photodetectors can be classified as chiral organic small molecules, chiral supramolecules, and chiral conjugated polymers.

The study of the chiral organic small molecules for CP light photodetectors began with the work of Fuchter and Campbell *et al*. [336]. They demonstrated CP light-detecting organic field-effect transistors (OFETs), using the asymmetric purely chiral helicene **68** as the active layer (this molecule which has been discussed in Section 3.1 for CP-OLED application), have a highly specific response to CP light (Figure 35a). Under a 365 nm CP light irradiation, the drain current of the device was increased ten-fold, when the spin direction of the CP light matches that of the helicene molecule (Figure 35b, c). The obtained OFETs also show fast and reversible switching under the time-dependent circularly polarized photoresponse measurement, where a rise time of 2.6 ms close to the theoretical limit of sensitivity in these devices was achieved. The inspiring optoelectronic performance of the device stems from the large chiral spacing of the helicene molecules giving them highly specific photoresponse and strong CD. In addition, the fully conjugated

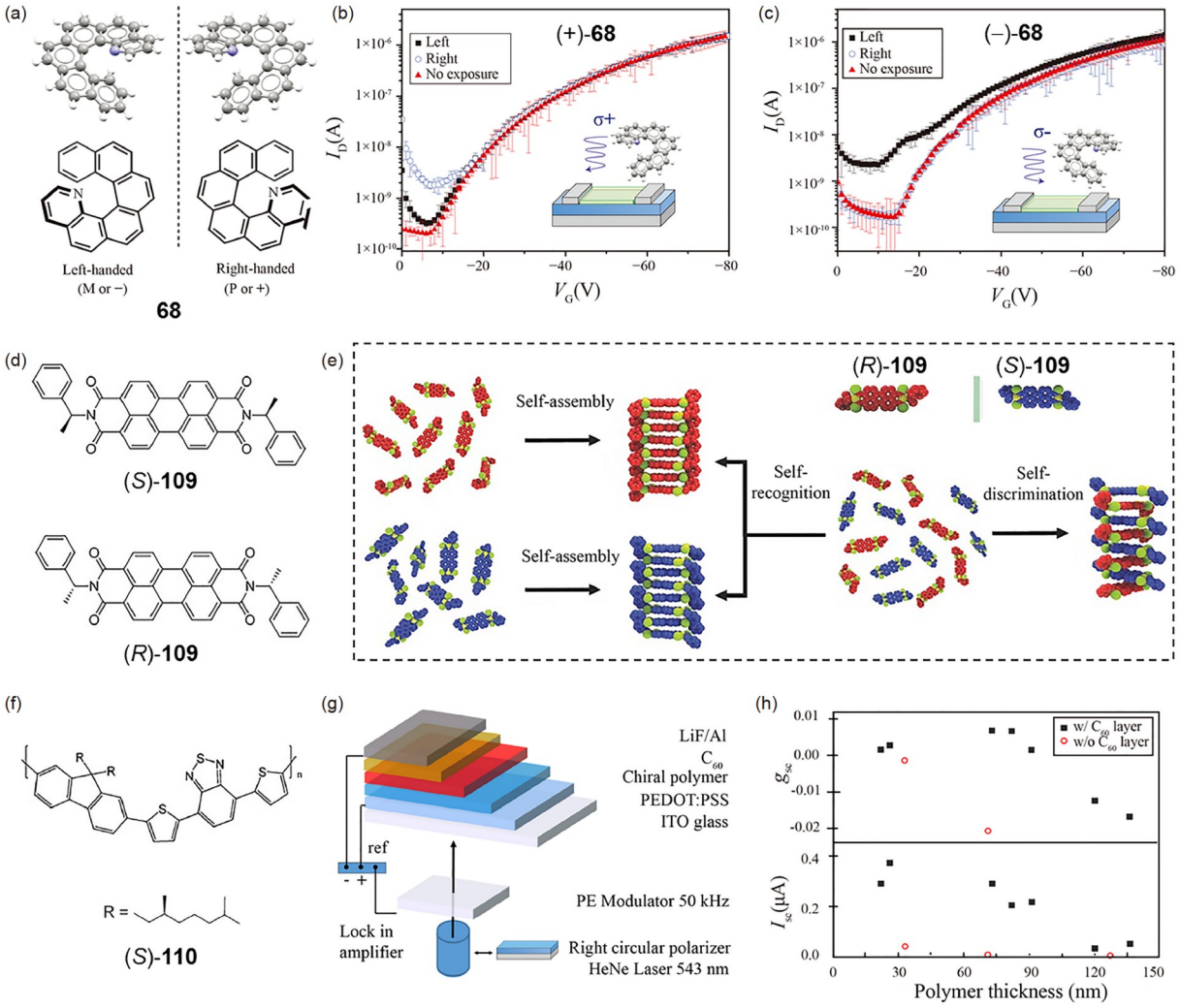

Figure 35 (a) Molecular structure of the left- and right-handed helicene **68**. (b, c) Response of (b) right-handed (+)-**68** and (c) left-handed (−)-**68** based OFETs upon exposure to different CP light [336]. (d) Molecular structure of the two helically chiral forms of **109**. (e) The self-sorting process in a mixed (*S*)- and (*R*)-**109** system [338]. (f) Molecular structure of the chiral polymer **110**. (g) The architecture of the photovoltaic cell and characterization system. (h) Circular selectivity in photocurrent generation (g_{sc}) and short-circuit photocurrent (I_{sc}) as the function of polymer thickness of **110** [339] (color online).

structure of this organic molecule is also essential for the transportation of photogenerated carriers.

Although chiral helicene molecules exhibit potentials in CP light detection, their electrical properties are strongly impeded by structural distortion of these helical aromatic rings, which reduces the dense stacking of solid-state film. The disturbed π-conjugation is unfavorable for electron delocalization. Besides, the helicene molecules usually only show chiral optical response in the UV and near-blue region, due to the small π-planes structure. To further improve the electrical performance of helicene-based CP light detectors and extend their applications in NIR light regions, Zhang *et al*. [337] reported a backbone incorporation method to combine the helicene with perylene diimide (PDI) possessing high carrier mobility and electron affinity. The obtained ortho-π-extended PDI double-[7] heterohelicene inherited well the high chirality and electron mobility from two-parent skeletons, and obtained NIR absorption and bipolar charge carrier transport ability. The corresponding OFETs thus show obvious and fast real-time photocurrent response with an asymmetry factor g_{res} of +0.010 and −0.009 under NIR CP light irradiation (λ = 730 nm, 1,400 μW/cm^2).

In addition to chiral small organic molecules, asymmetric supramolecular nanostructures can also be applied for CP light detection. Supramolecular nanostructures exhibit shorter π-plane distances and larger π-plane overlap as well as higher asymmetry factors than their monomeric analogues, due to the inerratic and dense molecular stacking form. Shang *et al*. [338] synthesized *N*,*N*′-bis-(1′-phenylethyl) perylene-3,4,9,10-tetracarboxyldiimide (*R*/*S*)-**109** as *n*-channel semiconductors containing chiral substituents (Figure 35d). Through a simple liquid phase self-assembly process, they prepared the chiral supramolecular nanowire (Figure 35e). Due to the trap-free molecular stacking and the

high crystallinity nature in the nanowires of **109**, the corresponding OFETs have a lower charge carrier transport barrier. In disordered films, the larger π-plane distance and less π-plane overlap hinder the charge transfer. In addition, the trap-induced charge carrier recombination in the amorphous region reduces the exciton dissociation efficiency, which further makes the devices exhibit a smaller exciton diffusion length and separation charge mobility. In the self-assembled supramolecular structures with high crystallinity, the chiral center is transferred from chiral small molecules to aggregates. The enhanced chirality of the supramolecular structures thus helps to distinguish CP light detection. OFETs based on **109** nanowire thus have much larger photocurrent variation under CP light irradiation than that of random film-based devices.

Conjugated polymers are also promising candidates for CP light detection, considering their extended large-π structures provide excellent electric properties. In fact, the first integrated device used for CP light detection was a polymer photodiode based on the poly(fluorene) copolymer **110** containing a chiral alkyl substituent (Figure 35f, g) [339]. In this example, poly(fluorene) copolymer films were obtained by alternating copolymerization of fluorene and di-thienyl benzothiadiazole. The obtained film showed a significant difference in the absorption under left-handed and right-handed CP light. The absorbance circular polarization of a 130 nm thick film is about −0.055 when exposed to CP light at 543 nm. The huge CD response of the film may be related to the existence of the CLCs phase. CLCs phases exhibit strong chiral selectivity due to the inherent periodic helical structure, which can reflect CP light with the same spin direction but absorb CP light with the opposite spin direction [340]. Moreover, the magnitude and sign of the circular selectivity of the generated photocurrent in the photodiode also show a high dependence on the thickness of the active layer. At a moderate active layer thickness (70–80 nm), the g_{res} reaches a maximum of ~0.007 (Figure 35h).

Conjugated polymer/chiral small molecule heterojunction films offer a practical solution for achieving both chiral amplification effect and good electrical properties. Kim *et al.* [341] obtained chiral optically active semiconductor films by mixing non-chiral polymer poly(3-alkylthiophene) (P3CT) and a general-purpose chiral molecule 1,1′-binaphthyl–2,2′-diamine (BN). In this hybrid film, chirality in small molecules extends to the non-chiral conjugated polymer, since that the intermolecular interactions between the two materials are an important chiral transfer mechanism [2]. The controllable phase separation and crystallization process of the mixture system also induces the formation of vertically separated heterojunction with top BN and bottom P3CT/BN mixture structure. The photoluminescence excitation results show that after hybridization with BN, the energy state density near the LUMO of P3CT increased, and two energy levels closer to the energy level of the BN molecule are newly generated. The electronic energy level reconstruction in the hybrid film thus makes the energy transfer from BN to P3CT more favorable. Photodiode using this hybrid heterojunction film was also fabricated. The device showed a highly specific response to CP light, and achieved an average g_{res} of 0.1. Chiral induction of achiral polymers also demonstrated a novel method for enabling direct CP light photodetectors of achiral organic semiconductors. Cheng *et al.* [342] demonstrated that the chirality of the external light source can induce circular polarization sense of the devices. Thus, the circular polarization resolution of these OFETs is achieved by external irradiation of the CP light instead of the use of chiral additives.

3.3.3 CP light photodetectors based on patterned inorganic nanostructures

Although CP light detectors based on chiral organic molecules have been extensively studied, organic CP light detectors still show limitations in many application scenarios. Organic materials are commonly unstable under environmental conditions; besides, response time and operating wavelength of organic CP light detectors are also limited. Inorganic materials thus show potential in the construction of high-performance CP light detectors for their inherent stability and high carrier mobility. Generally, inorganic metals or semiconductor compounds can achieve chirality by constructing asymmetric microstructures. Moreover, surface plasmonic polaritons of chiral nanoparticles exhibit strong electric magnetic resonances. Chiroptical effects were thus enhanced due to the strong local electric-magnetic field interaction [343,344]. For example, circular polarizers based on 3D spiral nanowires have achieved CD up to 0.8 [345]. Therefore, patterning inorganic materials to form twisted metamaterials has been demonstrated effective strategy for preparing CP light photodetectors. Li *et al.* [346] reported a silver (Ag) chiral periodic supramolecular array with a "Z"-shaped unit cell (Figure 36a). The CP light detector based on this chiral supramolecular array also contains a dielectric spacer silicon (Si) layer, a poly(methyl methacrylate) (PMMA) spacer layer and a reflective metal backplate (Figure 36b). Under CP light irradiation, the chiral metamaterial absorbs specific chiral photons and generates high-energy hot electrons over the Schottky interface, resulting in detectable currents (Figure 36c). They also simulated the selective absorption or reflection of CP light radiated on the chiral metamaterial. They found that the left-handed chiral metamaterial showed near-uniform absorption of left-handed CP light while reflecting nearly 90% of the right-handed CP light at the resonant wavelength (~1,340 nm). The resulting CD signal thus reaches up to 0.9. The high CD further contributes to the high CP light discrimination of the CP light photodetector. Devices based on this chiral metamaterial

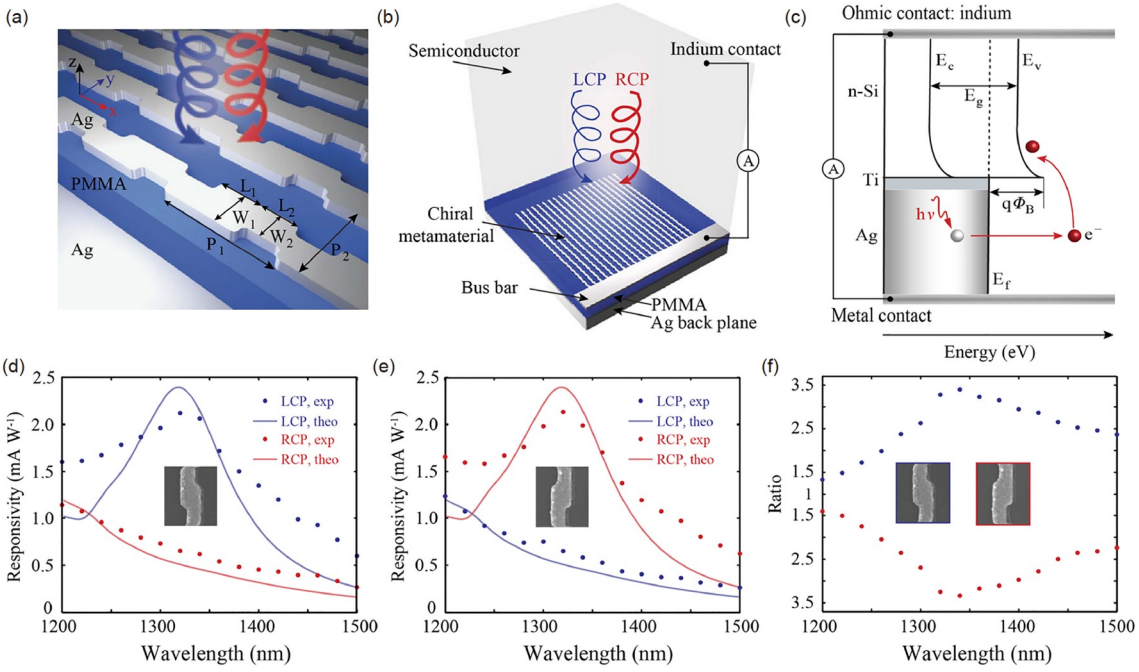

Figure 36 (a) Schematic of the Ag chiral periodic supramolecular array. (b) Schematic layout of the integrated CP light detector. (c) Energy band diagram and operating mechanism of the CP light detector. (d, e) Photoresponsivity spectra under different CP light illumination for CP light detector based on (d) left-handed and (e) right-handed metamaterials. (f) Photocurrent polarization discrimination ratio spectra for CP light detector based on left- and right-handed metamaterials [346] (color online).

achieved a photoresponsivity of 2.2 mA/W at the resonant wavelength, corresponding to a quantum efficiency of ~0.2%, a double improvement in efficiency compared to chiral OFETs (Figure 36d, e). This detector thus showed a huge CP light photocurrent difference and a polarization discrimination ratio (R_L/R_R) of 3.4 at 1,340 nm was achieved (Figure 36f). Similarly, Peng *et al*. [347] demonstrated CP light detectors based on chiral nanostructures with centrosymmetric "Y" shaped gold (Au) antennae. Such highly integrated photonic platforms simultaneously demonstrate the great potential for CP light imaging and sensing applications.

3.3.4 CP light photodetectors based on chiral organic-inorganic perovskites

In the early 2000s, Billing and co-workers [348,349] first synthesized chiral organic-inorganic perovskite single crystals. These chiral perovskites are composed of chiral small molecules and inorganic-frameworks, and most of them have 1D or 2D crystal structures. However, the optical physical properties of chiral perovskites have been systematically studied until 2017. Ahn *et al*. [350] revealed that the pure 2D perovskite with chiral organic cation (chiral-methylbenzylamine, *S*-MBA and *R*-MBA) exhibited opposite CD signals, depending on the configurations (*R* or *S*) of the enantiomers. In contrast, the racemic organic cations in the perovskite lattice did not induce the CD signal. In addition, the CD signal can be tuned by the morphology, thickness, and orientation of the film. The novel observation makes it possible for perovskite CP light photodetector.

Organic-inorganic perovskites typically have better optoelectronic properties than organic semiconductors [351,352]. Ma *et al*. [253,353] utilized chiral $(MBA)_2PbI_4$ to fabricate CP light photodetector (Figure 37a, b), and achieved a g_{res} of 0.23. However, the large single crystal of chiral $(MBA)_2PbI_4$ is difficult to grow. Besides, compared with 3D perovskite, large exciton binding energy and relatively poor carrier transport properties hinder the development of pure 2D perovskite. To solve these problems, Wang *et al*. [354] utilized a quasi-2D chiral $(\beta\text{-MPA})_2MAPb_2I_7$ (MPA: methylphenethylamine) film to fabricate CP light photodetector. The optimized device can reach a g_{res} of 0.2. In addition, the film can be fabricated on a flexible PET (polyethylene terephthalate) substrate, and exhibit negligible degradation after 100 cycles of bending. However, the CP light response spectral range and dissymmetry factor of the current perovskite CP light photodetectors still need to be improved. In addition to growing large single crystals, arranging chiral perovskites into an ordered array provides an efficient method to improve the performance of photodetection technology, as has been demonstrated in Section 3.3.3. In this context, Hu, Zhao and co-workers [355] recently fabricated large-scale single-crystalline nanowire arrays of $(S/R\text{-MBA})_2PbI_4$ through a micropillar template-assisted capillary-bridge rise approach, which showed excellent optoelectronic performance with the light ON/OFF

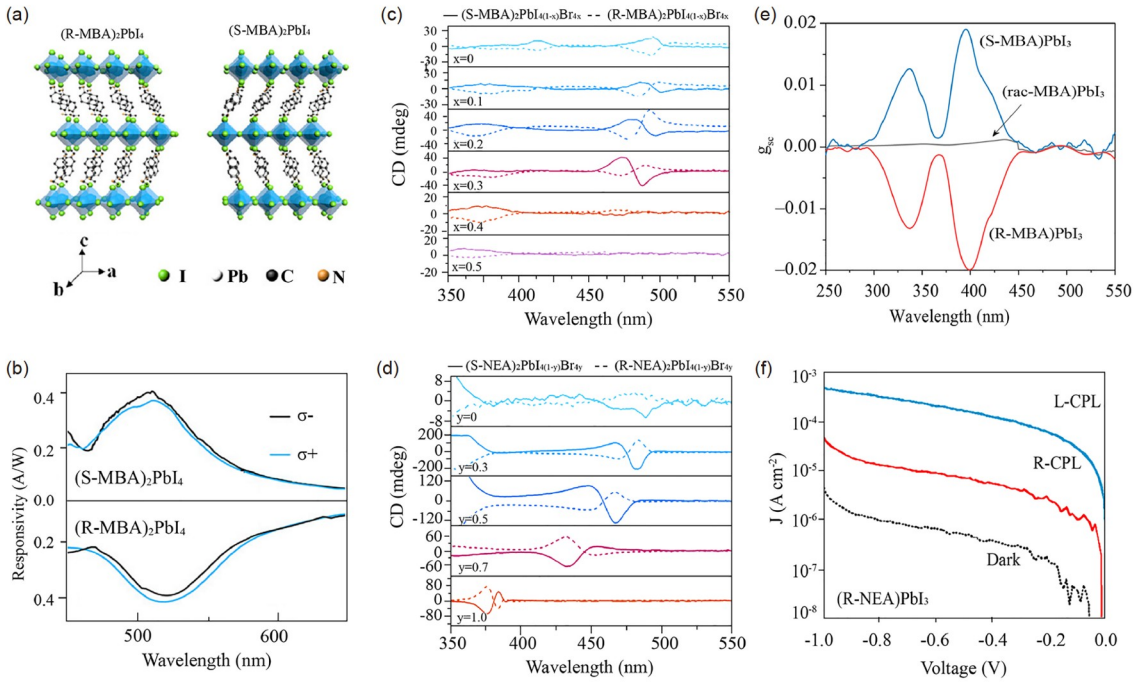

Figure 37 (a) The crystal structures of 2D chiral perovskite (*R*/*S*-MBA)$_2$PbI$_4$. (b) Spectral response of (*R*/S-MBA)$_2$PbI$_4$ based CP light photodetector [253]. CD spectra of (c) chiral (MBA)$_2$PbI$_{4(1-x)}$Br$_{4x}$ and (d) chiral (NEA)$_2$PbI$_{4(1-x)}$Br$_{4x}$ with different Br content [357]. (e) g_{CD} spectra of the (*R*/*S*-MBA)PbI$_3$ films [360]. (f) *J*-*V* curve of (*R*-NEA)PbI$_3$ CP light photodetector under L- and R-CP light at the wavelength of 395 nm, respectively [361] (color online).

ratio of 1.8 × 10^4, responsivity of up to 1.4 A/W, and anisotropy factor of 0.24 for photocurrent.

According to the previous report, due to the degenerate transition dipoles coupling, the strongest CD signal usually appears near the bandgap in the chiral perovskite. When the component of chiral perovskite changed, the crystal and electronic band structure will also change accordingly. Lu *et al*. [356] studied the chiral-optical properties of Pb-Sn alloyed (*R*/*S*-MBA)$_2$Pb$_{1-x}$Sn$_x$I$_4$ perovskites with different chemical components. Particularly, with different Sn alloys, the bandgap can be tuned from 2.31 to 2.52 eV, while the chiral activity extended from 500 to 300 nm according to the CD spectrum. Besides the Pb-Sn alloyed perovskite, the structure of chiral molecules and alloying of halides can also tune the chiral activity of the perovskite. Ahn *et al*. [357] found that increasing the ratio of Bromide in the perovskite can tune the chiroptical activity from 495 to 474 nm (Figure 37c). Further replacing the chiral MBA to chiral 1-(2-naphthyl)ethylamine (NEA), the CD signal can shift to 375 nm (Figure 37d). In general, the bandgap and chiroptical activity range of the perovskite can be easily tuned by the component engineering, similar to the pattern size adjustment of the inorganic metamaterial. The excellent CD performance gives them great potential in CP light detection.

For chiral perovskites, their different responses to *L*-/*R*-CP light may not only be ascribed to the difference in *L*-/*R*-CP light absorbance. The anisotropic response may also result from the inhomogeneous distribution of spin electrons due to the chirality-generated orbital angular momentum [358]. And the experiment results indeed demonstrated that the chiral perovskites have strong chiral induced spin selective (CISS) ability, which can enhance the anisotropy factor of the CP light photodetectors [359]. Therefore, some 1D perovskites with helix crystal structure and large spin-orbital coupling (SOC) were synthesized to fabricate the CP light photodetector.

Chen *et al*. [360] utilized the large chiral cation MBA to synthesize 1D (*R*/*S*)-MBAPbI$_3$ perovskite. The perovskite film exhibited a strong CD signal at 392 nm, as depicted in Figure 37e. The calculated g_{CD} (~0.02) of this 1D perovskite is about three times higher than its 2D counterpart [(*R*/*S*-MBA)$_2$PbI$_4$]. But the g_{res} of (*R*/*S*-MBA)PbI$_3$ is 0.1, which is still lower than those of (*R*/*S*-MBA)$_2$PbI$_4$. Subsequently, chiral NEA was applied to synthesize the 1D perovskite (*R*/*S*-NEA)PbI$_3$ by Ishii *et al*. [361]. The CD signal at 395 nm reached an amazing value of 3,000 mdeg, and the calculated g_{CD} (~0.04) was also twice of those of the (*R*/*S*-MBA)PbI$_3$. More importantly, as shown in Figure 37f, the R_L/R_R ratio is 25.4 (g_{res} = 1.92), which largely surpasses the inorganic metamaterials (usually < 4). This excellent performance may promote the applications of perovskite materials in the field of commercialized CP light detectors.

In this section, we have introduced the working mechanism of the CP light photodetectors and summarized their recent research progress. According to the composition of the active layer, we divided the CP light photodetectors into

three catalogs: chiral organic materials, inorganic metastructures, and emerging chiral hybrid perovskites. These types of mainly studied CP light photodetectors demonstrate impressive device performance. The wide sensing area, high responsivity and large anisotropy coefficient make these devices significant in many practical applications such as quantum communication and computing, encryption, and full stokes image. However, the development of CP light photodetectors is remaining fresh and fascinating. New materials with both high responsivity and large dissymmetry factor and multifunction and long-term stable CP light devices will receive increasing attention.

3.4 Recent advances in organic CP lasers and their display applications

Organic lasers that can generate strong coherent emission across full visible spectrum have attracted increasing attentions since the first appearance in the 1960s [362]. The combination of organic lasers with CP emission, which is defined as organic CP lasers, would not only show great promises in various applications ranging from optical communication to 3D displays, but also provide a powerful tool to investigate the chiral light-matter interactions. In this section, we summarize the latest advances in the field of organic CP lasers and corresponding applications in 3D displays.

3.4.1 Organic CP lasers

The key requirement to achieve organic CP laser is the combination of laser gain media and chiral environment. One typical strategy to enable CP lasing is the intracavity conversion from linearly polarized laser to CP laser by means of optical retardation. In 2008, Nunzi *et al*. [363] realized dynamic CP lasing based on a reflection pumping configuration by polarization modulation. By carefully controlling the interference of CP pumped laser beams, the refractive index of the dye-doped media was well-modulated and transient chiral photonic distributed feedback gratings were obtained, resulting in a CP laser emission output.

Another universal method to achieve CP laser through optical retardation is the utilization of chiral nematic liquid crystals as hosts for laser dyes [364–366], which has attracted wide attention since first discovered by Kopp and coworkers [367]. Due to their intrinsic twisting features, CLCs can form supramolecular helical assemblages. When laser dyes are encapsulated into the CLC media, the emission of gain materials can be selectively reflected by CLC with different circular polarization, and therefore CP laser emission can be achieved. In 2006, Furumi *et al*. [364] reported a detailed study of the chiroptical properties of dye-doped CLC laser systems. By tuning the ellipticity angle of the excitation beam, low-threshold CP lasing was achieved, which should be attributed to the collective effect of the ground-state chiroptical effect of achiral laser dye originating from the Borrmann effect in CLC media and the partial reflection of the obliquely incident light by CLC host.

Moreover, the physical parameters of the helicoidal superstructures in CLCs, such as helical pitch length, helical handedness and even the direction of the helical axis, can be dynamically manipulated by external stimuli, which is promising for tunable CP lasers. Yuan *et al*. [368] reported dye-doped CLC lasers with tunable wavelength and polarization in 2019 (Figure 38a). In the predesigned specific photoresponsive CLC system, reversible transformation of helical liquid crystal arrangement, among the common helicoidal helix, the special heliconical helix with different handedness, was achieved by carefully applying electric field and light exposure. This stimulus-directed diverse transformation in CLC superstructures provides new insights to the relationship between the nanoscale molecular interactions and the optical properties of the self-assembled superstructures for high-performance organic CP lasers. In addition to traditional CLC systems, strong CP laser emission was also reported by employing environmentally-friendly cellulose nanocrystals (CNCs) as chiral CLC media (Figure 38b) [162]. Owing to the oriented self-assembly of the CNCs, controlled chiral nematic structures as optical cavity were achieved and strong CP lasing with a dissymmetry factor up to 0.35 was further observed.

Although organic CP lasers based on optical retardation have been successively reported, direct generation and amplification of CP lasing from intrinsic chirality of gain media are extremely rare, which hinders the further investigation of chiral light-matter interaction for advanced CP laser applications. In 2017, de la Moya and co-workers [369] reported the direct CP laser emission from an enantiomeric couple of BODIPY-type laser dyes (*R*/*S*)-**111** (Figure 38c). In a transversally pumped cavity configuration, laser emission at 575 nm with efficiency as high as 68% was observed, which is the first demonstration of laser from any chiral compound so far. Nevertheless, the dissymmetric factor of the emission is too low to generate a detectable intrinsic CP laser signal, which should be attributed to the weak chiral light-matter coupling. Very recently, direct CP laser emission with high dissymmetric factor up to 0.29 was reported by Chen's group [370] (Figure 38d). By exploiting green fluorescent proteins and chiral biomolecules as gain materials, CP laser emission with two-order enhanced dissymmetry factor was demonstrated. Further studies discovered that the lasing dissymmetry factor is mainly determined by the molecular circular dichroism at lasing wavelength and this chirality enhancement reaches its maximum when the pump energy is near the lasing threshold. These results demonstrate that more information of chiral light-matter interactions can be revealed through the stimulated emission process, which not

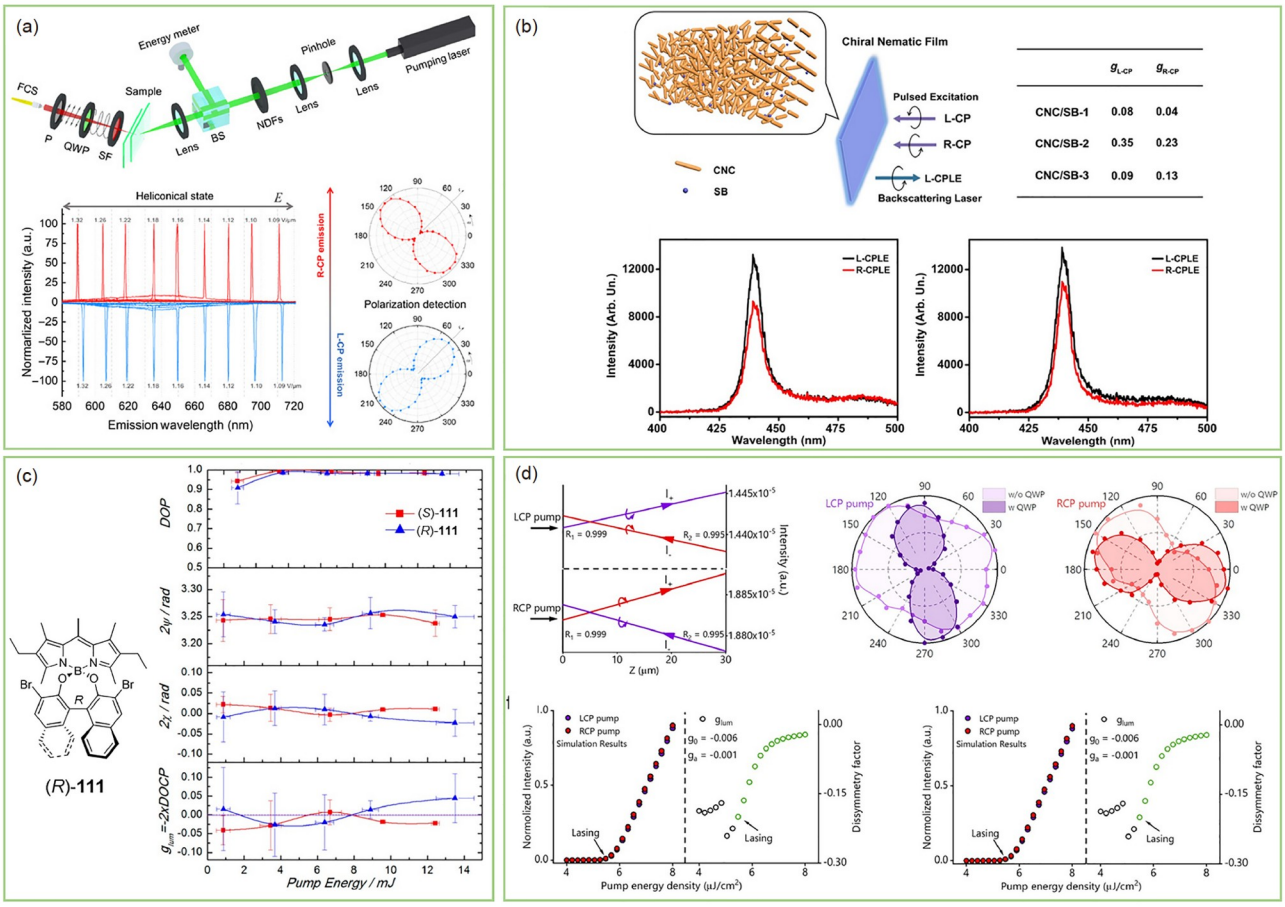

Figure 38 Latest advances in organic CP lasers. (a) Wavelength and polarization tunable CP lasing from the heliconical superstructure [368]. (b) Illustration of CNCs-based CP laser emission. SB = stilbene 420 [162]. (c) Laser emission polarization state parameters of chiral BODIPY dyes as a function of pump energy for a linear vertical pump polarization [369]. (d) CP lasing characteristics of fluorescein binding with chiral molecule in microcavity [370] (color online) (color online).

only provide more comprehensive insights into the chiral excited-state processes, but also promote the developments of advanced photonic devices.

3.4.2 3D displays based on organic CP lasers

Because of their capability to provide more abundant information to viewers than those in two-dimensional regime, 3D displays play an important role in modern display technologies [371], which is generally realized through linear-polarization-multiplexed approach. Direct emission of CP light could reduce perceived distortion and enhance contrast ratio of 3D displays [372], but the visual experience is limited due to their broadband emission. CP lasers allow for the implementation of 3D displays with wide color gamut, high saturation and so on, which therefore becomes an important branch of 3D displays. Very recently, Zhao *et al.* [373] reported the proof-of-concept full-color 3D laser displays based on chiral RGB microlaser arrays (Figure 39). The display panels were fabricated through microtemplate-assisted inkjet printing, comprising two sets of RGB microlaser pixel arrays with opposite CLC handedness. Benefiting from the intrinsic chiral superstructures of CLC matrix, ultrahigh circular polarization degree of the laser emission up to 1.6 was achieved, and stereoscopic images would be generated in viewer's mind by fusing together the two images with orthogonal CP laser emissions acquired by one's left and right eyes. These results offer a promising strategy for the development of self-emissive 3D laser displays and other lighting devices.

4 Summary and outlook

Intensive CPL research in the past decade has created extraordinary insights into photophysics, chemistry, and materials, while also launched applications in chiral photonics and electronics devices. As highlighted in the review, the electronic and magnetic transition dipole moments depend on the molecular structures of individual components as well as their aggregated structure. The CPL activity can be obtained from the intrinsic chirality of emissive materials, the chirality transfer or amplification chiral aggregates, or the

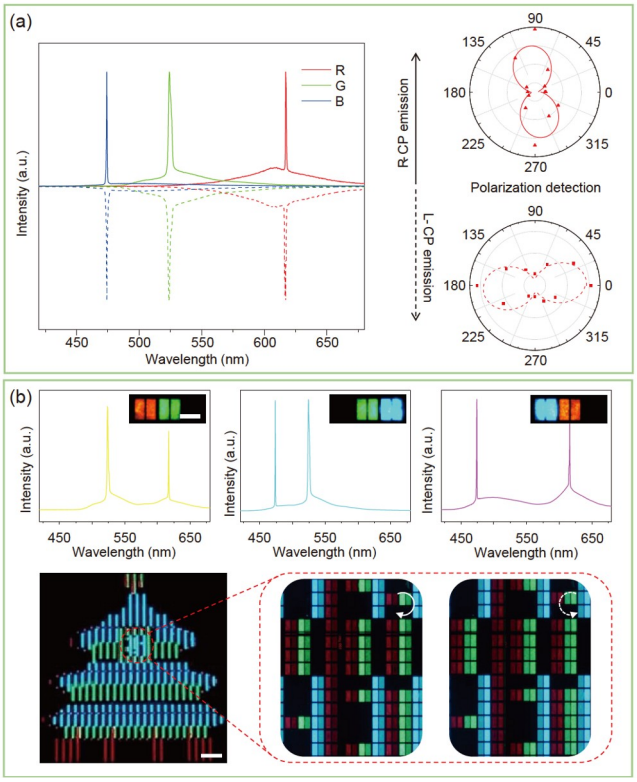

Figure 39 CLC-based 3D laser displays [373]. (a) CP lasing from the RGB CLC microunits. (b) Full-color 3D laser displays based on CP lasing (color online).

symmetry breaking of achiral chromophores. The CPL stemming directly from the intrinsic chirality of the system (molecules or their supermolecular structures) was significantly enhanced by rational molecular design and efficient synthesis, which could also be adjusted by interaction with cations and light irradiation and upon pH and solvent change. Combining chiral moieties with emerging materials, such as AIEgens, MOFs, metal clusters, perovskites, and TADF chromophores, enriches CPL-active materials with promising properties. In addition, single- or multi-component assembly has become an established method to optimize emission efficiency and CPL activities simultaneously.

Despite the remarkable progress in this field, several challenges are still impending. Firstly, due to the tradeoff between the emission efficiency Φ and luminescence dissymmetry factor g_{lum}, it remains challenging to develop CPL materials with both high factors. From the point of view of chiral emitters, the concept of ACQ and AIE has been greatly developed and researchers can more easily design chiral materials showing CPL activity. In addition, due to the tradeoff between Φ and g_{lum}, it becomes difficult to evaluate the comprehensive performance of CPL-active materials. For this reason, a number of new indicators have been proposed. Tang and Niu *et al.* [374] proposed the product of Φ and g_{lum} as a figure of merit (FM) for the evaluation of CPL performance (Eq. (7)). Considering that FM could not intuitively reflect the degree of energy loss, Zhao and Huang *et al.* [198] proposed the asymmetric quantum efficiency (φ_a) to evaluate the CPL performance, which was defined by the ratio of the left- or right-CPL light intensity (I_L or I_R) to the incident light intensity (I_0) (Eq. (8)). In addition, a brightness indicator for CPL (B_{CPL}) was proposed by Zinna *et al.* [17] according to Eq. (9), in which ε_λ is the molar coefficient measured at the excitation wavelength. However, the applicability and generality of these indicators remain to be explored.

$$\mathrm{FM} = \Phi \times g_{lum} \tag{7}$$

$$\varphi_a = I_L / I_0 \ \text{ or } \ \varphi_a = I_R / I_0 \tag{8}$$

$$B_{CPL} = \varepsilon_\lambda \times \Phi \times g_{lum} / 2 \tag{9}$$

Secondly, symmetry breaking of achiral molecules may not only provide CPL-active materials with reduced costs but also gain insights into the origin of molecular homochirality. Unfortunately, only limited examples are known to date and most of them were discovered by experimental serendipity in the beginning. It would be of high interest to develop general molecular frameworks or external conditions (*e.g.*, vortex mixing) for symmetry breaking with controlled handedness.

Thirdly, chirality transfer has been fully used in developing CPL-active materials, and the handedness inversion and/or the CPL sign inversion were reported in a considerable amount of examples. It is now in the sophisticated stage by further design and control of energy transfer modes, including Förster resonance energy transfer, radiative energy transfer, and photon upconversion, to amplify the g_{lum} value. However, the mechanism of the underlying chirality transfer or inversion has not been fully understood, which could be probed by *in-situ* spectroscopic and imaging characterizations on specific dynamic assembly processes with high time- and space-resolutions. More importantly, a theoretical understanding of the phenomenon on the excited-state chiral system is in urgent need.

Fourthly, although some representative CPL applications have been discussed here, these investigations are still in their infancy. Photonics and electronics applications would require CPL from a solid-state sample or thin-film, implying the necessity to induce aggregation into ordered dissymmetric structures upon thin film deposition, accompanying the requirement for accurate microscopic solid-state measurement. It has long been theoretically surmised that a single chiral molecule or molecular assembly showed anisotropic CPL. However, the regular CPL measurements usually get the averaged value at the larger aggregate scale, which will lose much more intrinsic information on the electronic states of the molecule. Thus, developing a microscopic study of spatially resolved CPL on the level of single-molecule or aggregate is attractive. In addition, the CPL activity could be influenced by phase retardation or the

optical effect occurring on the optical path between the emitter and the sample substrate. Further explorations and effort should be greatly devoted. We hope that the present work will help to further seed and stimulate the research area of CPL-active materials.

Acknowledgements This work was financially supported by the National Natural Science Foundation of China (21925112, 22090021, 21890734, 21975118, 51973011, 52003022, 91956119, 92061201, 21825106, 91856115, 21874058, 21771114, 91956130), the Research Grants Council of Hong Kong (C6014-20W), and the Innovation and Technology Commission (ITC-CNERC14SC01).

Conflict of interest The authors declare no conflict of interest.

1 Wang X, Wang Y, Gao W, Song L, Ran C, Chen Y, Huang W. *Adv Mater*, 2021, 33: 2003615
2 Ma S, Ahn J, Moon J. *Adv Mater*, 2021, 2005760
3 Ma J, Wang H, Li D. *Adv Mater*, 2021, 33: 2008785
4 Albano G, Pescitelli G, Di Bari L. *Chem Rev*, 2020, 120: 10145–10243
5 Clarke D, Grainger JF. *Polarized Light and Optical Measurement: International Series of Monographs in Natural Philosophy*. Vol. 35. Oxford: Pergamon, 2013
6 Sherson JF, Krauter H, Olsson RK, Julsgaard B, Hammerer K, Cirac I, Polzik ES. *Nature*, 2006, 443: 557–560
7 Richardson RD, Baud MGJ, Weston CE, Rzepa HS, Kuimova MK, Fuchter MJ. *Chem Sci*, 2015, 6: 3853–3862
8 Schadt M. *Annu Rev Mater Sci*, 1997, 27: 305–379
9 Han J, Guo S, Lu H, Liu S, Zhao Q, Huang W. *Adv Opt Mater*, 2018, 6: 1800538
10 Sang Y, Han J, Zhao T, Duan P, Liu M. *Adv Mater*, 2020, 32: 1900110
11 Emeis CA, Oosterhoff LJ. *Chem Phys Lett*, 1967, 1: 129
12 Nitti A, Pasini D. *Adv Mater*, 2020, 32: 1908021
13 Zhao T, Han J, Duan P, Liu M. *Acc Chem Res*, 2020, 53: 1279–1292
14 Kumar J, Nakashima T, Kawai T. *J Phys Chem Lett*, 2015, 6: 3445–3452
15 Song F, Zhao Z, Liu Z, Lam JWY, Tang BZ. *J Mater Chem C*, 2020, 8: 3284–3301
16 Ma JL, Peng Q, Zhao CH. *Chem Eur J*, 2019, 25: 15441–15454
17 Arrico L, Di Bari L, Zinna F. *Chem Eur J*, 2021, 27: 2920–2934
18 Zhao WL, Li M, Lu HY, Chen CF. *Chem Commun*, 2019, 55: 13793–13803
19 Yang D, Han J, Liu M, Duan P. *Adv Mater*, 2019, 31: 1805683
20 Zhang DW, Li M, Chen CF. *Chem Soc Rev*, 2020, 49: 1331–1343
21 Liang X, Liu TT, Yan ZP, Zhou Y, Su J, Luo XF, Wu ZG, Wang Y, Zheng YX, Zuo JL. *Angew Chem Int Ed*, 2019, 58: 17220–17225
22 Li M, Li SH, Zhang D, Cai M, Duan L, Fung MK, Chen CF. *Angew Chem Int Ed*, 2018, 57: 2889–2893
23 Jiang Z, Wang X, Ma J, Liu Z. *Sci China Chem*, 2019, 62: 355–362
24 Ma Z, Winands T, Liang N, Meng D, Jiang W, Doltsinis NL, Wang Z. *Sci China Chem*, 2020, 63: 208–214
25 Chen Y, Yekta S, Yudin AK. *Chem Rev*, 2003, 103: 3155–3212
26 Takaishi K, Takehana R, Ema T. *Chem Commun*, 2018, 54: 1449–1452
27 Takaishi K, Iwachido K, Takehana R, Uchiyama M, Ema T. *J Am Chem Soc*, 2019, 141: 6185–6190
28 Takaishi K, Hinoide S, Matsumoto T, Ema T. *J Am Chem Soc*, 2019, 141: 11852–11857
29 Takaishi K, Iwachido K, Ema T. *J Am Chem Soc*, 2020, 142: 1774–1779
30 Takaishi K, Matsumoto T, Kawataka M, Ema T. *Angew Chem Int Ed*, 2021, 60: 9968–9972
31 Sun ZB, Liu JK, Yuan DF, Zhao ZH, Zhu XZ, Liu DH, Peng Q, Zhao CH. *Angew Chem Int Ed*, 2019, 58: 4840–4846
32 Li M, Lu HY, Zhang C, Shi L, Tang Z, Chen CF. *Chem Commun*, 2016, 52: 9921–9924
33 He DQ, Lu HY, Li M, Chen CF. *Chem Commun*, 2017, 53: 6093–6096
34 Fang L, Li M, Lin WB, Shen Y, Chen CF. *J Org Chem*, 2017, 82: 7402–7409
35 Lin WB, Li M, Fang L, Shen Y, Chen CF. *Chem Asian J*, 2017, 12: 86–94
36 Li M, Zhang C, Fang L, Shi L, Tang Z, Lu HY, Chen CF. *ACS Appl Mater Interfaces*, 2018, 10: 8225–8230
37 Fang L, Li M, Lin WB, Chen CF. *Tetrahedron*, 2018, 74: 7164–7172
38 Lin WB, He DQ, Lu HY, Hu ZQ, Chen CF. *Chem Commun*, 2020, 56: 1863–1866
39 Qiu Z, Ju CW, Frédéric L, Hu Y, Schollmeyer D, Pieters G, Müllen K, Narita A. *J Am Chem Soc*, 2021, 143: 4661–4667
40 Kikuchi K, Nakamura J, Nagata Y, Tsuchida H, Kakuta T, Ogoshi T, Morisaki Y. *Chem Asian J*, 2019, 14: 1681–1685
41 Namba G, Mimura Y, Imai Y, Inoue R, Morisaki Y. *Chem Eur J*, 2020, 26: 14871–14877
42 Liu C, Yang JC, Lam JWY, Feng HT, Tang BZ. *Chem Sci*, 2021, doi: 10.1039/d1sc02305e
43 Roose J, Tang BZ, Wong KS. *Small*, 2016, 12: 6495–6512
44 Yang J, Fang M, Li Z. *Aggregate*, 2020, 1: 6–18
45 Kwok RTK, Leung CWT, Lam JWY, Tang BZ. *Chem Soc Rev*, 2015, 44: 4228–4238
46 Zhang C, Li S, Dong X, Zang S. *Aggregate*, 2021, 2: e48
47 Mei J, Leung NLC, Kwok RTK, Lam JWY, Tang BZ. *Chem Rev*, 2015, 115: 11718–11940
48 Yang J, Chi Z, Zhu W, Tang BZ, Li Z. *Sci China Chem*, 2019, 62: 1090–1098
49 Ou H, Dai S, Liu R, Ding D. *Sci China Chem*, 2019, 62: 929–932
50 Liu J, Su H, Meng L, Zhao Y, Deng C, Ng JCY, Lu P, Faisal M, Lam JWY, Huang X, Wu H, Wong KS, Tang BZ. *Chem Sci*, 2012, 3: 2737–2747
51 Li H, Xue S, Su H, Shen B, Cheng Z, Lam JWY, Wong KS, Wu H, Li BS, Tang BZ. *Small*, 2016, 12: 6593–6601
52 Ng JCY, Li H, Yuan Q, Liu J, Liu C, Fan X, Li BS, Tang BZ. *J Mater Chem C*, 2014, 2: 4615–4621
53 Ng JCY, Liu J, Su H, Hong Y, Li H, Lam JWY, Wong KS, Tang BZ. *J Mater Chem C*, 2014, 2: 78–83
54 Li H, Cheng J, Deng H, Zhao E, Shen B, Lam JWY, Wong KS, Wu H, Li BS, Tang BZ. *J Mater Chem C*, 2015, 3: 2399–2404
55 Xia Q, Meng L, He T, Huang G, Li BS, Tang BZ. *ACS Nano*, 2021, 15: 4956–4966
56 Zhang S, Wang Y, Meng F, Dai C, Cheng Y, Zhu C. *Chem Commun*, 2015, 51: 9014–9017
57 Zhang H, Li H, Wang J, Sun J, Qin A, Tang BZ. *J Mater Chem C*, 2015, 3: 5162–5166
58 Yang D, Duan P, Zhang L, Liu M. *Nat Commun*, 2017, 8: 15727
59 Shang H, Ding Z, Shen Y, Yang B, Liu M, Jiang S. *Chem Sci*, 2020, 11: 2169–2174
60 Xiong JB, Feng HT, Sun JP, Xie WZ, Yang D, Liu M, Zheng YS. *J Am Chem Soc*, 2016, 138: 11469–11472
61 Feng HT, Zheng X, Gu X, Chen M, Lam JWY, Huang X, Tang BZ. *Chem Mater*, 2018, 30: 1285–1290
62 Cheng Y, Liu S, Song F, Khorloo M, Zhang H, Kwok RTK, Lam JWY, He Z, Tang BZ. *Mater Horiz*, 2019, 6: 405–411
63 Li WJ, Gu Q, Wang XQ, Zhang DY, Wang YT, He X, Wang W, Yang HB. *Angew Chem Int Ed*, 2021, 60: 9507–9515
64 Lu N, Gao X, Pan M, Zhao B, Deng J. *Macromolecules*, 2020, 53: 8041–8049
65 Liu Q, Xia Q, Xiong Y, Li BS, Tang BZ. *Macromolecules*, 2020, 53: 6288–6298
66 Chen M, Chen Z, Chen H, Xu L, Kong X, Long L, Zheng L. *Sci China Chem*, 2021, 64: 1698–1702

67 Liao C, Zhang Y, Ye SH, Zheng WH. *ACS Appl Mater Interfaces*, 2021, 13: 25186–25192
68 Liu M, Zhang L, Wang T. *Chem Rev*, 2015, 115: 7304–7397
69 Yashima E, Ousaka N, Taura D, Shimomura K, Ikai T, Maeda K. *Chem Rev*, 2016, 116: 13752–13990
70 Ma K, Chen W, Jiao T, Jin X, Sang Y, Yang D, Zhou J, Liu M, Duan P. *Chem Sci*, 2019, 10: 6821–6827
71 Bai X, Sun Y, Jiang Y, Zhao G, Jiang J, Yuan C, Liu M. *Angew Chem Int Ed*, 2021, 60: 3745–3751
72 Huang Z, Jiang T, Wang J, Ma X, Tian H. *Angew Chem Int Ed*, 2021, 60: 2855–2860
73 Wang F, Gan F, Shen C, Qiu H. *J Am Chem Soc*, 2020, 142: 16167–16172
74 Wang Y, Li X, Li F, Sun WY, Zhu C, Cheng Y. *Chem Commun*, 2017, 53: 7505–7508
75 Wang Y, Wan K, Pan F, Zhu X, Jiang Y, Wang H, Chen Y, Shi X, Liu M. *Angew Chem Int Ed*, 2021, 60: 16615–16621
76 Li ZQ, Gong ZL, Shao JY, Yao J, Zhong YW. *Angew Chem Int Ed*, 2021, 60: 14595–14600
77 Li Y, Li Q, Miao X, Qin C, Chu D, Cao L. *Angew Chem Int Ed*, 2021, 60: 6744–6751
78 Chen W, Ma K, Duan P, Ouyang G, Zhu X, Zhang L, Liu M. *Nanoscale*, 2020, 12: 19497–19515
79 Zhang H, Zhao Z, Turley AT, Wang L, McGonigal PR, Tu Y, Li Y, Wang Z, Kwok RTK, Lam JWY, Tang BZ. *Adv Mater*, 2020, 32: 2001457
80 Han J, You J, Li X, Duan P, Liu M. *Adv Mater*, 2017, 29: 1606503
81 Cao H, Duan P, Zhu X, Jiang J, Liu M. *Chem Eur J*, 2012, 18: 5546–5550
82 Goto T, Okazaki Y, Ueki M, Kuwahara Y, Takafuji M, Oda R, Ihara H. *Angew Chem Int Ed*, 2017, 56: 2989–2993
83 Ma S, Jiang J, Liu Z, Jiang Y, Wu Z, Liu M. *Nanoscale*, 2020, 12: 7895–7901
84 Huo S, Duan P, Jiao T, Peng Q, Liu M. *Angew Chem Int Ed*, 2017, 56: 12174–12178
85 Shi Y, Duan P, Huo S, Li Y, Liu M. *Adv Mater*, 2018, 30: 1705011
86 Ru Y, Sui L, Song H, Liu X, Tang Z, Zang SQ, Yang B, Lu S. *Angew Chem Int Ed*, 2021, 60: 14091–14099
87 Hu S, Hu L, Zhu X, Wang Y, Liu M. *Angew Chem Int Ed*, 2021, 60: 19451–19457
88 Niu D, Ji L, Ouyang G, Liu M. *Chem Commun*, 2018, 54: 1137–1140
89 Cao Z, Zhu F, Hao A, Xing P. *J Phys Chem C*, 2020, 124: 7965–7972
90 Cao Z, Wang B, Zhu F, Hao A, Xing P. *ACS Appl Mater Interfaces*, 2020, 12: 34470–34478
91 Liang J, Hao A, Xing P. *ACS Appl Mater Interfaces*, 2020, 12: 45665–45672
92 Zhao J, Hao A, Xing P. *ACS Appl Mater Interfaces*, 2021, 13: 6830–6843
93 Wang Z, Li Y, Hao A, Xing P. *Angew Chem Int Ed*, 2021, 60: 3138–3147
94 Zhang H, Han J, Jin X, Duan P. *Angew Chem Int Ed*, 2021, 60: 4575–4580
95 Shen Z, Wang T, Shi L, Tang Z, Liu M. *Chem Sci*, 2015, 6: 4267–4272
96 Sang Y, Yang D, Duan P, Liu M. *Chem Sci*, 2019, 10: 2718–2724
97 Sang Y, Yang D, Shen Z, Duan P, Liu M. *J Phys Chem C*, 2020, 124: 17274–17281
98 Yang B, Zou G, Zhang S, Ni H, Wang H, Xu W, Yang C, Zhang H, Yu W, Luo K. *Angew Chem Int Ed*, 2021, 60: 10531–10536
99 Jiang H, Jiang Y, Han J, Zhang L, Liu M. *Angew Chem Int Ed*, 2019, 58: 785–790
100 Li P, Lü B, Han D, Duan P, Liu M, Yin M. *Chem Commun*, 2019, 55: 2194–2197
101 Li X, Shen Y, Liu K, Quan Y, Cheng Y. *Mater Chem Front*, 2020, 4: 2954–2961
102 Li Y, Yao K, Chen Y, Quan Y, Cheng Y. *Adv Opt Mater*, 2021, 9: 2100961
103 Yoshida S, Morikawa S, Ueda K, Hidaka M, Kaneko K, Kaneko K, Hanasaki T, Akagi K. *Adv Opt Mater*, 2020, 8: 2000936
104 Yao K, Shen Y, Li Y, Li X, Quan Y, Cheng Y. *J Phys Chem Lett*, 2021, 12: 598–603
105 Gao X, Qin X, Yang X, Li Y, Duan P. *Chem Commun*, 2019, 55: 5914–5917
106 Lin S, Sun H, Qiao J, Ding X, Guo J. *Adv Opt Mater*, 2020, 8: 2000107
107 Chen Y, Lu P, Li Z, Yuan Y, Ye Q, Zhang H. *ACS Appl Mater Interfaces*, 2020, 12: 56604–56614
108 Ikai T, Yoshida T, Awata S, Wada Y, Maeda K, Mizuno M, Swager TM. *ACS Macro Lett*, 2018, 7: 364–369
109 Dhbaibi K, Shen C, Jean M, Vanthuyne N, Roisnel T, Górecki M, Jamoussi B, Favereau L, Crassous J. *Front Chem*, 2020, 8: 237
110 Meng F, Li Y, Zhang W, Li S, Quan Y, Cheng Y. *Polym Chem*, 2017, 8: 1555–1561
111 Li F, Wang Y, Wang Z, Cheng Y, Zhu C. *Polym Chem*, 2015, 6: 6802–6805
112 Luo J, Xie Z, Lam JWY, Cheng L, Tang BZ, Chen H, Qiu C, Kwok HS, Zhan X, Liu Y, Zhu D. *Chem Commun*, 2001, 18: 1740–1741
113 Wang Z, Fang Y, Tao X, Wang Y, Quan Y, Zhang S, Cheng Y. *Polymer*, 2017, 130: 61–67
114 Ma J, Wang Y, Li X, Yang L, Quan Y, Cheng Y. *Polymer*, 2018, 143: 184–189
115 Zhang C, Li M, Lu HY, Chen CF. *RSC Adv*, 2018, 8: 1014–1021
116 Lee S, Kim KY, Jung SH, Lee JH, Yamada M, Sethy R, Kawai T, Jung JH. *Angew Chem Int Ed*, 2019, 58: 18878–18882
117 Zhang S, Sheng Y, Wei G, Quan Y, Cheng Y, Zhu C. *Polym Chem*, 2015, 6: 2416–2422
118 Zhao B, Pan K, Deng J. *Macromolecules*, 2018, 51: 7104–7111
119 Pan M, Zhao R, Zhao B, Deng J. *Macromolecules*, 2021, 54: 5043–5052
120 Fukao S, Fujiki M. *Macromolecules*, 2009, 42: 8062–8067
121 Nagata Y, Nishikawa T, Suginome M. *Chem Commun*, 2014, 50: 9951–9953
122 Yamada T, Nomura K, Fujiki M. *Macromolecules*, 2018, 51: 2377–2387
123 Liu WB, Xu XH, Kang SM, Song X, Zhou L, Liu N, Wu ZQ. *Macromolecules*, 2021, 54: 3158–3168
124 Kameta N, Shimizu T. *Nanoscale*, 2020, 12: 2999–3006
125 Hu Y, Song F, Xu Z, Tu Y, Zhang H, Cheng Q, Lam JWY, Ma D, Tang BZ. *ACS Appl Polym Mater*, 2019, 1: 221–229
126 Xu L, Wang C, Li YX, Xu XH, Zhou L, Liu N, Wu ZQ. *Angew Chem Int Ed*, 2020, 59: 16675–16682
127 Ikai T, Kojima Y, Shinohara K, Maeda K, Kanoh S. *Polymer*, 2017, 117: 220–224
128 Ikai T, Shimizu S, Awata S, Shinohara K. *Macromolecules*, 2018, 51: 2328–2334
129 Ikai T, Awata S, Shinohara K. *Polym Chem*, 2018, 9: 1541–1546
130 Ikai T, Takayama K, Wada Y, Minami S, Apiboon C, Shinohara KI. *Chem Sci*, 2019, 10: 4890–4895
131 Abdul Rahim NA, Fujiki M. *Polym Chem*, 2016, 7: 4618–4629
132 Duong ST, Fujiki M. *Polym Chem*, 2017, 8: 4673–4679
133 Mukherjee A, Pal DS, Kar H, Ghosh S. *Polym Chem*, 2020, 11: 7481–7486
134 Li Q, Yuan J, Liang H, Zheng F, Lu X, Yu C, Lu Q. *ACS Nano*, 2020, 14: 8939–8948
135 Guo S, Suzuki N, Fujiki M. *Macromolecules*, 2017, 50: 1778–1789
136 Guo S, Kamite H, Suzuki N, Wang L, Ohkubo A, Fujiki M. *Biomacromolecules*, 2018, 19: 449–459
137 Guo P, Jin R, Wang M, He Q, Cai C, Zhao Q, Bu W. *J Organomet Chem*, 2020, 931: 121616
138 Islam MJ, Kitagawa Y, Tsurui M, Hasegawa Y. *Dalton Trans*, 2021, 50: 5433–5436
139 Leo P, Orcajo G, García JA, Ortuño AM, Cuerva JM, Briones D, Calleja G, Rodríguez-Diéguez A, Sanz R, Cepeda J, Martínez F. *J*

Mater Chem C, 2021, 9: 5544–5553
140 Hasegawa Y, Miura Y, Kitagawa Y, Wada S, Nakanishi T, Fushimi K, Seki T, Ito H, Iwasa T, Taketsugu T, Gon M, Tanaka K, Chujo Y, Hattori S, Karasawa M, Ishii K. *Chem Commun*, 2018, 54: 10695–10697
141 Wang L, Suzuki N, Liu J, Matsuda T, Rahim NAA, Zhang W, Fujiki M, Zhang Z, Zhou N, Zhu X. *Polym Chem*, 2014, 5: 5920–5927
142 Liu J, Zhang J, Zhang S, Suzuki N, Fujiki M, Wang L, Li L, Zhang W, Zhou N, Zhu X. *Polym Chem*, 2014, 5: 784–791
143 Nakano Y, Liu Y, Fujiki M. *Polym Chem*, 2010, 1: 460–469
144 Wade J, Brandt JR, Reger D, Zinna F, Amsharov KY, Jux N, Andrews DL, Fuchter MJ. *Angew Chem Int Ed*, 2021, 60: 222–227
145 Zhao Y, Abdul Rahim NA, Xia Y, Fujiki M, Song B, Zhang Z, Zhang W, Zhu X. *Macromolecules*, 2016, 49: 3214–3221
146 Maeda K, Nozaki M, Hashimoto K, Shimomura K, Hirose D, Nishimura T, Watanabe G, Yashima E. *J Am Chem Soc*, 2020, 142: 7668–7682
147 Yu K, Fan T, Lou S, Zhang D. *Prog Mater Sci*, 2013, 58: 825–873
148 Sharma V, Crne M, Park JO, Srinivasarao M. *Science*, 2009, 325: 449–451
149 Sweeney A, Jiggins C, Johnsen S. *Nature*, 2003, 423: 31–32
150 Yan J, Ota F, San Jose BA, Akagi K. *Adv Funct Mater*, 2017, 27: 1604529
151 Chen Y, Lu P, Yuan Y, Zhang H. *J Mater Chem C*, 2020, 8: 13632–13641
152 Nagata Y, Uno M, Suginome M. *Angew Chem Int Ed*, 2016, 55: 7126–7130
153 Luo ZW, Tao L, Zhong CL, Li ZX, Lan K, Feng Y, Wang P, Xie HL. *Macromolecules*, 2020, 53: 9758–9768
154 Di Nuzzo D, Kulkarni C, Zhao B, Smolinsky E, Tassinari F, Meskers SCJ, Naaman R, Meijer EW, Friend RH. *ACS Nano*, 2017, 11: 12713–12722
155 Nagata Y, Takagi K, Suginome M. *J Am Chem Soc*, 2014, 136: 9858–9861
156 San Jose BA, Yan J, Akagi K. *Angew Chem Int Ed*, 2014, 53: 10641–10644
157 Khorloo M, Yu X, Cheng Y, Zhang H, Yu S, Lam JWY, Zhu M, Tang BZ. *ACS Nano*, 2021, 15: 1397–1406
158 Zheng H, Li W, Li W, Wang X, Tang Z, Zhang SXA, Xu Y. *Adv Mater*, 2018, 30: 1705948
159 Yu H, Zhao B, Guo J, Pan K, Deng J. *J Mater Chem C*, 2020, 8: 1459–1465
160 Jiang Y, Su W, Li G, Fu Y, Li Z, Qin M, Yuan Z. *Chem Eng J*, 2022, 430: 132780
161 Shi Y, Zhou Z, Miao X, Liu YJ, Fan Q, Wang K, Luo D, Sun XW. *J Mater Chem C*, 2020, 8: 1048–1053
162 Qu D, Archimi M, Camposeo A, Pisignano D, Zussman E. *ACS Nano*, 2021, 15: 8753–8760
163 Zhao B, Pan K, Deng J. *Macromolecules*, 2019, 52: 376–384
164 Zhao B, Yu H, Pan K, Tan Z', Deng J. *ACS Nano*, 2020, 14: 3208–3218
165 Zhao B, Gao X, Lu N, Deng J. *Adv Opt Mater*, 2020, 8: 2000858
166 Zhao B, Gao X, Pan K, Deng J. *ACS Nano*, 2021, 15: 7463–7471
167 Huang Z, Hu Y, Jin X, Zhao Y, Su J, Ma X. *Adv Opt Mater*, 2021, 9: 2100135
168 Zhang X, Xu Z, Zhang Y, Quan Y, Cheng Y. *J Mater Chem C*, 2020, 8: 15669–15676
169 Hong J, Kim S, Park G, Lee Y, Kim H, Kim S, Lee TW, Kim C, You Y. *Chem Sci*, 2021, 12: 8668–8681
170 He C, Yang G, Kuai Y, Shan S, Yang L, Hu J, Zhang D, Zhang Q, Zou G. *Nat Commun*, 2018, 9: 5117
171 Doistau B, Jiménez JR, Piguet C. *Front Chem*, 2020, 8: 555
172 Lunkley JL, Shirotani D, Yamanari K, Kaizaki S, Muller G. *J Am Chem Soc*, 2008, 130: 13814–13815
173 Wong HY, Lo WS, Yim KH, Law GL. *Chem*, 2019, 5: 3058–3095
174 Zinna F, Arrico L, Di Bari L. *Chem Commun*, 2019, 55: 6607–6609
175 Zinna F, Giovanella U, Di Bari L. *Adv Mater*, 2015, 27: 1791–1795
176 Liu D, Zhou Y, Zhang Y, Li H, Chen P, Sun W, Gao T, Yan P. *Inorg Chem*, 2018, 57: 8332–8337
177 Zhou Y, Li H, Zhu T, Gao T, Yan P. *J Am Chem Soc*, 2019, 141: 19634–19643
178 Yeung CT, Yim KH, Wong HY, Pal R, Lo WS, Yan SC, Yee-Man Wong M, Yufit D, Smiles DE, McCormick LJ, Teat SJ, Shuh DK, Wong WT, Law GL. *Nat Commun*, 2017, 8: 1128
179 Dai L, Zhang J, Chen Y, Mackenzie LE, Pal R, Law GL. *Inorg Chem*, 2019, 58: 12506–12510
180 Li XZ, Zhou LP, Yan LL, Yuan DQ, Lin CS, Sun QF. *J Am Chem Soc*, 2017, 139: 8237–8244
181 OuYang J, Crassous J. *Coord Chem Rev*, 2018, 376: 533–547
182 Hellou N, Srebro-Hooper M, Favereau L, Zinna F, Caytan E, Toupet L, Dorcet V, Jean M, Vanthuyne N, Williams JAG, Di Bari L, Autschbach J, Crassous J. *Angew Chem Int Ed*, 2017, 56: 8236–8239
183 Biet T, Cauchy T, Sun Q, Ding J, Hauser A, Oulevey P, Bürgi T, Jacquemin D, Vanthuyne N, Crassous J, Avarvari N. *Chem Commun*, 2017, 53: 9210–9213
184 Song J, Wang M, Zhou X, Xiang H. *Chem Eur J*, 2018, 24: 7128–7132
185 Song J, Wang M, Xu X, Qu L, Zhou X, Xiang H. *Dalton Trans*, 2019, 48: 4420–4428
186 Schulte TR, Holstein JJ, Krause L, Michel R, Stalke D, Sakuda E, Umakoshi K, Longhi G, Abbate S, Clever GH. *J Am Chem Soc*, 2017, 139: 6863–6866
187 Inoue R, Kondo R, Morisaki Y. *Chem Commun*, 2020, 56: 15438–15441
188 Lin J, Xie M, Zhang X, Gao Q, Chang X, Zou C, Lu W. *Chem Commun*, 2021, 57: 1627–1630
189 Ito H, Sakai H, Okayasu Y, Yuasa J, Mori T, Hasobe T. *Chem Eur J*, 2018, 24: 16889–16894
190 Tanaka Y, Murayama T, Muranaka A, Imai E, Uchiyama M. *Chem Eur J*, 2020, 26: 1768–1771
191 Kögel JF, Kusaka S, Sakamoto R, Iwashima T, Tsuchiya M, Toyoda R, Matsuoka R, Tsukamoto T, Yuasa J, Kitagawa Y, Kawai T, Nishihara H. *Angew Chem Int Ed*, 2016, 55: 1377–1381
192 Dee C, Zinna F, Kitzmann WR, Pescitelli G, Heinze K, Di Bari L, Seitz M. *Chem Commun*, 2019, 55: 13078–13081
193 Jiménez JR, Doistau B, Cruz CM, Besnard C, Cuerva JM, Campaña AG, Piguet C. *J Am Chem Soc*, 2019, 141: 13244–13252
194 Jiménez JR, Poncet M, Míguez-Lago S, Grass S, Lacour J, Besnard C, Cuerva JM, Campaña AG, Piguet C. *Angew Chem Int Ed*, 2021, 60: 10095–10102
195 Deng M, Mukthar NFM, Schley ND, Ung G. *Angew Chem Int Ed*, 2020, 59: 1228–1231
196 Ono T, Ishihama K, Taema A, Harada T, Furusho K, Hasegawa M, Nojima Y, Abe M, Hisaeda Y. *Angew Chem Int Ed*, 2021, 60: 2614–2618
197 Feng HT, Lam JWY, Tang BZ. *Coord Chem Rev*, 2020, 406: 213142–213155
198 Deng Y, Wang M, Zhuang Y, Liu S, Huang W, Zhao Q. *Light Sci Appl*, 2021, 10: 76
199 Ikeda T, Hirano K, Haino T. *Mater Chem Front*, 2018, 2: 468–474
200 Gong ZL, Zhong YW. *Sci China Chem*, 2021, 64: 788–799
201 Yang B, Ni H, Wang H, Hu Y, Luo K, Yu W. *J Phys Chem C*, 2020, 124: 23879–23887
202 Park G, Kim H, Yang H, Park KR, Song I, Oh JH, Kim C, You Y. *Chem Sci*, 2019, 10: 1294–1301
203 Zhang J, Liu Q, Wu W, Peng J, Zhang H, Song F, He B, Wang X, Sung HHY, Chen M, Li BS, Liu SH, Lam JWY, Tang BZ. *ACS Nano*, 2019, 13: 3618–3628
204 Wang Y, Li X, Yang L, Sun WY, Zhu C, Cheng Y. *Mater Chem Front*, 2018, 2: 554–558
205 Aoki R, Toyoda R, Kögel JF, Sakamoto R, Kumar J, Kitagawa Y, Harano K, Kawai T, Nishihara H. *J Am Chem Soc*, 2017, 139: 16024–16027
206 Weng GG, Zheng LM. *Sci China Chem*, 2020, 63: 619–636

207 Wang X, Sun M, Huang Z, Xie M, Huang R, Lu H, Zhao Z, Zhou X, Li D. *Adv Opt Mater*, 2021, 2002096
208 Shang W, Zhu X, Liang T, Du C, Hu L, Li T, Liu M. *Angew Chem Int Ed*, 2020, 59: 12811–12816
209 Zhang C, Yan ZP, Dong XY, Han Z, Li S, Fu T, Zhu YY, Zheng YX, Niu YY, Zang SQ. *Adv Mater*, 2020, 32: 2002914
210 Zeng M, Ren A, Wu W, Zhao Y, Zhan C, Yao J. *Chem Sci*, 2020, 11: 9154–9161
211 Hu L, Li K, Shang W, Zhu X, Liu M. *Angew Chem Int Ed*, 2020, 59: 4953–4958
212 Greenfield JL, Wade J, Brandt JR, Shi X, Penfold TJ, Fuchter MJ. *Chem Sci*, 2021, 12: 8589–8602
213 Jin Y, Zhang C, Dong XY, Zang SQ, Mak TCW. *Chem Soc Rev*, 2021, 50: 2297–2319
214 Chakraborty P, Nag A, Chakraborty A, Pradeep T. *Acc Chem Res*, 2019, 52: 2–11
215 Chakraborty I, Pradeep T. *Chem Rev*, 2017, 117: 8208–8271
216 Zeng C, Chen Y, Kirschbaum K, Lambright KJ, Jin R. *Science*, 2016, 354: 1580–1584
217 Huang RW, Wei YS, Dong XY, Wu XH, Du CX, Zang SQ, Mak TCW. *Nat Chem*, 2017, 9: 689–697
218 Dong XY, Si Y, Yang JS, Zhang C, Han Z, Luo P, Wang ZY, Zang SQ, Mak TCW. *Nat Commun*, 2020, 11: 3678–3686
219 Schaaff TG, Knight G, Shafigullin MN, Borkman RF, Whetten RL. *J Phys Chem B*, 1998, 102: 10643–10646
220 Nieto-Ortega B, Bürgi T. *Acc Chem Res*, 2018, 51: 2811–2819
221 Li Y, Zhou M, Song Y, Higaki T, Wang H, Jin R. *Nature*, 2021, 594: 380–384
222 Riehl JP, Richardson FS. *Chem Rev*, 1986, 86: 1–16
223 Hu M, Feng HT, Yuan YX, Zheng YS, Tang BZ. *Coord Chem Rev*, 2020, 416: 213329
224 Li Y, Zhou M, Jin R. *Adv Mater*, 2021, 2006591
225 Tan YL, Yang L, Yu TC, Yu H, Wang XY, Song YL, Niu Z, Lang JP. *Sci China Chem*, 2021, 64: 948–952
226 Zhang M, Li K, Zang S. *Adv Opt Mater*, 2020, 8: 1902152
227 Han Z, Dong XY, Luo P, Li S, Wang ZY, Zang SQ, Mak TCW. *Sci Adv*, 2020, 6: eaay0107
228 Kong YJ, Yan ZP, Li S, Su HF, Li K, Zheng YX, Zang SQ. *Angew Chem Int Ed*, 2020, 59: 5336–5340
229 Zhang MM, Dong XY, Wang ZY, Li HY, Li SJ, Zhao X, Zang SQ. *Angew Chem Int Ed*, 2020, 59: 10052–10058
230 Zhang MM, Dong XY, Wang ZY, Luo XM, Huang JH, Zang SQ, Mak TCW. *J Am Chem Soc*, 2021, 143: 6048–6053
231 Krishnadas KR, Sementa L, Medves M, Fortunelli A, Stener M, Fürstenberg A, Longhi G, Bürgi T. *ACS Nano*, 2020, 14: 9687–9700
232 Huang JH, Wang ZY, Zang SQ, Mak TCW. *ACS Cent Sci*, 2020, 6: 1971–1976
233 Li S, Yan ZP, Li XL, Kong YJ, Li HY, Gao GG, Zheng YX, Zang SQ. *Adv Sci*, 2020, 7: 2000738
234 Shi L, Zhu L, Guo J, Zhang L, Shi Y, Zhang Y, Hou K, Zheng Y, Zhu Y, Lv J, Liu S, Tang Z. *Angew Chem Int Ed*, 2017, 56: 15397–15401
235 Jin Y, Li S, Han Z, Yan BJ, Li HY, Dong XY, Zang SQ. *Angew Chem Int Ed*, 2019, 58: 12143–12148
236 Han Z, Zhao X, Peng P, Li S, Zhang C, Cao M, Li K, Wang ZY, Zang SQ. *Nano Res*, 2020, 13: 3248–3252
237 Wu H, He X, Yang B, Li CC, Zhao L. *Angew Chem Int Ed*, 2021, 60: 1535–1539
238 Jiang S, Chekini M, Qu ZB, Wang Y, Yeltik A, Liu Y, Kotlyar A, Zhang T, Li B, Demir HV, Kotov NA. *J Am Chem Soc*, 2017, 139: 13701–13712
239 Sun M, Xu L, Qu A, Zhao P, Hao T, Ma W, Hao C, Wen X, Colombari FM, de Moura AF, Kotov NA, Xu C, Kuang H. *Nat Chem*, 2018, 10: 821–830
240 Hao C, Xu L, Sun M, Ma W, Kuang H, Xu C. *Adv Funct Mater*, 2018, 28: 1802372
241 Ma W, Sun M, Fu P, Li S, Xu L, Kuang H, Xu C. *Adv Mater*, 2017, 29: 1703410
242 Meng D, Ma W, Wu X, Xu C, Kuang H. *Small*, 2020, 16: 2000003
243 Sun M, Xu L, Bahng JH, Kuang H, Alben S, Kotov NA, Xu C. *Nat Commun*, 2017, 8: 1847
244 Zhao X, Xu L, Sun M, Ma W, Wu X, Xu C, Kuang H. *Nat Commun*, 2017, 8: 2007
245 Wang J, Wu X, Ma W, Xu C. *Adv Funct Mater*, 2020, 30: 2000670
246 Mondal PC, Mtangi W, Fontanesi C. *Small Methods*, 2018, 2: 1700313
247 Hao C, Xu L, Kuang H, Xu C. *Adv Mater*, 2020, 32: 1802075
248 Ma W, Xu L, de Moura AF, Wu X, Kuang H, Xu C, Kotov NA. *Chem Rev*, 2017, 117: 8041–8093
249 Lee HE, Ahn HY, Mun J, Lee YY, Kim M, Cho NH, Chang K, Kim WS, Rho J, Nam KT. *Nature*, 2018, 556: 360–365
250 Ma W, Mao J, Hao C, Xu L, Xu C, Kuang H. *Appl Catal B-Environ*, 2019, 245: 691–697
251 Purcell-Milton F, McKenna R, Brennan LJ, Cullen CP, Guillemeney L, Tepliakov NV, Baimuratov AS, Rukhlenko ID, Perova TS, Duesberg GS, Baranov AV, Fedorov AV, Gun′ko YK. *ACS Nano*, 2018, 12: 954–964
252 Kim Y, Yeom B, Arteaga O, Jo Yoo S, Lee SG, Kim JG, Kotov NA. *Nat Mater*, 2016, 15: 461–468
253 Ma J, Fang C, Chen C, Jin L, Wang J, Wang S, Tang J, Li D. *ACS Nano*, 2019, 13: 3659–3665
254 Li S, Xu L, Ma W, Wu X, Sun M, Kuang H, Wang L, Kotov NA, Xu C. *J Am Chem Soc*, 2016, 138: 306–312
255 Ma W, Kuang H, Xu L, Ding L, Xu C, Wang L, Kotov NA. *Nat Commun*, 2013, 4: 2689
256 Ma W, Hao C, Sun M, Xu L, Xu C, Kuang H. *Mater Horiz*, 2018, 5: 141–161
257 Ma W, Xu L, Wang L, Xu C, Kuang H. *Adv Funct Mater*, 2019, 29: 1805512
258 Tohgha U, Deol KK, Porter AG, Bartko SG, Choi JK, Leonard BM, Varga K, Kubelka J, Muller G, Balaz M. *ACS Nano*, 2013, 7: 11094–11102
259 Cheng J, Hao J, Liu H, Li J, Li J, Zhu X, Lin X, Wang K, He T. *ACS Nano*, 2018, 12: 5341–5350
260 Li C, Jin X, Zhao T, Zhou J, Duan P. *Nanoscale Adv*, 2019, 1: 508–512
261 Hao C, Gao Y, Wu D, Li S, Xu L, Wu X, Guo J, Sun M, Li X, Xu C, Kuang H. *Adv Mater*, 2019, 31: 1903200
262 Xu M, Ma C, Zhou J, Liu Y, Wu X, Luo S, Li W, Yu H, Wang Y, Chen Z, Li J, Liu S. *J Mater Chem C*, 2019, 7: 13794–13802
263 Long G, Sabatini R, Saidaminov MI, Lakhwani G, Rasmita A, Liu X, Sargent EH, Gao W. *Nat Rev Mater*, 2020, 5: 423–439
264 Dong Y, Zhang Y, Li X, Feng Y, Zhang H, Xu J. *Small*, 2019, 15: 1902237
265 Zhao J, Zhang T, Dong XY, Sun ME, Zhang C, Li X, Zhao YS, Zang SQ. *J Am Chem Soc*, 2019, 141: 15755–15760
266 Dang Y, Liu X, Sun Y, Song J, Hu W, Tao X. *J Phys Chem Lett*, 2020, 11: 1689–1696
267 Kim YH, Zhai Y, Gaulding EA, Habisreutinger SN, Moot T, Rosales BA, Lu H, Hazarika A, Brunecky R, Wheeler LM, Berry JJ, Beard MC, Luther JM. *ACS Nano*, 2020, 14: 8816–8825
268 Chen W, Zhang S, Zhou M, Zhao T, Qin X, Liu X, Liu M, Duan P. *J Phys Chem Lett*, 2019, 10: 3290–3295
269 Liu P, Chen W, Okazaki Y, Battie Y, Brocard L, Decossas M, Pouget E, Müller-Buschbaum P, Kauffmann B, Pathan S, Sagawa T, Oda R. *Nano Lett*, 2020, 20: 8453–8460
270 Xu M, Wu X, Yang Y, Ma C, Li W, Yu H, Chen Z, Li J, Zhang K, Liu S. *ACS Nano*, 2020, 14: 11130–11139
271 Wang C, Chen K, Xu P, Yeung F, Kwok H, Li G. *Adv Funct Mater*, 2019, 29: 1903155
272 Cruz CM, Castro-Fernández S, Maçôas E, Cuerva JM, Campaña AG. *Angew Chem Int Ed*, 2018, 57: 14782–14786
273 Cruz CM, Márquez IR, Mariz IFA, Blanco V, Sánchez-Sánchez C, Sobrado JM, Martín-Gago JA, Cuerva JM, Maçôas E, Campaña AG.

Chem Sci, 2018, 9: 3917–3924
274 Deng WT, Qu H, Huang ZY, Shi L, Tang ZY, Cao XY, Tao J. *Chem Commun*, 2019, 55: 2210–2213
275 Reine P, Ortuño AM, Mariz IFA, Ribagorda M, Cuerva JM, Campaña AG, Maçôas E, Miguel D. *Front Chem*, 2020, 8: 306
276 Han J, Duan P, Li X, Liu M. *J Am Chem Soc*, 2017, 139: 9783–9786
277 Zhao T, Han J, Qin X, Zhou M, Duan P. *J Phys Chem Lett*, 2020, 11: 311–317
278 Yang X, Han J, Wang Y, Duan P. *Chem Sci*, 2019, 10: 172–178
279 Han D, Yang X, Han J, Zhou J, Jiao T, Duan P. *Nat Commun*, 2020, 11: 5659
280 Zhou M, Sang Y, Jin X, Chen S, Guo J, Duan P, Liu M. *ACS Nano*, 2021, 15: 2753–2761
281 Yang D, Duan P, Liu M. *Angew Chem Int Ed*, 2018, 57: 9357–9361
282 Jin X, Sang Y, Shi Y, Li Y, Zhu X, Duan P, Liu M. *ACS Nano*, 2019, 13: 2804–2811
283 Li W, Xu M, Ma C, Liu Y, Zhou J, Chen Z, Wang Y, Yu H, Li J, Liu S. *ACS Appl Mater Interfaces*, 2019, 11: 23512–23519
284 Yang X, Zhou M, Wang Y, Duan P. *Adv Mater*, 2020, 32: 2000820
285 Zhao T, Han J, Jin X, Zhou M, Liu Y, Duan P, Liu M. *Research*, 2020, 2020: 1–12
286 Zhao T, Han J, Shi Y, Zhou J, Duan P. *Adv Mater*, 2021, 33: 2101797
287 Jin X, Zhou M, Han J, Li B, Zhang T, Jiang S, Duan P. *Nano Res*, 2021, doi: 10.1007/s12274-021-3594-6
288 Tang CW, VanSlyke SA. *Appl Phys Lett*, 1987, 51: 913–915
289 Peeters E, Christiaans MPT, Janssen RAJ, Schoo HFM, Dekkers HPJM, Meijer EW. *J Am Chem Soc*, 1997, 119: 9909–9910
290 Geng Y, Trajkovska A, Culligan SW, Ou JJ, Chen HMP, Katsis D, Chen SH. *J Am Chem Soc*, 2003, 125: 14032–14038
291 Yang L, Zhang Y, Zhang X, Li N, Quan Y, Cheng Y. *Chem Commun*, 2018, 54: 9663–9666
292 Yang Y, da Costa RC, Smilgies DM, Campbell AJ, Fuchter MJ. *Adv Mater*, 2013, 25: 2624–2628
293 Kulkarni C, van Son MHC, Di Nuzzo D, Meskers SCJ, Palmans ARA, Meijer EW. *Chem Mater*, 2019, 31: 6633–6641
294 Wan L, Wade J, Salerno F, Arteaga O, Laidlaw B, Wang X, Penfold T, Fuchter MJ, Campbell AJ. *ACS Nano*, 2019, 13: 8099–8105
295 Lee DM, Song JW, Lee YJ, Yu CJ, Kim JH. *Adv Mater*, 2017, 29: 1700907
296 Jung JH, Lee DM, Kim JH, Yu CJ. *J Mater Chem C*, 2018, 6: 726–730
297 Zinna F, Pasini M, Galeotti F, Botta C, Di Bari L, Giovanella U. *Adv Funct Mater*, 2017, 27: 1603719
298 Brandt JR, Wang X, Yang Y, Campbell AJ, Fuchter MJ. *J Am Chem Soc*, 2016, 138: 9743–9746
299 Han J, Guo S, Wang J, Wei L, Zhuang Y, Liu S, Zhao Q, Zhang X, Huang W. *Adv Opt Mater*, 2017, 5: 1700359
300 Sakai H, Shinto S, Kumar J, Araki Y, Sakanoue T, Takenobu T, Wada T, Kawai T, Hasobe T. *J Phys Chem C*, 2015, 119: 13937–13947
301 Zhang X, Zhang Y, Li Y, Quan Y, Cheng Y, Li Y. *Chem Commun*, 2019, 55: 9845–9848
302 Zhang X, Zhang Y, Zhang H, Quan Y, Li Y, Cheng Y, Ye S. *Org Lett*, 2019, 21: 439–443
303 Wang Y, Zhang Y, Hu W, Quan Y, Li Y, Cheng Y. *ACS Appl Mater Interfaces*, 2019, 11: 26165–26173
304 Li TY, Jing YM, Liu X, Zhao Y, Shi L, Tang Z, Zheng YX, Zuo JL. *Sci Rep*, 2015, 5: 14912
305 Yan ZP, Liao K, Han HB, Su J, Zheng YX, Zuo JL. *Chem Commun*, 2019, 55: 8215–8218
306 Lu JJ, Tu ZL, Luo XF, Zhang YP, Qu ZZ, Liang X, Wu ZG, Zheng YX. *J Mater Chem C*, 2021, 9: 5244–5249
307 Yan ZP, Luo XF, Liao K, Zheng YX, Zuo JL. *Front Chem*, 2020, 8: 501
308 Wu ZG, Han HB, Yan ZP, Luo XF, Wang Y, Zheng YX, Zuo JL, Pan Y. *Adv Mater*, 2019, 31: 1900524
309 Wu ZG, Yan ZP, Luo XF, Yuan L, Liang WQ, Wang Y, Zheng YX, Zuo JL, Pan Y. *J Mater Chem C*, 2019, 7: 7045–7052
310 Hu Y, Yao J, Xu Z, Wang Z, Li L, Su SJ, Ma D, Huang F. *Sci China Chem*, 2020, 63: 897–903
311 Xie F, Zhou J, Zeng X, An Z, Li Y, Han D, Duan P, Wu Z, Zheng Y, Tang J. *Adv Opt Mater*, 2021, 9: 2100017
312 Tu Z, Lu J, Luo X, Hu J, Li S, Wang Y, Zheng Y, Zuo J, Pan Y. *Adv Opt Mater*, 2021, 9: 2100596
313 Frédéric L, Desmarchelier A, Plais R, Lavnevich L, Muller G, Villafuerte C, Clavier G, Quesnel E, Racine B, Meunier-Della-Gatta S, Dognon JP, Thuéry P, Crassous J, Favereau L, Pieters G. *Adv Funct Mater*, 2020, 30: 2004838
314 Yan ZP, Luo XF, Liu WQ, Wu ZG, Liang X, Liao K, Wang Y, Zheng YX, Zhou L, Zuo JL, Pan Y, Zhang H. *Chem Eur J*, 2019, 25: 5672–5676
315 Lu G, Wu Z-, Wu R, Cao X, Zhou L, Zheng Y-, Yang C. *Adv Funct Mater*, 2021, 31: 2102898
316 Yan Z, Liu T, Wu R, Liang X, Li Z, Zhou L, Zheng Y, Zuo J. *Adv Funct Mater*, 2021, 31: 2103875
317 Li M, Liu Y, Duan R, Wei X, Yi Y, Wang Y, Chen CF. *Angew Chem Int Ed*, 2017, 56: 8818–8822
318 Zhang L, Wang YF, Li M, Gao QY, Chen CF. *Chin Chem Lett*, 2021, 32: 740–744
319 Zhang Y, Zhang D, Tsuboi T, Qiu Y, Duan L. *Sci China Chem*, 2019, 62: 393–402
320 Imagawa T, Hirata S, Totani K, Watanabe T, Vacha M. *Chem Commun*, 2015, 51: 13268–13271
321 Feuillastre S, Pauton M, Gao L, Desmarchelier A, Riives AJ, Prim D, Tondelier D, Geffroy B, Muller G, Clavier G, Pieters G. *J Am Chem Soc*, 2016, 138: 3990–3993
322 Wang YF, Lu HY, Chen C, Li M, Chen CF. *Org Electron*, 2019, 70: 71–77
323 Song F, Xu Z, Zhang Q, Zhao Z, Zhang H, Zhao W, Qiu Z, Qi C, Zhang H, Sung HHY, Williams ID, Lam JWY, Zhao Z, Qin A, Ma D, Tang BZ. *Adv Funct Mater*, 2018, 28: 1800051
324 Sun S, Wang J, Chen L, Chen R, Jin J, Chen C, Chen S, Xie G, Zheng C, Huang W. *J Mater Chem C*, 2019, 7: 14511–14516
325 Sharma N, Spuling E, Mattern CM, Li W, Fuhr O, Tsuchiya Y, Adachi C, Bräse S, Samuel IDW, Zysman-Colman E. *Chem Sci*, 2019, 10: 6689–6696
326 Li M, Wang YF, Zhang D, Duan L, Chen CF. *Angew Chem Int Ed*, 2020, 59: 3500–3504
327 Tu ZL, Yan ZP, Liang X, Chen L, Wu ZG, Wang Y, Zheng YX, Zuo JL, Pan Y. *Adv Sci*, 2020, 7: 2000804
328 Wang YF, Li M, Zhao WL, Shen YF, Lu HY, Chen CF. *Chem Commun*, 2020, 56: 9380–9383
329 Yang SY, Wang YK, Peng CC, Wu ZG, Yuan S, Yu YJ, Li H, Wang TT, Li HC, Zheng YX, Jiang ZQ, Liao LS. *J Am Chem Soc*, 2020, 142: 17756–17765
330 Zhang YP, Liang X, Luo XF, Song SQ, Li S, Wang Y, Mao ZP, Xu WY, Zheng YX, Zuo JL, Pan Y. *Angew Chem Int Ed*, 2021, 60: 8435–8440
331 Li M, Wang YF, Zhang DW, Zhang D, Hu ZQ, Duan L, Chen CF. *Sci China Mater*, 2021, 64: 899–908
332 Li M, Wang MY, Wang YF, Feng L, Chen CF. *Angew Chem Int Ed*, 2021, 60: 20728–20733
333 Intaravanne Y, Chen X. *Nanophotonics*, 2020, 9: 1003–1014
334 El Gemayel M, Treier M, Musumeci C, Li C, Müllen K, Samorì P. *J Am Chem Soc*, 2012, 134: 2429–2433
335 Yu H, Bao Z, Oh JH. *Adv Funct Mater*, 2013, 23: 629–639
336 Yang Y, da Costa RC, Fuchter MJ, Campbell AJ. *Nat Photon*, 2013, 7: 634–638
337 Zhang L, Song I, Ahn J, Han M, Linares M, Surin M, Zhang HJ, Oh JH, Lin J. *Nat Commun*, 2021, 12: 142
338 Shang X, Song I, Ohtsu H, Lee YH, Zhao T, Kojima T, Jung JH, Kawano M, Oh JH. *Adv Mater*, 2017, 29: 1605828
339 Gilot J, Abbel R, Lakhwani G, Meijer EW, Schenning APHJ, Mes-

kers SCJ. *Adv Mater*, 2010, 22: E131–E134
340 Stranks SD, Wood SM, Wojciechowski K, Deschler F, Saliba M, Khandelwal H, Patel JB, Elston SJ, Herz LM, Johnston MB, Schenning APHJ, Debije MG, Riede MK, Morris SM, Snaith HJ. *Nano Lett*, 2015, 15: 4935–4941
341 Kim NY, Kyhm J, Han H, Kim SJ, Ahn J, Hwang DK, Jang HW, Ju BK, Lim JA. *Adv Funct Mater*, 2019, 29: 1808668
342 Cheng J, Ge F, Zhang C, Kuai Y, Hou P, Xiang Y, Zhang D, Qiu L, Zhang Q, Zou G. *J Mater Chem C*, 2020, 8: 9271–9275
343 Valev VK, Baumberg JJ, Sibilia C, Verbiest T. *Adv Mater*, 2013, 25: 2517–2534
344 Fan JA, Wu C, Bao K, Bao J, Bardhan R, Halas NJ, Manoharan VN, Nordlander P, Shvets G, Capasso F. *Science*, 2010, 328: 1135–1138
345 Gansel JK, Thiel M, Rill MS, Decker M, Bade K, Saile V, von Freymann G, Linden S, Wegener M. *Science*, 2009, 325: 1513–1515
346 Li W, Coppens ZJ, Besteiro LV, Wang W, Govorov AO, Valentine J. *Nat Commun*, 2015, 6: 8379
347 Xiao W, Shi X, Zhang Y, Peng W, Zeng Y. *Phys Scr*, 2019, 94: 085501
348 Billing DG, Lemmerer A. *Acta Crystlogr E Struct Rep Online*, 2003, 59: m381–m383
349 Billing DG, Lemmerer A. *CrystEngComm*, 2006, 8: 686–695
350 Ahn J, Lee E, Tan J, Yang W, Kim B, Moon J. *Mater Horiz*, 2017, 4: 851–856
351 Han P, Zhang X, Mao X, Yang B, Yang S, Feng Z, Wei D, Deng W, Pullerits T, Han K. *Sci China Chem*, 2019, 62: 1405–1413
352 Li J, Liu X, Cui P, Li J, Ye T, Wang X, Zhang C, Zhao YS. *Sci China Chem*, 2019, 62: 1257–1262
353 Wang J, Fang C, Ma J, Wang S, Jin L, Li W, Li D. *ACS Nano*, 2019, 13: 9473–9481
354 Wang L, Xue Y, Cui M, Huang Y, Xu H, Qin C, Yang J, Dai H, Yuan M. *Angew Chem Int Ed*, 2020, 59: 6442–6450
355 Liu Z, Zhang C, Liu X, Ren A, Zhou Z, Qiao C, Guan Y, Fan Y, Hu F, Zhao YS. *Adv Sci*, 2021, 2102065
356 Lu H, Xiao C, Song R, Li T, Maughan AE, Levin A, Brunecky R, Berry JJ, Mitzi DB, Blum V, Beard MC. *J Am Chem Soc*, 2020, 142: 13030–13040
357 Ahn J, Ma S, Kim JY, Kyhm J, Yang W, Lim JA, Kotov NA, Moon J. *J Am Chem Soc*, 2020, 142: 4206–4212
358 Wang Z, Gao M, Hao X, Qin W. *Appl Phys Lett*, 2020, 116: 053301
359 Lu H, Wang J, Xiao C, Pan X, Chen X, Brunecky R, Berry JJ, Zhu K, Beard MC, Vardeny ZV. *Sci Adv*, 2019, 5: eaay0571
360 Chen C, Gao L, Gao W, Ge C, Du X, Li Z, Yang Y, Niu G, Tang J. *Nat Commun*, 2019, 10: 1927
361 Ishii A, Miyasaka T. *Sci Adv*, 2020, 6: eabd3274
362 Kuehne AJC, Gather MC. *Chem Rev*, 2016, 116: 12823–12864
363 Chen F, Gindre D, Nunzi JM. *Opt Express*, 2008, 16: 16746
364 Furumi S, Sakka Y. *Adv Mater*, 2006, 18: 775–780
365 Furumi S. *Chem Record*, 2010, 10: 394–408
366 Coles H, Morris S. *Nat Photon*, 2010, 4: 676–685
367 Kopp VI, Fan B, Vithana HKM, Genack AZ. *Opt Lett*, 1998, 23: 1707–1709
368 Yuan CL, Huang W, Zheng ZG, Liu B, Bisoyi HK, Li Y, Shen D, Lu Y, Li Q. *Sci Adv*, 2019, 5: eaax9501
369 Jiménez J, Cerdán L, Moreno F, Maroto BL, García-Moreno I, Lunkley JL, Muller G, de la Moya S. *J Phys Chem C*, 2017, 121: 5287–5292
370 Yuan Z, Zhou Y, Qiao Z, Eng Aik C, Tu WC, Wu X, Chen YC. *ACS Nano*, 2021, 15: 8965–8975
371 Downing E, Hesselink L, Ralston J, Macfarlane R. *Science*, 1996, 273: 1185–1189
372 Huang L, Chen X, Mühlenbernd H, Zhang H, Chen S, Bai B, Tan Q, Jin G, Cheah KW, Qiu CW, Li J, Zentgraf T, Zhang S. *Nat Commun*, 2013, 4: 2808
373 Zhan X, Xu FF, Zhou Z, Yan Y, Yao J, Zhao YS. *Adv Mater*, 2021, 33: 2104418
374 Yao L, Niu G, Li J, Gao L, Luo X, Xia B, Liu Y, Du P, Li D, Chen C, Zheng Y, Xiao Z, Tang J. *J Phys Chem Lett*, 2020, 11: 1255–1260